REPUBLIQUE DU CAMEROUN
Paix-Travail-Patrie
****
UNIVERSITE DE YAOUNDE I
****
CENTRE DE RECHERCHE ET DE FORMATION DOCTORALE EN SCIENCES TECHNOLOGIE ET GEOSCIENCES
****

UNITE DE RECHERCHE ET DE FORMATION DOCTORALE PHYSIQUE ET APPLICATIONS

****
DÉPARTEMENT DE PHYSIQUE

B.P.812 Yaoundé

Email : crfdstg@uy1.uninet.cm

REPUBLIC OF CAMEROON
Peace –Work – Fatherland
****
THE UNIVERSITY OF YAOUNDE I
****
POSTGRADUATE SCHOOL OF SCIENCE, TECHNOLOGY & GEOSCIENCES
****

RESEARCH AND POSTGRADUATE TRAINING UNIT FOR PHYSICS AND APPLICATIONS

****
DEPARTMENT OF PHYSICS

P.O. Box 812 Yaounde

Email: crfdstg@uy1.uninet.cm

LABORATORY OF MECHANICS, MATERIALS AND STRUCTURES

LABORATOIRE DE MECANIQUE, MATERIAUX ET STRUCTURES

STRUCTURE AND STABILITY OF ALUMINUM CLUSTERS: A MOLECULAR DYNAMICS STUDY WITH GUPTA POTENTIAL

Thesis submitted for the obtention of Doctorate/PhD in Physics

Option : **Material Science**

By

KEYAMPI WATIO Martial

Matricle : 12W1848

Masters in Physics

Under the Supervision of :

NANA Bonaventure

Associate Professor (University of Bamenda)

And

ZEKENG Serge Sylvain

Professor (University of Yaounde I)

Year 2021

UNIVERSITÉ DE YAOUNDÉ I
THE UNIVERSITY OF YAOUNDE I

FACULTÉ DES SCIENCES
FACULTY OF SCIENCE

DÉPARTEMENT DE PHYSIQUE
DEPARTMENT OF PHYSICS

ATTESTATION DE CORRECTION DE LA THÈSE DE DOCTORAT/Ph.D

Nous, Professeur **DJUIDJE KENMOE Germaine épouse ALOYEM et** Professeur **BEN-BOLIE Germain Hubert** respectivement Examinatrice et Président du jury de la Thèse de Doctorat/Ph.D de Monsieur **KEYAMPI WATIO Martial**, Matricule **12W1848**, préparée sous la direction du Professeur **ZEKENG Serge Sylvain** et du Professeur **NANA Bonaventure,** intitulée : « **Structure and stability of aluminum clusters : a molecular dynamics study with Gupta potential**», soutenue le **Mercredi, 07 Avril 2021**, en vue de l'obtention du grade de Docteur/Ph.D en Physique, Spécialité **Mécanique, Matériaux et Structures ,** Option **Science Des Matériaux,** attestons que toutes les corrections demandées par le jury de soutenance ont été effectuées.

En foi de quoi, la présente attestation lui est délivrée pour servir et valoir ce que de droit.

Fait à Yaoundé le ……19 APR 2021……

Examinatrice	Le Chef de Département de Physique	Le Président du jury
Pr DJUIDJE KENMOE Germaine Epouse ALOYEM	Pr NDJAKA Jean-Marie Bienvenu	Pr BEN-BOLIE Germain Hubert

DEDICATION

To GOD for providing me with life and health and to my wife TSASSE TIWA Stephanie, my three children: Samuel, Filardy, Darryl and finally to my dear parents WATIO Bernard and LONTSI Juliette, for all their love and encouragements.

ACKNOWLEDGMENTS

I am very thankful to my Supervisor Pr. ZEKENG Serge Sylvain, for his encouragement and guidance throughout this work.

I am very thankful to my Director Pr. NANA Bonaventure, for his guidance throughout this work and his infinite tolerance and patience.

I would like to thank Pr. NDJAKA Jean-Marie, Head of Department of Physics, for his constant willingness to solve our problems.

I would like to thank Pr. BEN-BOLIE Germain Hubert, President of this Jury, for his lectures and willingness to solve our problems.

I am grateful to all the members of Jury (Pr. NDJAKA Jean-Marie, Pr. NDOP Joseph, Pr. DJUIDJE KENMOE Germaine and Pr. FEWO Serge) for their willingness to evaluate this work during the predefense.

I am grateful to all the members of Jury (Pr. BEN-BOLIE Germain Hubert, Pr. DJUIDJE KENMOE Germaine, Pr. BODO Bertrand, and Pr. SIEWE SIEWE Martin) for their willingness to evaluate this work during the Audition.

I am grateful to all the members of Jury (Pr. BEN-BOLIE Germain Hubert, Pr. DJUIDJE KENMOE Germaine, Pr. NANA NBENDJO Blaise Romèo, Pr. NDOP Joseph, and Pr. TCHANGNWA NYA Fridolin) for their willingness to evaluate this work during the defense of this Thesis.

I would like to thank my wife TSASSE Tiwa Stephanie for all her help in typesetting and computations during this work.

I am very grateful to all my teachers and lecturers who taught me throughout my educational carrier, for their effort and determination to carry out competitive students with good background.

I would like to thank all my brothers, sisters and my in-laws for their encouragements throughout this work.

I would not forget my elders in research and all my classmates for their friendship and

collaborations in the work.

I would like to thank all those who have contributed scientifically and spiritually for the realization of this work especially for those whose names are not mentioned here.

Contents

LIST OF ABBREVIATIONS

BCC	Body Centered Cubic
BCGA	Birmingham Cluster Genetic Algorithm
C	Cyclic
CI	Configuration Interaction
CGR	Conjugate Gradient Relaxation
D	Decahedral
EAM	Embedded Atom Method
FCC	Face Centered Cubic
GA	Genetic Algorithm
GM	Global Minimization
hcp	hexagonal close packed
HOMO	Highest Occupied Molecular Orbital
I	Icosahedral
IC	Intercrystaline Corrosion
L-BFGS	Quasi Newton Minimization Algorithm
LUMO	Lowest unoccupied Molecular Orbital
MD	Molecular Dynamics
NP-B	Truhlar potential
O	Octahedron
ODE	Ordinary Differential Equation
PES	Potential Energy Surface
PG	Point Group
T	Tetrahedron
TB	Tight Binding

List of Tables

List of Figures

ABSTRACT

In this thesis, we have determined the ground-state geometries and energies of aluminum, $A\ell_N(3 \leq N \leq 170)$ clusters. We have developed a classical Molecular dynamics code using the Gupta potential. The Gupta parameters have been fixed according to the experimental values of the cohesive energy and lattice parameters. For each minimum, the energy and Point Group (PG) have been obtained. The optimized structures are in good agreement with previous ones obtained using Murrell-Mottram potential as well as those obtained using the Glue potential. Aluminum clusters have shown some degree of stability through the little fluctuations observed for few clusters with their number of atoms, known as magic numbers which is due to the saturation of electronic orbitals generated by the entire atomic aggregate. A simple relation between the ground state energy and the number of atoms has been proposed which can permit one to predict the ground state for any cluster size with a known number of atoms. We have obtained the cohesion energy of the aluminum crystal with an accuracy of 99.81%. We have shown in our work that the centered cubic structure is not the optimized structure of $A\ell_9$ as mentioned in the literature. However, it remains an isomer because its energy is 2.0318 eV greater than that of the optimized structure obtained in this work. Finally, we have obtained with the best precision (98.13%), the distance between the two aluminum atoms of the $A\ell_2$ dimer .

Keywords: Aluminum cluster, Ground state, Gupta potential, Molecular dynamics, Magic numbers, Optimized structures.

RESUME

Dans cette thèse, nous avons déterminé les géométries et les énergies de l'état fondamental des clusters d'aluminium, $A\ell_N(N \leq 170)$. Nous avons développé un code de dynamique moléculaire en utilisant le potentiel de Gupta. Les paramètres du potentiel de Gupta ont été fixés en fonction des valeurs expérimentales de l'énergie de cohésion et du paramètre de maille du cristal d'aluminium. Les structures optimisées sont en très bon accord avec celles obtenues en utilisant les potentiels de Murrell-Mottram et de Glue. Parmi les structures optimisées obtenues, nous avons déterminé les structures les plus stables. Ces dernières sont constituées d'un certain nombre d'atomes appelé nombre magique et sont caractérisés par la saturation des orbitales électroniques. Une relation simple entre l'énergie de l'état fondamental et le nombre d'atomes a été proposée, ceci permet de prédire l'état fondamental d'un cluster quelconque des lors que le nombre d'atomes est connu. Nous avons obtenu l'énergie de cohésion du cristal d'aluminium avec une précision de 99.81%. Il ressort de notre travail que la structure cubique centrée n'est pas la structure optimisée du cluster $A\ell_9$ comme mentionné dans la littérature. Elle reste cependant un isomère, car son énergie est de $2,0318$ eV supérieure à celle de la structure optimisée obtenue dans ce travail. Enfin, nous avons obtenu avec la meilleure précision (98.13%), la distance entre les deux atomes d'aluminium du dimère $A\ell_2$.

Mots clés: Cluster d'aluminium, état fondamental, Potentiel de Gupta, Dynamique moléculaire, Nombre magique, Structures optimisées.

GENERAL INTRODUCTION

Aluminum is one of the most abundant elements on earth. It is estimated that the solid portion of the earth's crust to a depth of ten miles is about 8% aluminum, surpassed only by oxygen (47%) and silicon (28%). Aluminum is a major constituent of clay and almost all common rocks. Aluminum is never found as a pure metal in nature but only in chemical compounds with other elements and especially with oxygen, with which it combines strongly [1]. Aluminum can form clusters with itself or with other elements.

Clusters are known to be aggregates composed of several to thousands of atoms (molecules) bonded in certain physical or chemical forces, that exist stably in microscopic state [2]. It has become a great interest for studies due to its unique physical and chemical properties and potential applications in many fields such as the new material physics, the nanoelectronics and the nano-catalyst [3–8].

Aluminum nanoclusters have attracted much attention for their rich display of interesting basic-physics problems and possible applications [9–12]. For any research fields and technological applications which include catalysis, cluster deposition [13], microelectronics [14], and superconductivity [15, 16], atomic distribution on their surfaces play a fundamental role, where the surface structure and its quality are of primary importance.

In other to find their lowest energy configurations, sophisticated minimization techniques have been put in place [17, 18]. It is clearly known that finding the global minimum on a cluster is a difficult problem [19]. This is because the number of structurally distinct minima increases almost exponentially with increasing nuclearity, due to the high dimensionality of configuration space.

Ab-initio electronic structure methods are often used to determine the lowest energy structure. However, a very long time for convergence is needed when the number of atoms making up the cluster increases, which is a drawback. As such, many empirical potentials which adequately describe interactions between atoms in clusters have been developed [20]. For more accuracy in the determination of the energy, the potential should incorporate well modeled

different external surface twin planes, different crystal structures, and the response to strain. Furthermore, vibrational properties need to be well described so as to model the potential temperature dependence of the structure [21]. Therefore, the prediction of the correct structure of a cluster represents a tough challenge for the potential in use.

The understanding of the structure of metal clusters has seen many developments in recent years. However, there is still much to be learnt. A vast number of investigations have attempted to specifically address the stability of various metal-containing clusters [22–27]. From the theoretical perspective, for example, only recently developed global optimization techniques have become sufficiently powerful to find the most stable structures of metal clusters with up to 100 atoms even when described by relatively simple many-body potentials. This has led to many interesting new structures being revealed that go beyond those classified for pair potentials, but there are still probably many classes of structure that remain undiscovered.

The first objective of this work is to fix the Gupta parameters taking into account the experimental values of the cohesive energy and lattice parameters of the Aluminum clusters. The second objective is to use the many body Gupta potential to obtain the lowest energy, which corresponds to the global minima (stable configuration), for each Aluminum cluster with sizes ranging from 3 to 170 atoms. We then compared our results to those obtained using the Murrell-Mottram potential, Glue potential, Sutton-Chen potential, Truhlar potential and the Cleri-Rosato potential [28–32]. As the third objective of this thesis, we will determine some characteristics of our proposed Aluminum clusters.

This thesis is subdivided into three chapters as follows:

The first Chapter is devoted to the physical background of clusters, properties of atomic and molecular clusters, size dependant characteristics of clusters (the Jellium model), past developments and current motivation of Aluminum clusters, importance of Aluminum clusters and features of Aluminum clusters.

The second Chapter deals with the description of the methodology put in place. Here, we presented the calculation method used in this work, exposing the reasons that justify our choice for the many body Gupta potential, we describe the many-body Gupta potential model followed by describing the molecular dynamics method which include the discretization of the ordinary differential equation, global optimization technique, assigning initial values and velocities.

In Chapter 3 focused on the results, we presented our optimized structures, their respective energies and some global minima cluster structures obtained from our calculations. Our structures are then compared to those obtained using different potentials. The stability of the optimized structures is analyzed, the cohesive energy and some characteristics of the Aluminum

clusters are determined.

The document ends with a general conclusion where the principal results of the work are summarized and where perspectives for future investigations are proposed.

Chapter 1

LITERATURE REVIEW

Introduction

In this chapter, we shall look at the ordered type of structures that simple atomic clusters adopt at their ground state, followed by presenting the difference between clusters and their bulk materials. We will also look at the melting behavior of clusters with respect to their sizes and an emphasis shall be made concerning the stability of clusters as well as the reasons why clusters are called superatoms. Clusters preparation together with the motivations for studying clusters shall also be detailly regarded, followed by details on the physical, electrical, optical, magnetic and chemical properties. Next, we shall present the size dependent characteristics of clusters (the Jellium model) as well as an emphasis on the electronic and geometric magic numbers. Furthermore, we shall present the different simulation methods used in stabilizing clusters as well as the different types of potentials that can be used for the global optimization of clusters. Finally, we shall lay emphasis on the problems to be solved in this thesis.

1.1 GENERALITIES ON CLUSTERS

1.1.1 Definition of clusters

Clusters in general, are aggregates of atoms that are too large compared to atoms and molecules and too small compared to small pieces of crystals (bulk materials). The atoms and molecules as well as the bulk materials have been studied many years ago by chemists and physicists and their properties are now fairly well understood. As a whole, cluster does not have the same structure or atomic arrangement as a bulk solid and can change its structure with the addition of just one or few atoms.

One of the most interesting aspects of cluster structure is the possibility of non-crystallographic symmetry which arises from the absence of translational periodicity. In particular, many clus-

ters are found to have fivefold axes of symmetry. The four main types of ordered structure that simple atomic clusters adopt are tetrahedral, octahedral, decahedral and icosahedral. Examples of each are given in Figure 1.1. The decahedral structures have a single fivefold axis of symmetry and are based on pentagonal bipyramids, and the icosahedral structures have six fivefold axes of symmetry.

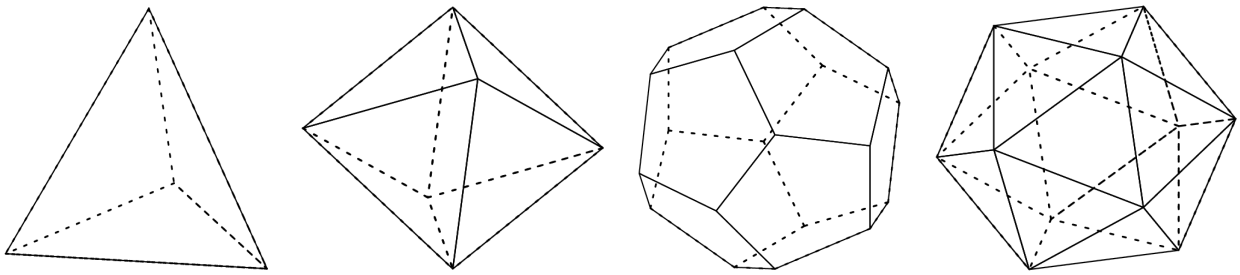

a) b) c) d)

Figure 1.1: The four main types of ordered structure adopted by simple atomic clusters, a) the regular tetrahedron, b) the regular octahedron, c) the regular dodecahedron and d) the regular icosahedron.

The tetrahedron (Figure 1.1a)) has four faces, all of which are triangles. It also has four vertices and six edges. Three faces meet at each vertex. The octahedron (Figure 1.1b)) has eight faces, all of which are triangles. It also has six vertices and twelve edges. Four faces meet at each vertex. The dodecahedron (Figure 1.1c)) has twelve faces, all of which are pentagons. It also has twenty vertices and thirty edges. Three faces meet at each vertex. The icosahedron (Figure 1.1d)) has twenty faces, all of which are triangles. It also has twelve vertices and thirty edges. Five faces meet at each vertex.

1.1.2 Clusters and bulk materials

The wonderful experiment-theory effort is revealing specific characteristics to the reduced-size dimensions and opening up new opportunities. A good example is the possibility of creating new materials using atomic or compound clusters as the building blocks [27, 33, 34]. From this, materials with desirable collective traits would be designed from the level of atomic control realized in the properties of clusters. Clusters may be classified as metallic or nonmetallic according to the atoms they are made up of and in general, some metallic character persist from small clusters to bulk matter of the same composition and no metal-insulator transition have been observed. As the number of atoms in the cluster increases, the bulk structure is established and the addition of atoms has no more effect on the structure.

Nevertheless, there will be some rearrangement of the atoms on the surface of this bulk

structure, but since the surface to volume ratio is very low in bulk materials, it can be neglected with a good approximation. However, in the case of clusters, most of the atoms lie on the surface (extremely high surface to volume ratio) and such rearrangement produces a drastic effect. Owing to their high surface to volume ratio, the surface science from both chemical and physical points of view has become crucial in order to collect data and information about such systems. The manner of study of such a small cluster is nearly the same manner in which they have been fabricated. With Bottom-up approach (chemical point of view) these clusters are formed from atoms and/or molecules by assembling them together to form the cluster and there are many calculations based on this view point. Also these clusters can be fabricated, starting from the bulk material by reducing its dimension somehow, which is the Top-down approach.

1.1.3 Melting behaviors of clusters

The melting behaviors of clusters are completely different from that of the bulk materials and the melting points of clusters usually decrease with decreasing cluster size. Moreover, there are apparent premelting temperature intervals of clusters. For the small clusters, their melting behaviors are accompanied by obvious size effects. For example, the experimental study of the melting behaviors of simple monovalent Na clusters [35] show that the melting points of clusters change oscillatorily for clusters containing less than 200 atoms. The negative heat capacity for Na_{147} cluster [7] has also been observed. Some exotic behaviors are also observed, for example, for the simple trivalent Ga clusters in a small size regime, the melting temperatures are observed to be higher than the bulk melting point [8,36]. The preeminent heat conductivity and malleability of trivalent Aluminum crystal have brought extensive applications in social practice. The study of Aluminum clusters has also revealed a series of singular behaviors.

For example, the ferromagnetic properties of extremely small Aluminum clusters [37] and the super-stability of $A\ell_{13}^-$ cluster which can provide a great potential as being cluster-assembled material [38] with good performance in catalyst [39]. Recently, Jarrold and co-workers conducted numerous experiments on the melting properties of small and medium-sized $A\ell_N$ ($N < 200$) cluster and observed generally irregular phenomenon on the heat capacity curves of small-sized $A\ell_N$ ($N < 100$) clusters [40] (if the heat capacity curve has no clear peak, then considered irregular). Moreover, a double-peak feature in heat capacity has been clearly observed for some larger-sized $A\ell_N$ ($N > 100$) clusters and the authors also conjectured the reason of the double-peak [41], but there is still lack of specific dynamic description at atomic level (like molecular dynamics simulation study).

1.1.4 Stability of clusters

For more than a decade ago, Khanna and Jena [27] discussed the possibility of designing stable metallic clusters that could form the building blocks of solids. Their arguments were derived from two different mass spectrometric experiments on simple metal clusters. The first experiment was the observation by Knight et al. [42] who used small sodium clusters, containing magic numbers of 2, 8, 18, 20, 34, 40 atoms, with the help of a simple Jellium model(as further explained in section 1.3) to explain the enhanced stability at these magic numbers. Here, one assumed that the positive charges of the free-electron metal nuclei within a cluster are evenly distributed over a sphere, that is the size of the cluster and that of the energy levels for a spherical Jellium potential, determined by considering all of the free electrons to be bounded by this potential to have $1s^2$ $1p^6$ $1d^{10}$ $2s^2$ $1f^{14}$ $2p^6$, shell closures. Like the noble gas atoms, the magic-number clusters correspond to filled electronic shells, thereby indicating the role of the total number of itinerant electrons on stability. Basing on the magic numbers in clusters that contain more than a few dozen atoms, the second experiment showed that the most stable species correspond to sizes with complete geometric shells in an icosahedral or cuboctahedral atomic arrangement [43].

Alkali metal clusters, at least for sizes of up to thousands of atoms, conform to the Jellium model in that, certain nuclearities are relatively stable, the so-called magic numbers, due to their filled electronic shells [42]. Hakkinen and Manninen have also shown that, even for molten clusters, the shapes of small sodium clusters are determined by electronic shell effects since electron counts which do not correspond to closed Jellium shells, give rise to deformations of the otherwise spherical liquid drop [44]. By contrast, clusters of alkaline earth elements such as Ca and Sr (which have s^2 closed sub-shell electronic configurations), exhibit magic numbers which correspond to clusters consisting of concentric polyhedral shells (geometric shells) of atoms where the relative stability of a given cluster is determined by the competition between packing and surface energy effects [45].

In the case of Aluminum, due to the higher atomic valency (+3), the higher density of electronic states and the involvement of p, as well as s orbitals in bonding, the situation is more complex [46]. It is believed that the crossover from the regime where electronic factors determine cluster stability to where packing and surface energy effects dominate, occurs at lower nuclearities than for the alkali metals where Jellium effects is possibly being important in the range $40 < N < 300$ [46–48]. Variable temperature experiments by Baguenard et al. have shown, however, that Jellium effects can be seen at much higher nuclearities when the

Aℓ clusters are generated at temperatures such that they are either molten or have molten surfaces [49]. Martin and co-workers have demonstrated that the observation of electronic shells or geometric shells is also strongly temperature dependent in the case of large sodium clusters [50]. Finally, mass spectroscopic studies by Martin and co-workers indicate that Aℓ clusters, with up to a few hundred atoms, have octahedral shell structures based on face centered cubic packing [45].

1.1.5 Chemical representation of clusters

The description of the electronic structure of clusters in terms of electronic shells raised the interesting possibility that clusters can be regarded as superatoms. There are several reasons for such an analogy. The ionization potentials of simple metal clusters exhibit local maxima at sizes corresponding to filled electronic shells, as well as atoms [51]. Furthermore, clusters can sometimes behave chemically similar to atomic species with like electronic valences. A proof of this concept came from the experiments by Leuchtner et al. [52] who studied the reactivity of Aℓ_n^- clusters with oxygen. They showed that while other Aℓ_n^- species were etched away by oxygen, the species Aℓ_{13}^- , Aℓ_{23}^-, and $A\ell_{37}^-$ were not. Since Aℓ_{13} has 40 valence electrons, its inertness could be understood in terms of a closed electronic shell meaning aluminum cluster anions also showed Jellium shell closures for the 23 and 37 atoms.

These and other observations show that the Jellium picture though extremely simplistic and marked by indisputable limitations, is amazingly successful in describing many of the globally observed electronic features of a variety of systems, [53] which allows the description of certain metallic clusters as superatoms. It is important to emphasize that although the electronic shells are introduced through the Jellium model, the existence of electronic shells in fermionic systems is known to occur for a far wider range of potentials [51]. For example, the energy levels in a three dimensional harmonic oscillator, those in an intermediate and square well potential and the energy levels in nuclei under a different class of potentials all lead to shells that would produce closings at the magic number electrons.

1.1.6 Preparation of clusters

Clusters can be prepared in a number of ways. A large proportion of experimental studies are now performed on clusters that are produced in molecular beams by free-jet expansion. The discovery of this technique was one of the most important factors in the growth of cluster studies.

The resulting clusters can then be mass-selected and subjected to many types of high-resolution spectroscopies. However, although this technique allows very detailed and sensitive studies to be performed, it is not so suitable for producing large quantities of (size-selected) clusters a likely requirement for industrial applications and it is hard to make direct measurements of structure.

One alternative that circumvents the latter problem is to deposit the clusters on a surface, where their structure can then be probed by techniques such as high resolution electron microscopy, and scanning tunneling microscopy [54–56]. However, the effects of the surface on the cluster is then to be taken into account.

The oldest route for the preparation of clusters is by colloidal chemistry: back in 1856 Faraday famously investigated the optical properties of gold colloids [57]. Typically, clusters produced by this method are stabilized by the addition of a passivating layer, as compared to the naked clusters produced in molecular beams. One of the main advantages of this method is that large quantities of clusters can be produced. Furthermore, significant advances have now been made in controlling the size, shape and structure of these particles [58–60].

1.1.7 Motivation of studying clusters

If we look back into the early cluster literature, three motivations are particularly common. Firstly, clusters provide a bridge between the limits of isolated atoms and molecules and bulk matter, and so much interest has focused on the evolution of properties with size, particularly those, such as phase transitions, which have no counterpart in atomic physics, and which must therefore emerge as collective behavior becomes possible. The hope is that such knowledge will provide a new perspective on and an increased understanding of the behavior that occurs at the more familiar limits.

A second motivation to study clusters, particularly from the theoretical viewpoint, is to try to understand nucleation at an atomistic level, rather than by the continuum theories of classical nucleation theory. However, these ambitions have never been fully realized; this task is a far more difficult problem than perhaps was originally conceived.

Thirdly, much work has been, and is still, driven by the prospect that a fundamental understanding of the properties, particularly the chemical reactivity, of metal clusters could have far-reaching consequences for catalysis. Small metal particles and clusters (supported, for instance, within a zeolite) could provide both a large surface area to volume ratio and properties, such as activity and selectivity that have been tailored to catalyze a specific reaction.

1.2 PROPERTIES OF ATOMIC AND MOLECULAR CLUSTERS

In case of clusters, its energy levels are neither too discrete nor do they form bands whereas bulk systems form bands of energy and atoms have discrete energy levels. This is due to the presence of large amount of electrons. The unusual electronic structure of clusters is due to the quantum confinement of electrons belonging to molecular orbitals. Other significant properties of clusters are their physical, electric, magnetic, optical and chemical properties.

1.2.1 Physical states

Clusters share some of the physical properties of bulk matter, a few of which are rather surprising. Clusters of all substances except helium and possibly hydrogen are solidlike at low temperatures as expected. The atoms or molecules of a cluster remain close to their equilibrium positions, vibrating around these positions in moderately regular motions of small amplitude. This is characteristic of all solids; their atoms are constrained to stay roughly in the same position at all times. In a liquid or a gas, the atoms or molecules are free to wander through the space accessible to the substance. A gas or vapor has so much empty space relative to the volume occupied by the particles that the particles move almost unhindered, colliding only occasionally with other particles or with the walls of the container [61,62]. A liquid is typically almost as dense as a solid but has some empty spaces into which the atoms or molecules can easily move.

Clusters can be liquidlike if they are warm enough, but typically the temperatures at which clusters can become liquid are much lower than the melting points of the corresponding bulk solids. If temperatures are measured on the Kelvin scale, small clusters become liquidlike at temperatures of roughly half the bulk melting temperatures. For example, solid argon melts at approximately 80 K, while small clusters of argon become liquid at about 40 K [63].

Some clusters are expected to show a gradual transition from solidlike to liquidlike, appearing slushy in the temperature range between their solidlike and liquidlike zones. Other clusters are expected to show, as seen in computer simulations, distinct solidlike and liquidlike forms that qualitatively resemble bulk solids and liquids in virtually every aspect, even though they may exhibit quantitative differences from the bulk [64]. Solid clusters, for example, show virtually no diffusion, but the particles of a liquid cluster can and do diffuse. The forces that hold a particle in place in a solid cluster are strong, comparable to those of a bulk solid; but those

in a liquid cluster include, in addition to forces comparable in strength to those in solids, some forces weak enough to allow a particle to wander far from its home base and find new equilibrium positions. Those same weak forces are responsible for making a liquid cluster compliant; that is, weak forces allow the liquid to accommodate any new force, say, a finger inserted into water.

The greatest differences between bulk solids and liquids and solid and liquid clusters arise from the fact that a large fraction of the particles of a cluster are on its surface. As a result, the particle mobility that characterizes liquids and enables them to exhibit diffusion and physical compliance is enhanced in a cluster, for the cluster can easily expand by enlarging the spaces between particles and can also transfer particles from its interior to its surface, leaving vacancies that enhance the mobility of the interior particles. An important consequence is that the vapor pressure of a cluster is higher than the vapor pressure of the corresponding bulk, and accordingly the boiling point of a liquid cluster, the temperature at which the vapor pressure of a liquid is equal to the pressure of the surrounding atmosphere-is lower than that of the corresponding bulk liquid. The vapor pressure of clusters decreases with increasing cluster size, while the boiling point increases [65].

Perhaps the greatest difference between clusters and bulk matter with regard to their transformation between solid and liquid is the nature of the equilibrium between two phases. Bulk solids can be in equilibrium with their liquid forms at only a single temperature for any given pressure or at only a single pressure for any given temperature. Clusters differ sharply from bulk matter in that solid and liquid clusters of the same composition are capable of coexisting within a band of temperatures and pressures. At any chosen pressure, the proportion of liquid clusters to solid clusters increases with temperature [66]. At low temperatures the clusters are solid, as described above. As the temperature is increased, some clusters transform from solid to liquid. If the temperature is raised further, the proportion of liquid clusters increases, passing through 50 percent, so that the mixture becomes predominantly liquid clusters. At sufficiently high temperatures all the clusters are liquid.

No cluster remains solid or liquid all the time; liquidlike clusters occasionally transform spontaneously into solidlike clusters and vice versa. The fraction of time that a particular cluster spends as a liquid is precisely the same as the fraction of clusters of that same type within a large collection that are liquid at a given instant [66]. That is to say, the time average behavior gives the same result as the ensemble average, which is the average over a large collection of identical objects. This equivalence is not limited to clusters; it is the well-known ergodic property that is expected of all but the simplest real systems.

1.2.2 Electric properties

The electric properties of clusters, such as their conductivity and metallic or insulating character, depend on the substance and the size of the cluster. Quantum theory attributes wavelike character to matter, a behavior that is detectable only when matter is examined on the scale of atoms and electrons. At a scale of millimeters or even millionths of millimeters, the wavelengths of matter are too short to be observed. Clusters are often much smaller than that, with the important consequence that many are so small that when examined their electrons and electronic states can exhibit the wavelike properties of matter. In fact, quantum properties may play an important role in determining the electrical character of the cluster. In particular, as described previously, if a cluster is extremely small, the energy levels or quantum states of its electrons are not close enough together to permit the cluster to conduct electricity [61, 67].

Moreover, an alternative way to view this situation is to recognize that a constant electric force and an alternating force can behave differently in a cluster. Direct current cannot flow in an isolated cluster and probably cannot occur in a small cluster even if it is sandwiched between slabs of metal. The current flow is prohibited both because the electrons that carry the current encounter the boundaries of the cluster and because there are no quantum states readily available at energies just above those of the occupied states, which are the states that must be achieved to allow the electrons to move.

However, if a field of alternating electric force is applied with a frequency of alternation so high that the electrons are made to reverse their paths before they encounter the boundaries of the cluster, then the equivalent of conduction will take place [67, 68]. Ordinary 60 Hz alternating voltage and even alternations at radio-wave frequencies switch direction far too slowly to produce this behavior in clusters; microwave frequencies are required.

1.2.3 Optical properties

The optical properties of weakly bound clusters are much like those of their component atoms or molecules; the small differences are frequently useful diagnostics of how the cluster is bound and what its structure may be. Optical properties of metal clusters are more like those of the corresponding bulk metals than like those of the constituent atoms [69, 70]. These properties reveal which cluster sizes are unusually stable and therefore correspond to magic-number sizes. Optical properties of covalently bound clusters are in most cases unlike those of either the component atoms or the bulk but are important clues to the structure and bonding of the cluster [71–73].

1.2.4 Magnetic properties

Magnetic properties of clusters, in contrast, appear to be rather similar to those of bulk matter. They are not identical, because clusters contain only small numbers of electrons, which are the particles whose magnetic character makes clusters and bulk matter magnetic. As a result, the differences between magnetic properties of clusters and of bulk matter are more a matter of degree than of kind. Clusters of substances being magnetic in the bulk also tend to be magnetic. The larger the cluster, the more nearly will the magnetic character per atom approach that of the bulk. The degree of this magnetic character depends on how strongly the individual electron magnets couple to each other to become aligned in the same direction; the larger the cluster, the stronger is this coupling.

Magnetic dipole moments of free atoms of Sc, V, Ti, Cr, Mn, Fe, Co and Ni are μ_b, $2\mu_b$, $3\mu_b$, $6\mu_b$, $5\mu_b$, $4\mu_b$, $3\mu_b$, $2\mu_b$ respectively. While magnetism in Cr remains unchanged on benzenes, the magnetic moments change dramatically for others [74–76]. For example, magnetic elements (Fe, Co and Ni) exhibit reduced magnetic moments whereas Sc, V, Ti show increased moments. This peculiar behavior suggests that magnetism in organometallic systems is greatly influenced by supporting molecules.

1.2.5 Chemical properties

This is one of the most important properties of clusters. Here, organic molecules can be seen binding to various sites of inorganic or metal clusters. Metal atoms, metal clusters and metal surfaces can be observed to bind to various organic molecules thus providing great information in the organometallic field [74,75,77–82]. With regard to these situations, transition metal clusters bound with such organic molecules to achieve exceptional stability. Few examples have been studied concerning the favorite binding positions of metal atoms on given organic molecules or changes in the structure of clusters as multiple organic molecules attached themselves to metal clusters. For example, the structural study of various 3d transition metal atoms like Sc, Ti, V, Cr, Mn, Fe, Co and Ni attached to a benzene ring or a coronene (this is a benzene ring surrounded by six other benzenes) [77, 83]. From the $M_n(Bz)_m^+$ mass spectra, it is observed that only structures with $m = n + 1$ for M = Sc, Ti, V are favored. A single highest peak corresponding to ($n = 1$, $m = 2$) is observed for Cr and Mn thus showing that transition metal is sandwiched between stacking of benzene rings. In this process, the maximum number of benzene rings in a stable cluster hardly exceeds four meanwhile, the number of metal atoms

can exceed the number of benzene rings. For this reason, the reactivity of transition metal decreases. Magnetism in such organometallic complexes has also been found to be unusual.

Many properties of cluster depend on their size, shape, composition and charge. So, some clusters from their electronic structure are considered to be artificial elements. Theoretical predictions and experimental evidence showed that, clusters behave as atoms. These type of clusters are called superatoms and they are building blocks of the new three-dimensional periodic table [84]. Castleman et al. observed that $A\ell_{13}^-$ has very less reactivity than its neighboring clusters [52]. Since $A\ell$ atom has three valence electrons, $A\ell_{13}$ will have 39 electrons, making electron affinity of $A\ell_{13}$ very large so as to attain the magic number which is 40. Like the normal salt, this cluster can form salt with alkali metals [85]. This was experimentally confirmed by Wang [12] and Bowen [86] and their co-workers. Hence, $A\ell_{13}$ became the first superatom or rather superhalogen. On the other hand, Li_3O cluster has ionization potential (3.54 eV), lower than that of any alkali metal and $H_{12}F_{13}$ recorded highest electron affinity (13.87 eV), higher than any halogen [87, 88]. Some boron clusters mimic the properties hydrocarbons [89] while thiol protected gold cluster $[Au_{25}(SR)_{18}]^-$ behaves as noble gas [90]. Clusters consisting of all-inorganic elements can be used as ligands [91, 92].

Although Jellium model is successful in describing the magical stability of alkali metal clusters, it cannot be applied to study the stability of covalently bonded systems, such as fullerene or planar boron clusters. However, for these systems a simple electron counting rule can give a great understanding of stability. This is called the Hückel rule which says; if the system has delocalized π electrons and if they are equal to $4n+2$ (n is integer), then the system is said to be aromatic and will be extra stable. If it is equal to 4n, then it is called antiaromatic and will destabilize the system. For example benzene, it has 6π electrons and it is aromatic. A planarity is also applied by the Hückel rule for aromaticity.

This rule is successfully applied to a large number of carbon and boron-based clusters and are found to be aromatic [89, 91, 93–98]. Boron clusters B_N ($N \leq 20$) prefer to be planar and they are governed by aromatic nature. A three-dimensional structure of B_{12} also shows enhanced stability mainly because of largest HOMO-LUMO (Highest Occupied Molecular Orbital-Lowest Unoccupied Molecular Orbital) gap and the most stable isomer of B_{12} is a planar structure having 6π electrons like that of benzene. Based on the Hückel rule, several metallic clusters are also found to exhibit aromaticity. $A\ell_4^{2-}$, for instance, is aromatic and square-planar due to two π electrons, whereas $A\ell_4^{4-}$ with four π electrons is antiaromatic [99, 100]. An aromatic, planar boron cluster having wheel shape rotates when shined by a circularly polarized light [101, 102]. This can be termed as the smallest aromatic nano-motor.

1.3 THE JELLIUM MODEL: SIZE DEPENDANT CHARACTERISTICS OF CLUSTERS

1.3.1 Definition

Jellium, also known as the uniform electron gas or homogeneous electron gas, is a quantum mechanical model of interacting electrons in a solid where the positive charges (atomic nuclei) are assumed to be uniformly distributed in space; the electron density is a uniform quantity as well in space. This model allows one to focus on the effects in solids that occur due to the quantum nature of electrons and their mutual repulsive interactions (due to like charge) without explicit introduction of the atomic lattice and structure making up a real material.

Jellium is often used in solid-state physics as a simple model of delocalized electrons in a metal, where it can qualitatively reproduce features of real metals such as screening, plasmons, Wigner crystallization and Friedel oscillations. At zero temperature, the properties of Jellium depend solely upon the constant electronic density. This lends it to a treatment within density functional theory; the formalism itself provides the basis for the local-density approximation to the exchange-correlation energy density functional.

1.3.2 Applications of the Jellium model

Jellium is the simplest model of interacting electrons. It is employed in the calculation of properties of metals, where the core electrons and the nuclei are modeled as the uniform positive background and the valence electrons are treated with full rigor. Semi-infinite Jellium slabs are used to investigate surface properties such as work function and surface effects such as adsorption; near surfaces the electronic density varies in an oscillatory manner, decaying to a constant value in the bulk [103–105].

Within density functional theory, Jellium is used in the construction of the local-density approximation, which in turn is a component of more sophisticated exchange-correlation energy functionals. From quantum Monte Carlo calculations of Jellium, accurate values of the correlation energy density have been obtained for several values of the electronic density, which have

been used to construct semi-empirical correlation functionals [106,107]. The Jellium model has been applied to superatoms, and used in nuclear physics.

1.3.3 Electronic and geometric magic numbers

Magic numbers based on electronic shells were first observed in mass spectra of alkali metal clusters [108]. These features are now well understood in the framework of the self-consistent spherical Jellium model, in which the nearly-free valence electrons are assumed to move in a homogeneous spherical ionic background. Further refinements, such as allowing the cluster to deform into an ellipsoidal shape for incomplete electronic shells, improve the agreement with experiment [109].

In experiments on large sodium clusters by Martin et al. electronic shell structure was found to persist up to about 1000 atoms and above this size geometric magic numbers were observed [110]. These magic numbers are associated with the completion of shells of the Mackay icosahedron. Further temperature-dependent experiments have shown that for $N > 1000$ the geometric magic numbers disappear as the temperature is increased [111]. This has been attributed to the loss of icosahedral structure on melting (or surface melting) of the cluster and so has been used to examine the size dependence of the melting temperature. At sufficiently high temperatures, electronic magic numbers have been observed up to at least 3000 sodium atoms [112]. Similarly, experiments on large Aluminum clusters have shown that as the temperature is increased the observed magic numbers change from geometric (due to octahedra [113]) to electronic [114].

The Jellium-type models can provide a good description of the alkali metals because these elements most closely approximate free electron systems and understanding the electronic effects becomes more difficult as one goes further from this limit. Our results lead us to expect that for metals with shorter-ranged potentials geometric magic numbers could be seen at much smaller sizes than for sodium. This may provide an explanation for the behavior of group II metals: barium clusters of less than 50 atoms show magic numbers consistent with an icosahedral growth sequence and magnesium and calcium have magic numbers due to Mackay icosahedra from 147 atoms upwards [115–117]. However, it is hard to judge the role many-body forces may play in the energetic competition between regular and disordered structures in these systems.

1.4 COMPUTER MODELING AND MOLECULAR DYNAMICS

1.4.1 Computer modeling of clusters

One of the simplest to describe, yet most difficult to solve, problems in computational chemistry is the determination of molecular conformation. A molecular conformation problem can be described as finding the global minimum of a suitable potential energy function, which depends on relative atom positions. Progress toward solution techniques will facilitate drug design, synthesis and utilization of pharmaceutical and material products.

The methods of quantum chemistry are quite suited to predict the geometric, electronic and energy features of known and unknown molecules. However, it remains too expensive in terms of computer time and nearly intractable, even at the simplest, semi-empirical level, for many organic molecules or biological macromolecular structures.

In the modern nanotechnology age, microscopic analysis methods are indispensable in order to generate new functional materials and investigate physical phenomena on a molecular level. These methods treat the constituent species of a system, such as molecules and fine particles. Macroscopic and microscopic quantities of interest are derived from analyzing the behavior of these species.

These approaches, called molecular simulation methods, are represented by the Monte Carlo (MC) and molecular dynamics (MD) methods. Monte Carlo methods exhibit a powerful ability to analyze thermodynamic equilibrium, but are unsuitable for investigating dynamic phenomena. Molecular dynamics methods are useful for thermodynamic equilibrium and are more advantageous for investigating the dynamic properties of a system in a nonequilibrium situation.

1.4.2 Molecular Dynamics

Molecular dynamics is a computer simulation method for analyzing the physical movements of atoms and molecules. The atoms and molecules are allowed to interact for a fixed period of time, giving a view of the dynamic evolution of the system. In the most common version, the trajectories of atoms and molecules are determined by numerically solving Newton's equations

of motion for a system of interacting particles, where forces between the particles and their potential energies are often calculated using interatomic potentials or molecular mechanics force fields. Because molecular systems typically consist of a vast number of particles, it is impossible to determine the properties of such complex systems analytically; Molecular dynamics simulation circumvents this problem by using numerical methods.

1.4.3 Areas of application

First used in theoretical physics, the Molecular dynamics method gained popularity in materials science afterward, and since the 1970s is also common in biochemistry and biophysics. Molecular dynamics is frequently used to refine 3-dimensional structures of proteins and other macromolecules based on experimental constraints from X-ray crystallography.

In physics, Molecular dynamics is used to examine the dynamics of atomic-level phenomena that cannot be observed directly, such as thin-film growth and ion-subplantation, and also to examine the physical properties of nanotechnological devices that have not yet been created.

In biophysics and structural biology, the method is frequently applied to study the motions of macromolecules such as proteins and nucleic acids, which can be useful for interpreting the results of certain biophysical experiments and for modeling interactions with other molecules, as in ligand docking.

In principle Molecular dynamics can be used for ab-initio prediction of protein structure by simulating folding of the polypeptide chain from random coil.

1.4.4 Design constraints

The design of a molecular dynamics simulation should account for the available computational power. Simulation size (n =number of particles), time step, and total time duration must be selected so that the calculation can finish within a reasonable time period. However, the simulations should be long enough to be relevant to the time scales of the natural processes being studied. To make statistically valid conclusions from the simulations, the time span simulated should match the kinetics of the natural process. Otherwise, it is analogous to making conclusions about how a human walks when only looking at less than one footstep.

1.5 POTENTIALS IN MOLECULAR DYNAMICS SIMULATIONS

1.5.1 Generalities

A molecular dynamics simulation requires the definition of a potential function, or a description of the terms by which the particles in the simulation will interact. In chemistry and biology this is usually referred to as a force field and in materials physics as an interatomic potential. Potentials may be defined at many levels of physical accuracy; those most commonly used in chemistry are based on molecular mechanics and embody a classical mechanics treatment of particle-particle interactions that can reproduce structural and conformational changes but usually cannot reproduce chemical reactions.

The reduction from a fully quantum description to a classical potential entails two main approximations. The first one is the Born-Oppenheimer approximation, which states that the dynamics of electrons are so fast that they can be considered to react instantaneously to the motion of their nuclei. As a consequence, they may be treated separately. The second one treats the nuclei, which are much heavier than electrons, as point particles that follow classical Newtonian dynamics. In classical molecular dynamics, the effect of the electrons is approximated as one potential energy surface, usually representing the ground state.

When finer levels of detail are needed, potentials based on quantum mechanics are used; some methods attempt to create hybrid classical/quantum potentials where the bulk of the system is treated classically but a small region is treated as a quantum system, usually undergoing a chemical transformation.

1.5.2 Empirical potentials

Empirical potentials used in chemistry are frequently called force fields, while those used in materials physics are called interatomic potentials. Most force fields in chemistry are empirical and consist of a summation of bonded forces associated with chemical bonds, bond angles, bond dihedrals, and non-bonded forces associated with van der Waals forces and electrostatic charge. Empirical potentials represent quantum-mechanical effects in a limited way through ad-hoc functional approximations.

These potentials contain free parameters such as atomic charge, van der Waals parameters reflecting estimates of atomic radius, and equilibrium bond length, angle, and dihedral; these are obtained by fitting against detailed electronic calculations or experimental physical properties

such as elastic constants, lattice parameters and spectroscopic measurements.

Because of the non-local nature of non-bonded interactions, they involve at least weak interactions between all particles in the system. Its calculation is normally the bottleneck in the speed of MD simulations. To lower the computational cost, force fields employ numerical approximations such as shifted cutoff radii, reaction field algorithms, particle mesh Ewald summation, or the newer particle-particle-particle-mesh.

Chemistry force fields commonly employ preset bonding arrangements (an exception being ab initio dynamics), and thus are unable to model the process of chemical bond breaking and reactions explicitly. On the other hand, many of the potentials used in physics, such as those based on the bond order formalism can describe several different coordination of a system and bond breaking [54, 55]. Examples of such potentials include the Brenner potential [56] for hydrocarbons and its further developments for the C-Si-H [57] and C-O-H [58] systems. The ReaxFF potential [59] can be considered a fully reactive hybrid between bond order potentials and chemistry force fields.

1.5.3 Pair potentials versus many-body potentials

The potential functions representing the non-bonded energy are formulated as a sum over interactions between the particles of the system. The simplest choice, employed in many popular force fields, is the "pair potential", in which the total potential energy can be calculated from the sum of energy contributions between pairs of atoms. Therefore, these force fields are also called "additive force fields". An example of such a pair potential is the non-bonded Lennard-Jones potential (1.1), used for calculating van der Waals forces.

$$U(r_{ij} = \varepsilon \left[\left(\frac{r_{min}}{r_{ij}} \right)^{12} - 2 \left(\frac{r_{min}}{r_{ij}} \right)^{6} \right] \tag{1.1}$$

The attractive long-range term α - $\frac{1}{r^6}$ is due to mutual polarization of the interacting atoms. The indicated form of the repulsion term, α $\frac{1}{r^{12}}$ has no theoretical justification. In addition to the Lennard-Jones potential, we have the Morse potential, Dzugutov potential and the Quasi Sutton Chen potential as describe in section 1.6.

Another example is the Born (ionic) model of the ionic lattice. The first term in this model is the Coulomb's law for a pair of ions, the second term is the short-range repulsion explained

by Pauli's exclusion principle and the final term is the dispersion interaction term. Usually, a simulation only includes the dipolar term, although sometimes the quadrupolar term is also included [60, 118].

In many-body potentials, the potential energy includes the effects of three or more particles interacting with each other [119]. In simulations with pair-wise potentials, global interactions in the system also exist, but they occur only through pair-wise terms. In many-body potentials, the potential energy cannot be found by a sum over pairs of atoms, as these interactions are calculated explicitly as a combination of higher-order terms. In the statistical view, the dependency between the variables cannot in general be expressed using only pair-wise products of the degrees of freedom.

For example, the Tersoff potential (1.2), [120] which was originally used to simulate carbon, silicon, and germanium, and has since been used for a wide range of other materials, involves a sum over groups of three atoms, with the angles between the atoms being an important factor in the potential.

$$U_{tot} = \frac{1}{2}\sum_{i}\sum_{i\neq j} f_{cut}(r_{ij})\left[a_{ij}U_R(r_{ij}) - b_{ij}U_A(r_{ij})\right]. \tag{1.2}$$

The repulsive U_R and attractive U_A energy terms are given by

$U_R(r_{ij}) = A\exp(\text{-}\lambda_1 r_{ij})$ and $U_A(r_{ij}) = B\exp(\text{-}\lambda_2 r_{ij})$ Where A, B, λ_1 and λ_2 are parameters of the potential. In addition to the Tersoff potential, we have the Sutton Chen potential, Stillinger-Weber potential and the Gupta potential as describe in section 1.7.

Other examples are the embedded-atom method (EAM), [121] the EDIP, [119] and the Tight-Binding Second Moment Approximation (TBSMA) potentials, [122] where the electron density of states in the region of an atom is calculated from a sum of contributions from surrounding atoms, and the potential energy contribution is then a function of this sum.

1.5.4 Semi-empirical potentials

Semi-empirical potentials make use of the matrix representation from quantum mechanics. However, the values of the matrix elements are found through empirical formulae that estimate the degree of overlap of specific atomic orbitals. The matrix is then diagonalized to determine the occupancy of the different atomic orbitals, and empirical formulae are used once again to determine the energy contributions of the orbitals.

There are a wide variety of semi-empirical potentials, termed tight-binding potentials, which vary according to the atoms being modeled.

1.6 OTHER TYPES OF PAIR POTENTIALS

1.6.1 Morse Potential

The Morse potential is a convenient model for the potential energy of a diatomic molecule. It is a better approximation for treating the vibrational structure of a molecule than the harmonic oscillator because it explicitly includes the effects of bond breaking. It also accounts for the anharmonicity of chemical bonds. The Morse potential is implemented in the most general form (1.3). The parameter r_0 is the radial distance to the minimum of the potential, $\varepsilon(\kappa - 1)$ is the depth of the potential well, the parameters β (in units of inverse length) and κ (dimensionless) define the steepness of the potential. The curves in Figure 1.2 show the Morse potential calculated for several values of β

$$U(r_{ij}) = \varepsilon[exp(-\kappa\beta(r_{ij} - r_o)) - \kappa exp(-\beta(r_{ij} - r_o))] \tag{1.3}$$

1.6.2 Dzugutov Potential

The Dzugutov pairwise potential is known to favor icosahedral ordering in the first neighbour shell and was originally developed as a model of simple glass-forming liquid metals [123]. The potential is constructed to suppress crystallization common to most monoatomic systems by the introduction of a repulsive term representing the Coulomb interactions that are present in a liquid metal. This term gives rise to a maximum that is needed to prevent particles residing in the second neighbour shell from finding energetically favorable sites as in an FCC or BCC configuration. The Dzugutov potential (1.4)

$$U(r_{ij}) = A\left(\frac{1}{r_{ij}^m - B}\right) exp\left(\frac{c}{r_{ij} - a}\right)\Theta(a - r_{ij}) + Bexp\left(\frac{d}{r_{ij} - b}\right)\Theta(b - r_{ij}), \tag{1.4}$$

where Θ (χ) is the Heaviside step function (1.5):

$$\Theta(\chi) = \{^{1,if\chi>0}_{0,if\chi<0} \tag{1.5}$$

The parameters a, b, c and d are measured in units of length, m is an integer, the units of A and B are not fixed. The curves in Figure 1.3 illustrate the behaviour of the Dzugutov potential for several values of the parameter a (as indicated) and for fixed values of other parameters.

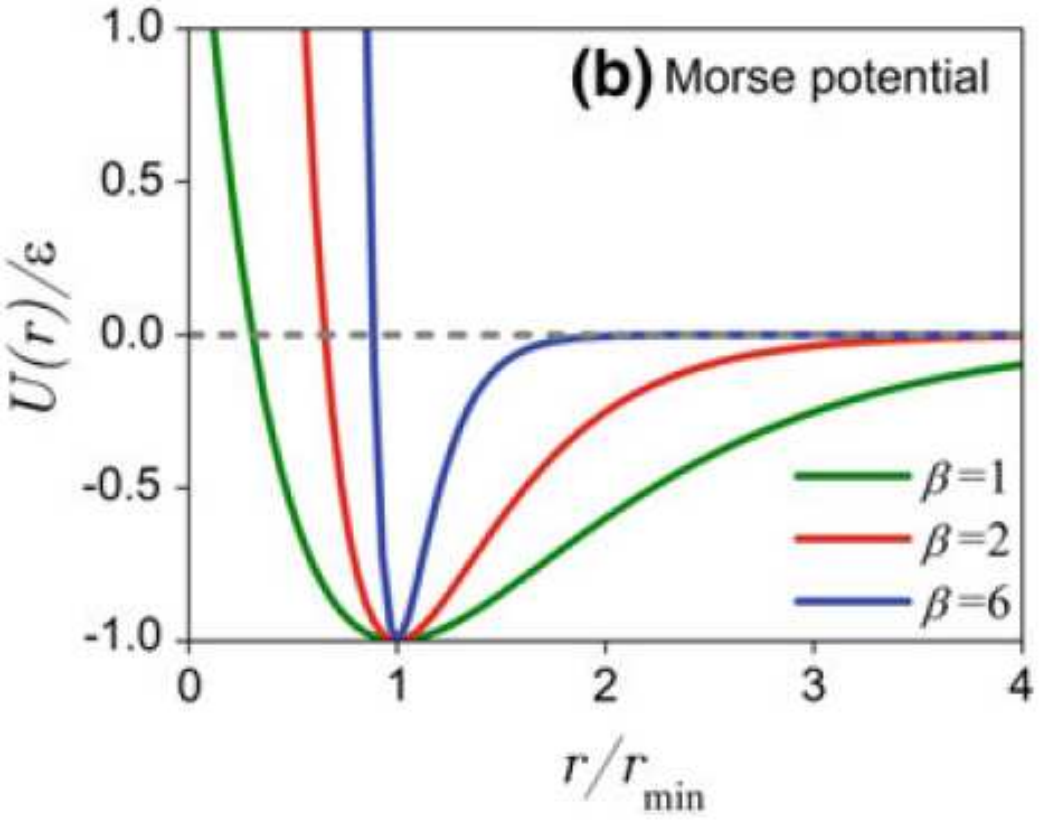

Figure 1.2: *The Morse potential (scaled by ε) as a function of the radial distance r . The curves correspond to κ = 2, r_0 = 1 (arb. units) and for three indicated values of β (in arb. units) [123].*

1.6.3 Quasi Sutton-Chen Potential

The pairwise Quasi Sutton-Chen potential is a pairwise potential, which is a simplified version of the many-body Sutton-Chen potential discussed below. The quasi Sutton-Chen potential is more convenient in some simulations because of its simple parametrisation, (1.6).

$$U(r_{ij}) = \{ \begin{matrix} +\infty, & r_{ij}<r_0 \\ \frac{a}{(r_{ij}-r_0)^n} - \frac{b}{r_{ij}^m}, & r_{ij}\geq r_0 \end{matrix} \tag{1.6}$$

where n,m are integers, the parameter r_0 is measured in units of length and the parameters a, b are measured in $[EnergyLength^n]$ and $[EnergyLength^m]$, respectively. Figure 1.4 illustrates the quasi Sutton-Chen potential calculated for several sets (n,m) as indicated and for fixed values of other parameters as specified in the caption.

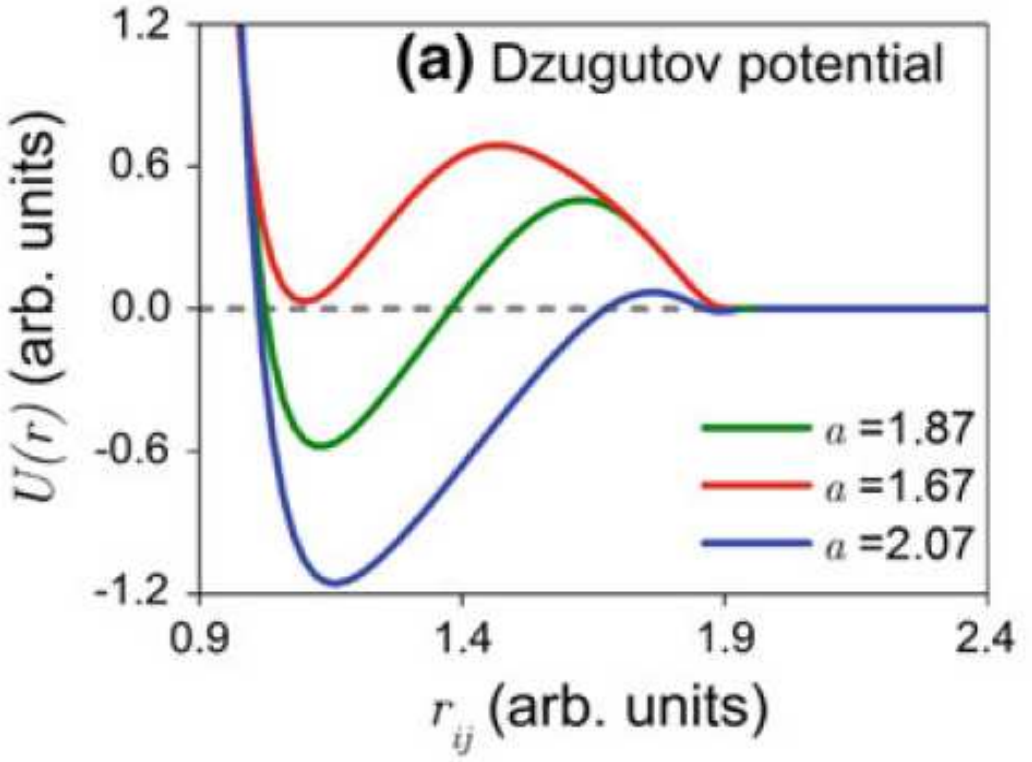

Figure 1.3: *The Dzugutov potential as a function of the radial distance r . The curves correspond to b = 1.94, c = 1.1, d = 0.27, A = 5.82, B = 1.28 (all in arb. units), m = 16, and to three values of a (arb. units) as indicated [123].*

1.7 OTHER TYPES OF MANY BODY POTENTIALS

1.7.1 Sutton-Chen Potential

The Sutton-Chen potential is often employed for the description of the interaction between metal atoms, for example, those which constitute a metallic cluster or a nanoparticle [123]. The total potential energy of N atoms can be written as a sum of the repulsive, U_R, and the attractive, U_A, terms (1.7).

$$U(tot) = U_R + U_A \tag{1.7}$$

The repulsive part of the Sutton-Chen potential is written in terms of the sum of pairwise power potentials (1.8),

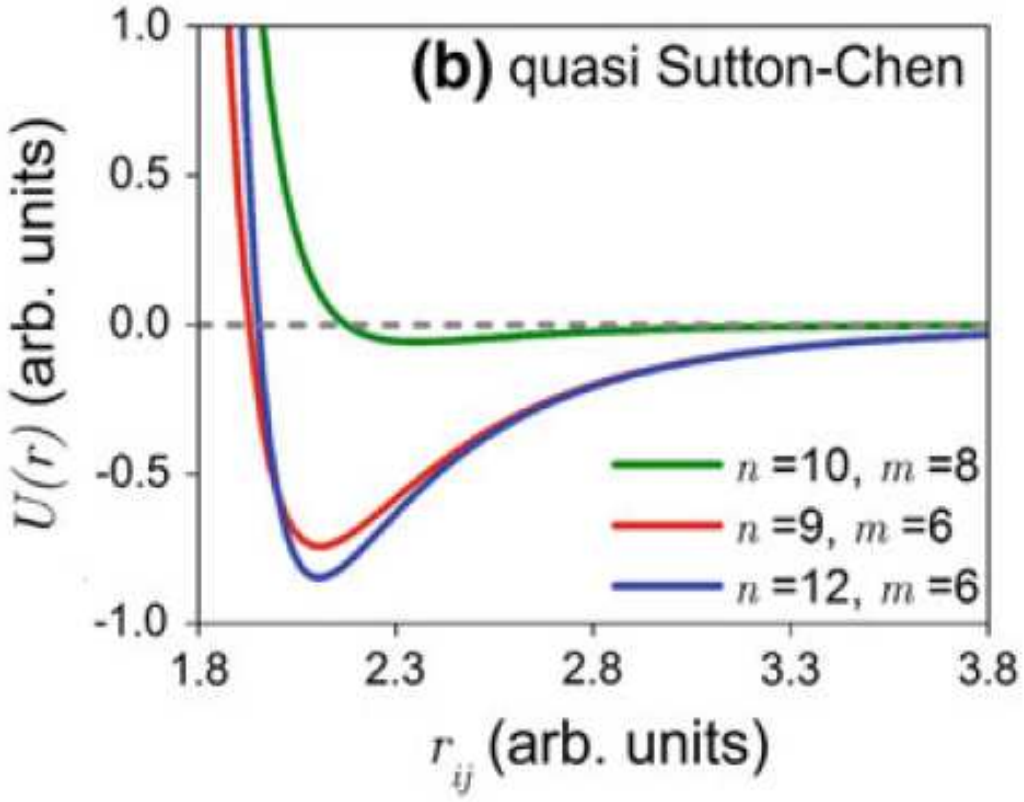

Figure 1.4: *The Quasi Sutton-Chen potential as a function of the radial distance r . The curves correspond to r_0 = 1, a = 1, b = 100 (arb. units) and for three indicated sets of the integers n and m [123].*

$$U(R) = \frac{\varepsilon}{2}\sum_{j\neq i}^{N} U(r_{ij}), \qquad U(r_{ij}) = \left(\frac{a}{r_{ij}}\right)^{n} \tag{1.8}$$

The attractive term accounts for the non-local effects of the interatomic interaction (1.9):

$$U(A) = -C\varepsilon\sum_{i=1}^{N}\sqrt{\rho(r_i)}, \qquad \rho(r_i) = \sum_{j\neq i}\left(\frac{a}{r_{ij}}\right)^{m} \tag{1.9}$$

In these formulae, the parameters of the Sutton-Chen potential are introduced: a and c (in units of length) and dimensionless integers n,m.

1.7.2 Gupta Potential

The Gupta family of potentials can be used to model a variety of metals. Similar to the Sutton-Chen potential, the Gupta potential can be written in the form indicated in (1.10) but with the repulsive and attractive parts expressed in terms of the exponential potentials (1.11):

$$U(R) = A\sum_{j\neq i}^{N} U(r_{ij}), \qquad U(r_{ij}) = exp\left[-p\left(\frac{r_{ij}}{r_0} - 1\right)\right], \tag{1.10}$$

$$U(A) = -\xi\sum_{i=1}^{N}\sqrt{\rho(r_i)}, \qquad \rho(r_i) = \sum_{j\neq i}\left[-2q\left(\frac{r_{ij}}{r_0} - 1\right)\right] \tag{1.11}$$

where the parameters A and ξ are measured in units of energy, r_0 in units of length and p, q are dimensionless. More detailed information on the parameters as well as on their derivation will be presented in chapter2.

1.7.3 Stillinger-Weber Potential

Simulation of the structure of carbon-like structures for example, single diamond, Si and Ge crystals as well as of the superlattice Si1-xGex by means of molecular dynamics can be performed by means of bond-ordered Tersoff and Brenner potentials. Another potential, allowing this is the Stillinger-Weber. The Stillinger-Weber potential is written as a combination of two-body and three body interactions (1.12) [123]:

$$U(tot) = \sum_{i<j} V_2(i,j) + \sum_{i<j<k} V_3(i,j,k) \tag{1.12}$$

Here the first term stands for the contribution of the two-body interactions (1.13),

$$V_2(i,j) = \begin{cases} \varepsilon_{ij}A\left[B\left(\frac{\sigma_{ij}}{r_{ij}}\right)^p - \left(\frac{\sigma_{ij}}{r_{ij}}\right)^q\right] exp(\frac{r_{ij}}{\sigma_{ij}} - a)^{-1}, & if \frac{r_{ij}}{\sigma_{ij}} < a \\ 0, & if otherwise \end{cases} \tag{1.13}$$

Dimensionless parameters A, B, as well as the cut-off radius a are used to tune the pairwise potential. If the system in question consist of identical atoms, then for all pairs (i, j) the energy parameters ε_{ij} and the length ones σ_{ij} are set equal, that is $\varepsilon_{ij} \longrightarrow \varepsilon$, $\sigma_{ij} \longrightarrow \sigma$. For a binary system, which consist of the atoms of two types, a1 and a2 (e.g., a Si-Ge superlattice) one introduces $\varepsilon_{\alpha\beta} = \sqrt{\varepsilon_\alpha \varepsilon_\beta}$ and $\sigma_{\alpha\beta} = \frac{(\sigma_\alpha + \sigma_\beta)}{2}$($\alpha$,$\beta$ = 1, 2). The three-body interaction is parametrised as shown in (1.14), (1.15), (1.16) and (1.17)

$$V_a(i,j,k) = \varepsilon_{ijk} h\left(\frac{r_{ij}}{\sigma_{ij}}\right), \left(\frac{r_{ik}}{\sigma_{ik}}, \theta_{ijk}\right) \Theta\left(a - \frac{r_{ij}}{\sigma_{ij}}\right) \Theta\left(a - \frac{r_{ik}}{\sigma_{ik}}\right) \tag{1.14}$$

$$V_b(i,j,k) = \varepsilon_{jik} h\left(\frac{r_{ji}}{\sigma_{ji}}\right), \left(\frac{r_{jk}}{\sigma_{jk}}, \theta_{jik}\right) \Theta\left(a - \frac{r_{ji}}{\sigma_{ji}}\right) \Theta\left(a - \frac{r_{jk}}{\sigma_{jk}}\right) \tag{1.15}$$

$$V_c(i,j,k) = \varepsilon_{kij} h\left(\frac{r_{ki}}{\sigma_{ki}}\right), \left(\frac{r_{kj}}{\sigma_{kj}}, \theta_{kij}\right) \Theta\left(a - \frac{r_{ki}}{\sigma_{ki}}\right) \Theta\left(a - \frac{r_{kj}}{\sigma_{kj}}\right). \tag{1.16}$$

$$V_3(i,j,k) = V_a(i,j,k) + V_b(i,j,k) + V_c(i,j,k) \tag{1.17}$$

Here, $\Theta\ (\chi)$ is the Heaviside step function, θ_{ijk} is the angle between r_{ij} and r_{ik}. The energy parameters ε_{ijk} are set equal in a homogenous material but defines $\varepsilon_{\alpha\beta\gamma} = \sqrt{\varepsilon_{\alpha\beta}\varepsilon_{\beta\gamma}}$ in the case of a binary structure $((\alpha,\beta,\gamma) = 1,2)$. The function h is given by (1.18)

$$h\left(\frac{r_{ij}}{\sigma_{ij}}, \frac{r_{ik}}{\sigma_{ik}}, \theta_{ijk}\right) = \lambda_{ijk} exp\left(\mu\left[(\frac{r_{ij}}{\sigma_{ij}} - a)^{-1} + (\frac{r_{ik}}{\sigma_{ik}} - a)^{-1}\right]\right) \times \left(\cos\theta_{ijk} + \frac{1}{3}\right)^2 \tag{1.18}$$

where λ_{ijk} and μ are dimensionless parameters.

1.8 PROBLEMS TO SOLVE IN THIS THESIS

The study of clusters has become an increasingly interesting topic of research in both physics and chemistry in recent years, since they span the gap between the microscopic and macroscopic materials. The determination of structural and electronic properties and the growth pattern of coinage Aluminum clusters are of much interest both experimentally [124] and theoretically [28–32, 83].

In addition, there remain uncertainties about the thermal behavior of crystal structures, atomic configurations, cohesive energy and electronic structures for various intermediate phases. The authors of references [28], [30], [31], [32], [83] and [29] have used respectively the Murrell-Mottram potential, the Glue potential, the Gupta potential, the Sutton-Chen potential, the Truhlar potential and the Cleri-Rosato potential to determine the optimized configurations of Aluminum clusters. In the first five works mentioned previously, their optimized configurations and the corresponding energies are not in agreement with the experimental results. On the other hand, the configurations are obtained with good precision in the sixth work, but the energy levels have some errors. Therefore, these authors have not succeeded to determine the cohesive energy and the lattice parameter of the Aluminum crystal.

The first problem to solve in this thesis is to determine the parameters of the Gupta potential taking into account the cohesive energy and the lattice parameter of the Aluminum crystal. As such, Jasper et al. have used the Gupta potential in their work but the parameters of the potential was not well fitted [31].

The determination of the optimized configurations of Aluminum clusters and their fundamental energies will be the second problem to address. From these data, the cohesive energy of the Aluminum crystal can be deduced and the stable configurations are also determined.

Conclusion

Studies have shown that optimized clusters usually adopt one of the following four types of structures: Tetrahedral, Octahedral, Decahedral and Icosahedral. Atomic arrangement in clusters and their bulk material have shown that the addition of atoms to bulk materials have no effect though there is rearrangement of surface atoms whereas there is a drastic effect in the case of clusters. The melting point of clusters depend on their sizes, in addition, some clusters are extremely stable due to their completely filled electronic orbitals and they are called magic number clusters. Chemically, clusters are similar to atomic species in behavior and in electronic valencies thus giving them the name superatoms. The fact that clusters have provided a link between isolated atoms, molecules and the bulk material so as to make phase-transition studies very possible (just to name a few), have attracted many researchers to the field of clusters. Physically, clusters exist in the solid, liquid and gaseous states with very large ranges of temperature at phase-transition and isolated clusters do not conduct electricity even when sandwished between two metal slabs, except under high alternating electric forces and frequencies. Magnetically, clusters are similar to those of their bulk materials. In addition, Thermodynamic equilibrium and the dynamic properties of nonequilibrium systems can be analyzed using both the Monte Carlo and Molecular Dynamic simulation methods.

Chapter 2

MATERIAL AND METHODOLOGY

Introduction

In this chapter, we shall present the various steps involved in our calculation method. We shall begin by showing how the ground state electronic properties of the clusters were determined from the non relativistic Schrödinger equation, followed by showing the important part played by the Gupta potential for our system. In addition, the mathematical model of our system shall be presented together with other reasons for using the Gupta potential in this work. The verlet algorithm together with the initial conditions shall be used to further explain the global optimization method used for the cluster structures. Through the convergence criteria, we shall show how the multiple independent simulation can be used to check a single stable configuration and how the Basin hopping method is used to search the local minima, ensuring that the potential energy surface for a particular minima does not change. A flow chart for the verlet algorithm with multiple independent simulation methods shall be made, followed by showing all the symmetry elements involved in a given point group. Finally, all the materials used in this work shall be mentioned.

2.1 MODELING OF THE SYSTEM

2.1.1 Ground states determination

In this subsection, we are concerned with the ground state electronic properties of a finite isolated system of N_a atoms each containing N_e electrons. The coordinates of atoms and electrons are denoted respectively by $\overrightarrow{r}$ and $\overrightarrow{R}$. The non relativistic time independent Schrödinger equation for the system is described as

$$H\psi\left(\overrightarrow{r_1},\cdots,\overrightarrow{r_{N_a}},\overrightarrow{R_1},\cdots,\overrightarrow{R_{N_e}}\right)=E\psi\left(\overrightarrow{r_1},\cdots,\overrightarrow{r_{N_a}},\overrightarrow{R_1},\cdots,\overrightarrow{R_{N_e}}\right) \tag{2.1}$$

where E is the ground state energy and the operator hamiltonian H is defined as follows:

$$H = -\sum_{m=1}^{N_a} \frac{\hbar^2}{2M_a}\nabla_m^2 - \sum_{n=1}^{N_e} \frac{\hbar^2}{2m_e}\nabla_n^2 + \frac{1}{4\pi\varepsilon_0}\left[\sum_{n<\ell}^{N_a,N_a} \frac{e^2}{|\overrightarrow{r_n} - \overrightarrow{r_\ell}|} + \sum_{m<k}^{N_e,N_e} \frac{Z^2e^2}{\left|\overrightarrow{R_m} - \overrightarrow{R_k}\right|} - \sum_{n,m}^{N_a,N_e} \frac{Ze^2}{\left|\overrightarrow{r_n} - \overrightarrow{R_m}\right|}\right]. \tag{2.2}$$

The first and second terms of equation (2.2) represent the kinetic energies of nucleus and electron respectively. The third and fourth terms represent the nucleus-nucleus interaction and electron-electron interaction respectively while the fifth term represents the electron-nucleus interaction. Here, M_a and Z are mass and atomic number of the nucleus, the electron mass and charge are denoted by m_e and $-e$, and ε_0 is the vacuum permittivity. Equation (2.1) is obviously an insoluble problem without making approximations. The Born-Oppenheimer approximation makes it possible to compute the wavefunction in two less formidable, consecutive steps.

We can then consider electronic motion for fixed nuclei and factorize the total wavefunction as $\psi\left(\overrightarrow{r_1}, \cdots, \overrightarrow{r_{N_a}}, \overrightarrow{R_1}, \cdots, \overrightarrow{R_{N_e}}\right) = \Theta\left(\overrightarrow{R_1}, \cdots, \overrightarrow{R_{N_e}}\right)\Phi\left(\overrightarrow{r_1}, \cdots, \overrightarrow{r_{N_a}}, \overrightarrow{R_1}, \cdots, \overrightarrow{R_{N_e}}\right)$, where $\Theta\left(\overrightarrow{R_1}, \cdots, \overrightarrow{R_{N_e}}\right)$ describes the nuclei, and $\Phi\left(\overrightarrow{r_1}, \cdots, \overrightarrow{r_{N_a}}, \overrightarrow{R_1}, \cdots, \overrightarrow{R_{N_e}}\right)$ depends parametrically on R_i and describes the electrons. The problem then can be reformulated in terms of two separate Schrödinger equations:

$$H_{el}\Phi\left(\overrightarrow{r_1}, \cdots, \overrightarrow{r_{N_a}}, \overrightarrow{R_1}, \cdots, \overrightarrow{R_{N_e}}\right) = V\left(\overrightarrow{R_1}, \cdots, \overrightarrow{R_{N_e}}\right)\Phi\left(\overrightarrow{r_1}, \cdots, \overrightarrow{r_{N_a}}, \overrightarrow{R_1}, \cdots, \overrightarrow{R_{N_e}}\right). \tag{2.3}$$

$$H_i\Theta\left(\overrightarrow{R_1}, \cdots, \overrightarrow{R_{N_e}}\right) = E\Theta\left(\overrightarrow{R_1}, \cdots, \overrightarrow{R_{N_e}}\right). \tag{2.4}$$

where

$$H_{el} = -\sum_{n=1}^{N_e} \frac{\hbar^2}{2m_e}\nabla_n^2 + \frac{1}{4\pi\varepsilon_0}\left[\sum_{n<\ell}^{N_a,N_a} \frac{e^2}{|\overrightarrow{r_n} - \overrightarrow{r_\ell}|} + \sum_{m<k}^{N_e,N_e} \frac{Z^2e^2}{\left|\overrightarrow{R_m} - \overrightarrow{R_k}\right|} - \sum_{n,m}^{N_a,N_e} \frac{Ze^2}{\left|\overrightarrow{r_n} - \overrightarrow{R_m}\right|}\right] \tag{2.5}$$

and

$$H_i = -\sum_{m=1}^{N_a} \frac{\hbar^2}{2M_a}\nabla_m^2 + V\left(\overrightarrow{R_1}, \cdots, \overrightarrow{R_{N_e}}\right)$$

The equation (2.3) for the electronic problem gives the energy $V\left(\overrightarrow{R_1}, \cdots, \overrightarrow{R_{N_e}}\right)$ that depends parametrically on the coordinates of the nuclei, R_i. Once found, $V\left(\overrightarrow{R_1}, \cdots, \overrightarrow{R_{N_e}}\right)$ enters

equation (2.4) which describes the motion of nuclei. The later equation does not include any electronic degrees of freedom, all the electronic effects are incorporated in $V\left(\overrightarrow{R_1},\cdots,\overrightarrow{R_{N_e}}\right)$ that is called interatomic potential.

Hence, in Molecular Dynamics, we can use potential function $V\left(\overrightarrow{R_1},\cdots,\overrightarrow{R_{N_e}}\right)$ to describe interaction among atoms. But we know that in real materials the dynamics of atoms is controlled by the laws of quantum mechanics and the bonding is defined by the electrons that are not present in classical Molecular Dynamics.

2.1.2 System and potential

In order to use Molecular Dynamics we have to define the rules that are governing interaction of atoms in the system. In classical and semi-classical simulations these rules are often expressed in terms of potential functions. The potential function $V\left(\overrightarrow{r_1},\ \overrightarrow{r_2},\cdots,\overrightarrow{r_N}\right)$ describes how the potential energy of a system of N atoms depends on the coordinates of the atoms, $\overrightarrow{r_1},\ \overrightarrow{r_2},\cdots,\overrightarrow{r_N}$. It is assumed that the electrons adjust to new atomic positions much faster than the motion of the atomic nuclei.

In this work, we will use the many body Gupta potential. The Gupta potential, was originally proposed to study relaxation near surfaces and impurities in bulk transition metals [125]. The principal part of the many body Gupta potential rests on the tight binding model originally proposed by Ducastelle [16] and Friedel [17]. The main idea consists of constructing a functional within the second momentum approximation [18,19,126] which takes into account the essential band character of the metallic bond. The cohesive energy of the system depends on five parameters. It is written in terms of repulsive pair and attractive many body terms which are obtained by summing over all atoms. Its expression given in equation 2.6 results from the summation of the total bonding energy between N atoms.

$$V=\sum_{i=1}^{N}\left[\sum_{j>i}^{N}V_{ij}^{r}\left(r_{ij}\right)-\sqrt{\sum_{j>i}^{N}V_{ij}^{a}\left(r_{ij}\right)}\right], \tag{2.6}$$

with

$$V_{ij}^{r}=Ae^{-p\left(\frac{r_{ij}}{r_0}-1\right)}\ \text{ and }\ V_{ij}^{a}=B^2e^{-2q\left(\frac{r_{ij}}{r_0}-1\right)}. \tag{2.7}$$

A is the index to measure the interatomic repulsive strength and B is an effective jump integral only related to the type of atoms. p and q are adjustable parameters, V_{ij}^{r} and V_{ij}^{a} are respectively the repulsive potential and the attractive potential. r_0 is the equilibrium distance

between atoms and $r_{ij} = \|\overrightarrow{r_j} - \overrightarrow{r_i}\|$ represents the distance between the i^{th} and the j^{th} atoms. N is the total number of atoms with equal mass m.

2.1.3 Mathematical model of the system

In the molecular dynamics simulation methods the emphasis is on the motion of individual atoms within an assembly of N atoms, or molecules, that make up the nanostructure under study. The force acting on the i^{th} atom and due to the potential is given by the gradient of the potential energy (the force on atom i is a vector pointing in the direction of the steepest decent of the potential energy):

$$\overrightarrow{F_i} = -\overrightarrow{\nabla} V = \left[\frac{p}{r_0} \sum_{\substack{j=1 \\ j \neq i}}^{N} V_{ij}^{r}(r_{ij}) - \frac{q}{r_0} \frac{1}{\sqrt{\sum_{\substack{j=1 \\ j \neq i}}^{N} V_{ij}^{a}(r_{ij})}} \sum_{\substack{j=1 \\ j \neq i}}^{N} V_{ij}^{a}(r_{ij}) \right] \frac{\overrightarrow{r_{ij}}}{r_{ij}}. \tag{2.8}$$

By applying the second law of Newton to the i^{th} atom , the equations of motion take the form given as

$$m\frac{d^2\overrightarrow{r_i}}{dt^2} + \lambda\frac{d\overrightarrow{r_i}}{dt} + \left[\frac{p}{r_0} \sum_{\substack{j=1 \\ j \neq i}}^{N} V_{ij}^{r}(r_{ij}) - \frac{q}{r_0} \frac{1}{\sqrt{\sum_{\substack{j=1 \\ j \neq i}}^{N} V_{ij}^{a}(r_{ij})}} \sum_{\substack{j=1 \\ j \neq i}}^{N} V_{ij}^{a}(r_{ij}) \right] \frac{\overrightarrow{r_{ij}}}{r_{ij}} = \overrightarrow{0}, \tag{2.9}$$

where λ is the damping coefficient and $i = 1, \cdots, N$.

However, all the quantities in molecular dynamics simulations are very small. It is therefore usual to introduce measurement units that are adapted to the task. This means that we measure lengths in units of r_0 and time in units of $\frac{1}{\omega_0}$. Hence, to conveniently describe the system, the dimensionless equations of the system are established using the transformations $\tau = \omega_0 t$ and $\overrightarrow{r_i} = r_0\overrightarrow{R_i}$ $(i = 1, \cdots, N)$, where τ and $\overrightarrow{R_i}$ are dimensionless variables. Let us introduce these new variables inside equations (2.9), after some mathematical manipulations; the mathematical model of the system is given as

$$\frac{d^2\overrightarrow{R_i}}{dt^2}+\beta\frac{d\overrightarrow{R_i}}{dt}+\left[p_0\sum_{\substack{j=1\\j\neq i}}^{N}U_{ij}^{r}\left(R_{ij}\right)-\frac{q_0}{\sqrt{\sum_{\substack{j=1\\j\neq i}}^{N}U_{ij}^{a}\left(R_{ij}\right)}}\sum_{\substack{j=1\\j\neq i}}^{N}U_{ij}^{a}\left(R_{ij}\right)\right]\frac{\overrightarrow{R_{ij}}}{R_{ij}}=\overrightarrow{0}. \tag{2.10}$$

with $i=1,\cdots,N$. The new introduced parameters and functions are defined as follows:

$$\beta=\frac{\lambda}{m\omega_0},\ \ p_0=\frac{p}{m\omega_0^2r_0^2},\ \ q_0=\frac{q}{m\omega_0^2r_0^2},\ U_{ij}^{r}=Ae^{-p(R_{ij}-1)}\ \text{ and }\ U_{ij}^{a}=B^2e^{-2q(R_{ij}-1)}. \tag{2.11}$$

2.1.4 Reasons for using the Gupta potential

Accurately simulating atoms for metal materials, using molecular dynamics technique, entirely depends on the choice of the empirical potentials. Generally, the pair potentials such as Lennard-Jones potential, Morse potential are unable to describe metals due to their many-body effects in metallic cohesion, that is, the interaction strength per bond decreases with increasing number of neighboring atoms [127]. It is based on this consideration that, in the 1980s, a variety of empirical many-body potentials, such as the tight-binding (TB) potential by Gupta [125] and Cleri and Rosato [122], Embedded Atom Method (EAM) potential by Daw and Baskes [128], Finnis-Sinclair potential [129], Glue potential by Ercolessi et al. [130], were independently developed and today, they are successfully applied to metals and alloys of face-centered cubic (fcc), body-centered cubic (bcc) and hexagonal close packed (hcp) phases, respectively. Among these potentials, the Gupta potential has distinguished itself due to its simplest form as well as fewest parameters. Many body potentials do have environmental dependence for example atom in the bulk is not similar to the atom on the surface or near a defect site.

In reality, the strength of the individual bonds should decrease as the local environment becomes too crowded as mentioned by the Pauli's principle, but since many body potentials do depend on the environment, it can account for this decrease. Furthermore, many body potentials do account for directional nature of the bond and so, the covalent contributions, of the transition metals can be described. Originally, Gupta potential was developed to calculate the surface relaxation of fcc transition metals and only included the first nearest neighboring atoms [125]. From this basis, Cleri and Rosato [122] interpreted the Gupta potential form in terms of the second-moment approximation of TB theory and fitted a series of potential parameters for those common in fcc and hcp transition metals (Ni, Cu, Rh, Ti, Zr, Co, etc)

that can successfully reproduce the fundamental properties such as elastic moduli and melting points. Nowadays, the Gupta potential has been parameterized for wide atomistic simulations of clusters, liquids, surfaces and alloys of different transition metals [131–135].

2.2 GLOBAL OPTIMIZATION METHOD

In molecular dynamics, the most commonly used time integration algorithm is probably the so-called Verlet algorithm [136]. The basic idea is to assume that the positions, velocities and accelerations can be approximated by a Taylor series expansion.

2.2.1 Verlet algorithm

The algorithm was rediscovered by Verlet in 1960's for molecular dynamics simulations after Delambre in 1791. It was also used by Cowell and Crommelin in 1909 to compute the orbit of Halleys comet and by Störmer in 1907 to study the motion of electrical particles in a magnetic field [137]. To simplify our analysis, we assume that the model of the system is given by the following equation:

$$\frac{d^2\overrightarrow{R_i}}{d\tau^2} = \overrightarrow{a_i}(\tau), \quad i = 1, \cdots, N. \tag{2.12}$$

The $3N$ coupled differential equations of motion can then be solved by a variety of numerical finite-difference techniques, one of which is the velocity Verlet algorithm, according to which the positions, $\overrightarrow{R_i}$, and velocities, $\overrightarrow{\mathcal{V}_i}$, of the particles are updated at each time step, h, by

$$\overrightarrow{R_i}(\tau + h) = \overrightarrow{R_i}(\tau) + h\overrightarrow{\mathcal{V}_i}(\tau) + \frac{1}{2}h^2\overrightarrow{a_i}(\tau), \quad i = 1, \cdots, N. \tag{2.13}$$

$$\overrightarrow{\mathcal{V}_i}(\tau + h) = \overrightarrow{\mathcal{V}_i}(\tau) + h\overrightarrow{a_i}(\tau), \quad i = 1, \cdots, N. \tag{2.14}$$

As we can immediately see, the truncation error of the algorithm when evolving the system by h is of the order of h^4, even if third derivatives do not appear explicitly. This algorithm is at the same time simple to implement, accurate and stable, explaining its large popularity among molecular dynamics simulators.

2.2.2 Assigning initial conditions

Molecular dynamics simulation starts from an initial configuration of atoms and determines the trajectories of all the atoms. The initial condition for such a simulation consists of all the positions, $\overrightarrow{R_i}(0)$ and velocities $\overrightarrow{\mathcal{V}_i}(0)$ at the initial time. In order to model a realistic system, it is important to choose the initial configuration with some care.

In particular, since most potentials such as the Gupta potential increase very rapidly as the interatomic distance R_{ij} goes to zero, it is important not to place the atoms too close to each other. We therefore often place the atoms regularly in space, on a lattice, with initial random velocities. We generate a lattice by first constructing a unit cell and then copying this unit cell to each position of a lattice to form a regular pattern of unit cells. In this work, we have used cubic and hexagonal unit cells of length r_0.

2.3 CONVERGENCE CRITERIA

Convergence to equilibrium is an essential requirement for molecular simulation output to be accurate and reproducible. In the absence of any general technique for a prior prediction of run lengths, it is necessary to carry out some form of statistical analysis in order to assess convergence. These procedures, which are called convergence diagnostics, fall into two general categories: those based solely on the output values (positions, velocities and energy) of the simulation, and those that also use additional information about the target density. The methods described in this work are the entire first category.

2.3.1 Multiple independent simulations

In this work, we have used a quantitative method for monitoring convergence based on multiple independent simulations starting from four different initial configurations [138]. For illustration, an example is shown in Figure 2.1 where the energies of a certain system starting from four different initial configurations are sketched.

In this particular case, the system converges to one stable configuration as all the curves have approximately the same value for a sufficient long time.

We quantify the distance between the independent cluster population vectors using the distance $\delta(t)$ defined as:

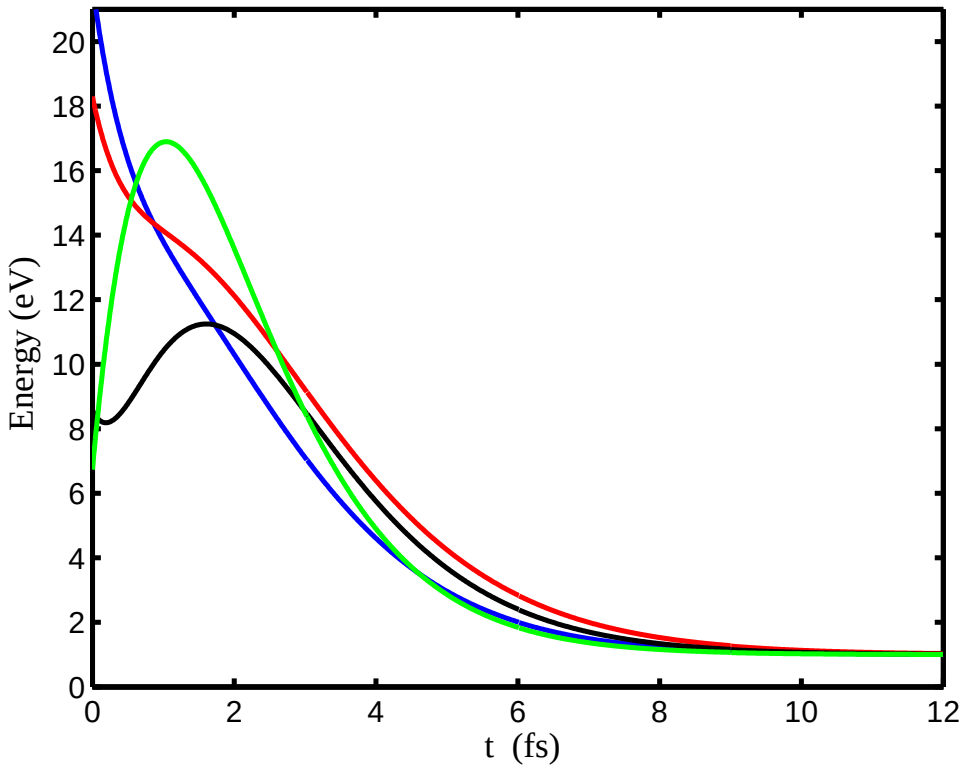

Figure 2.1: The energies of a certain system according to four different initial configurations.

$$\delta(t) = \frac{1}{2} \max_j \left(\sum_{i=1}^{N} \left\| R_{ij}(t) - \overline{R_i(t)} \right\| \right), \tag{2.15}$$

where $R_{ij}(t)$ is the position of the i$^{\text{th}}$ particle of the j$^{\text{th}}$ simulation at time t, $\overline{R_i(t)} = \frac{1}{4} \sum_{j=1}^{4} R_{ij}(t)$, and N is the number of atoms. This distance is computed against time and the system considered equilibrated when it decreases below a pre-chosen threshold and remains below. A 10^{-2} threshold has been used in this thesis.

2.3.2 Basin-hopping method

In applied mathematics, Basin-hopping is a global optimization technique that iterates by performing random perturbation of coordinates, performing local optimization, and accepting or rejecting new coordinates based on a minimized function value. The algorithm was described in 1997 by David J. Wales and Jonathan Doye [139]. It is a particularly useful algorithm for global optimization in very high-dimensional landscapes, such as finding the minimum energy structure for molecules.

The basic idea of the method rests on monitoring an initial Potential Energy Surface (PES) $V(r_{ij})$ of N atoms which is transformed so that the resulting PES does not change the global minimum or the relative energies of local minima [139, 140]. In other words, the PES of $V(r_{ij})$ is deformed into a multidimensional staircase topography $\widetilde{V}(r_{ij})$ given by equation (2.16),

$$\widetilde{V}(r_{ij}) = \min\left[V(r_{ij})\right], \tag{2.16}$$

where the $\min(\cdot)$ represents a local energy minimization starting from the coordinates $\overrightarrow{r_i}$ of N atoms. For illustration, an example of the energy of the original surface and its corresponding transformed energy are shown in Figure 2.2.

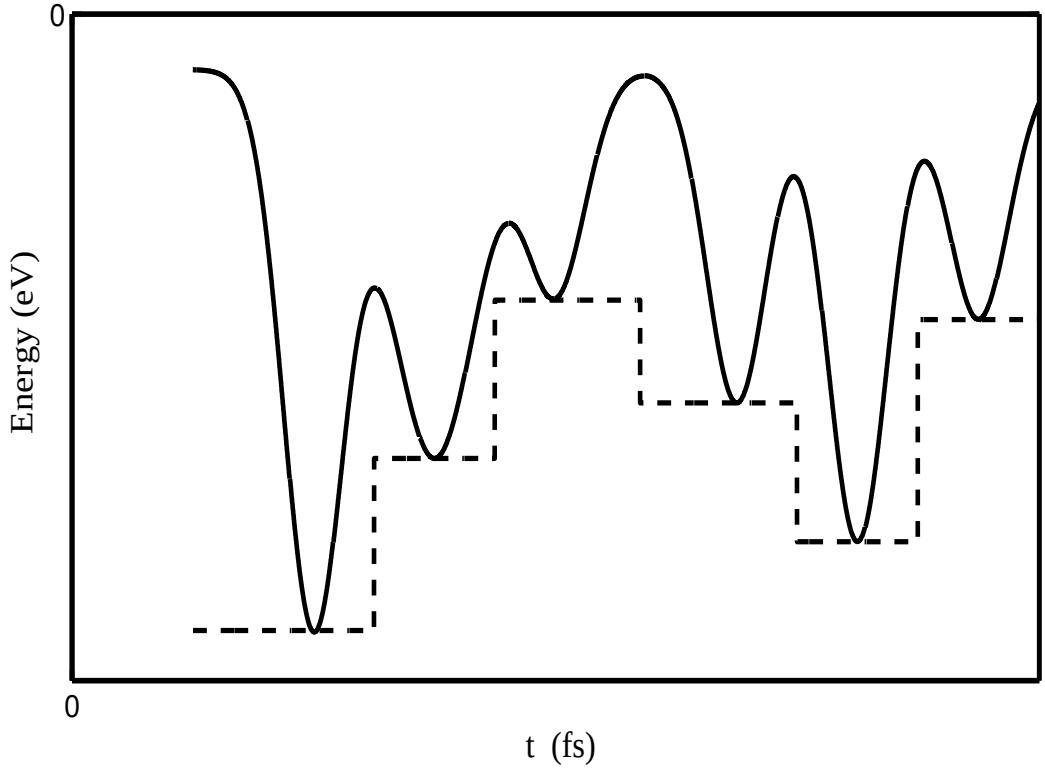

Figure 2.2: A schematic diagram illustrating the effects of our energy transformation for a one-dimensional example. The solid line is the energy of the original surface and the dashed line is the transformed energy $\widetilde{V}$.

Technically the numerical procedure runs as follows: For a cluster of N atoms, we randomly generate an atomic configuration that is confined inside a sphere of radius R_d defined as follows:

$$R_d = r_0\left(1 + \sqrt[3]{\frac{3N}{4\pi\sqrt{2}}}\right), \tag{2.17}$$

where r_0 represents the nearest-neighbor distance, whose origin is located at the center-of-mass of the cluster. The confinement of N atoms within R_d is done to prevent the whole cluster from evaporating.

It is next identified with precision (pinpoint) that particular atom whose location r_{max} from the origin is farthest compared with others. Given the configuration of a cluster, the potential energy is calculated using (2.16).

Some technical points on the method include:

1) Angular move and random displacement

Given the configuration of an N-atoms cluster, the local minimum is determined as follows, the angular moves and random displacements to the n-atoms cluster is applied. This process is called a step. For an additive potential, it is easy to write down the energy as in equation (2.18),

$$E = \frac{1}{2}\sum_{i=1}^{N} V(i). \tag{2.18}$$

$V(i)$ refers to the potential of the i^{th} atom due to its interaction with all the other atoms at (R_i). Among the $V(i)$, $i = 1, \cdots, N$ the two particles with the lowest, V_ℓ, and the highest, V_h, energies are sorted out. If $V_h > \nu V_\ell$, where the constant ν satisfies $0 < \nu < 1$, the V_h atom is moved to the surface of $R_{\max}$ and displaces all others by a random number δ that lies in the range $0 < \delta < 1$.

2) Seeding

To reduce computing time, the existing set of coordinates for the initial configuration is used. This procedure is applied in parallel with a randomly generated configuration (no seeding) to check the reliability of the calculated results.

3) Limited BFGS algorithm

This is one of the variable metric methods and it is an efficient approach in searching the local minimum [141]. The basic idea lies in the usual Monte Carlo moves where the root-mean-square gradient is applied to determine how far the moves are to be accepted during the iterations of the L-BFGS. Initially the convergence criterion needs not be very tight, thus saving a lot of computing time. In the final stage the L-BFGS is carried out again now using a tightly convergence criterion.

4) Quenching

Based on Markov's process, the Monte Carlo simulation starts by going downhill, which leads to a local but not necessarily a global minimum. Statistically the system must obey

a Boltzmann probability distribution $P(E)$ in thermal equilibrium at temperature T for all different energy states E that satisfies equation (2.19)

$$P\left(E\right) \simeq \exp\left(-\frac{\Delta E}{KT}\right). \tag{2.19}$$

Although the original Monte Carlo method is used at a constant Temperature, in the basin hopping method the temperature may still increase or decrease in the course of taking steps. For example, supposing $\Delta E > 0$ which only happens when the search for the energy landscape is difficult, the temperature may be varied to find the range of energy states so that the later difficulty can be resolved. In general, after a few intervals of steps, the temperature is lowered slowly, which corresponds to narrowing the range of energy states.

2.3.3 Flow-chart of the code used in this work

We show in Figure 2.3 the flow chart of our energy optimization procedure for the genetic algorithm strategy. Technically, the genetic algorithm is a search procedure inspired by the Darwinian evolution process. Numerically it is an iterative, algorithm maintaining a population of atoms. Each individual atom in the system consists of three unknown variables (position) in the Cartesian coordinates.

The potential is computed using the set of equations (2.2) and (2.3). In the other hand, the force, the positions and the velocities are computed using the equations (2.8), (2.13) and (2.14) respectively. The distance δ between clusters is evaluated according to equation (2.15).

2.4 POINT GROUPS DETERMINATION

2.4.1 Definition

Each molecule has at least one point which is unique and which remains unchanged, no matter how many or what type of symmetry operations are performed. Such point is termed singular point. The number and nature of the symmetry elements of a given molecule are conveniently denoted by its point group. These point groups belong to the classes of C groups, D groups and special groups, the latter containing groups that possess special symmetries, that is, tetrahedral (T_d), octahedral (O_h) and icosahedral (I_h) [142]. The complete set of symmetry operations that characterize a molecule's overall symmetry is known as the Point group (PG).

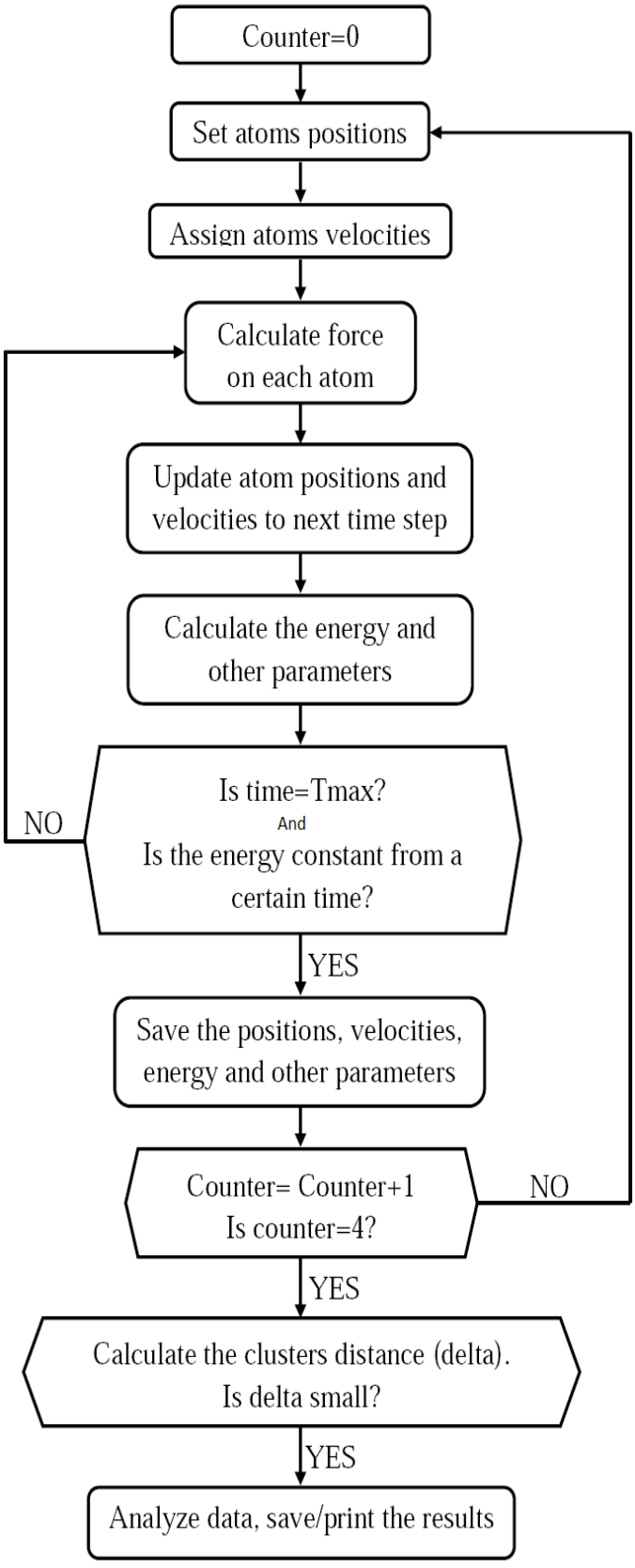

Figure 2.3: Flow chart for the Verlet algorithm combined with the multiple independent simulations method.

2.4.2 Point groups

To determine the point group of a certain molecule or cluster, we have to identify all its symmetry elements. Below are the most important classes of point groups, involving their characteristics type of symmetry elements.

PG	**Symmetry elements**
C_s	One symmetry plane or mirror
C_i	One inversion center
C_n	One C_n axis
C_{nv}	One C_n axis and $n\sigma_v$ planes
C_{nh}	One C_n axis, one σ_h plane, one $S_n \equiv C_n$ axis
D_{nh}	One C_n axis, nC_2 axes, one σ_h plane, $n\sigma_v$ planes, one S_n-fold axis
D_{nd}	One C_n axis, nC_2 axes, $n\sigma_v$ planes, one S_{2n}-fold axis
T_d	$8C_3$ axes, $3C_2$ axes, $6S_4$ axes and $6\sigma_d$
T	$4C_3$ axes, $4C_3^2$ axes and $3C_2$ axes
T_h	$4C_3$ axes, $4C_3^2$ axes, $3C_2$ axes, i, $4S_6$, $4S_6^5$ axes and $3\sigma_h$
O_h	$8C_3$ axes, $6C_2$ axes, $6C_4$ axes, $3C_2$ axes, i, $6S_4$, $8S_6$, $3\sigma_h$ and $6\sigma_d$
O	$8C_3$ axes, $6C_2$ axes, $6C_4$ axes and $3C_2$ axes
I_h	$12C_5$ axes, $12C_5^2$ axes, $20C_3$ axes, $15C_2$ axes, i, $12S_{10}$, $12S_{10}^3$, $20S_6$ and 15σ
I	$12C_5$ axes, $12C_5^2$ axes, $20C_3$ axes and $15C_2$ axes

Table 2.1: Different Point groups and their corresponding symmetry elements.

2.5 SOFTWARES USED

For the realization of this thesis, we have used four fundamental softwares, and each for a precise task. For writing the codes and their compilation, FORTRAN 90 (FORmula TRANslator) software was used. It is a general-purpose, compiled imperative programming language that is especially suited to numeric computation and scientific computing. MATLAB (MAtrix LABoratory) software has been used to plot the graphs. For the visualization of the clusters, we chose RASTOP and for the determination of the point groups, we have used CHEMCRAFT software.

2.5.1 Some important features involved in Fortran 90 (formula translator) software that were used when writting this code and to compile

To set the project, we opened the Project Settings dialog box Figure 2.4 from where the project workspace was opened and in the project menu, we clicked on setting. The Fortran tab of the dialog box will presented options grouped under different categories. We then selected the category from the Category drop-down list:

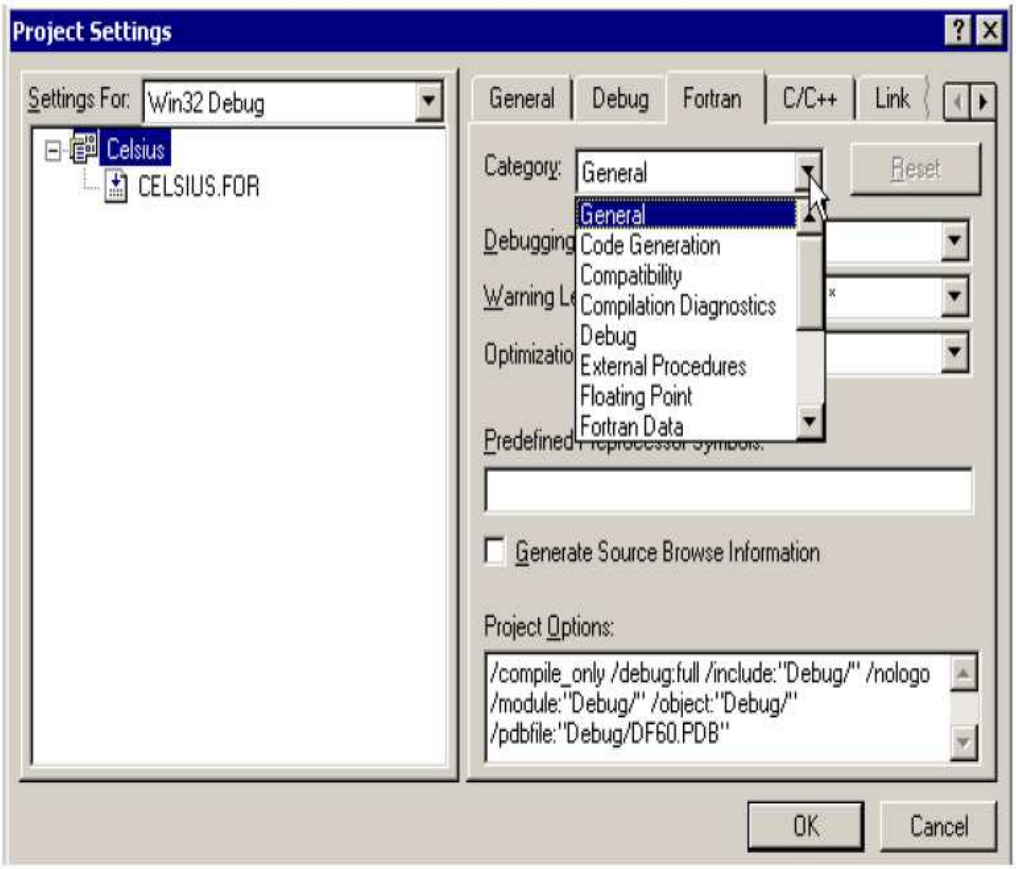

Figure 2.4: Project settings dialog box [143].

To save the project settings Fortran environment Figure 2.5, we opened to the appropriate workspace and modified the Project Settings dialog box as needed. If the actual file names for output is specified, then we use the default file naming conventions. In the File menu, we clicked Save Fortran Environment or clicked the green tree on the Fortran toolbar. A window resembling the following dialog box appeared.

The Tool Combo box allowed us to view the project settings for either the Fortran or the

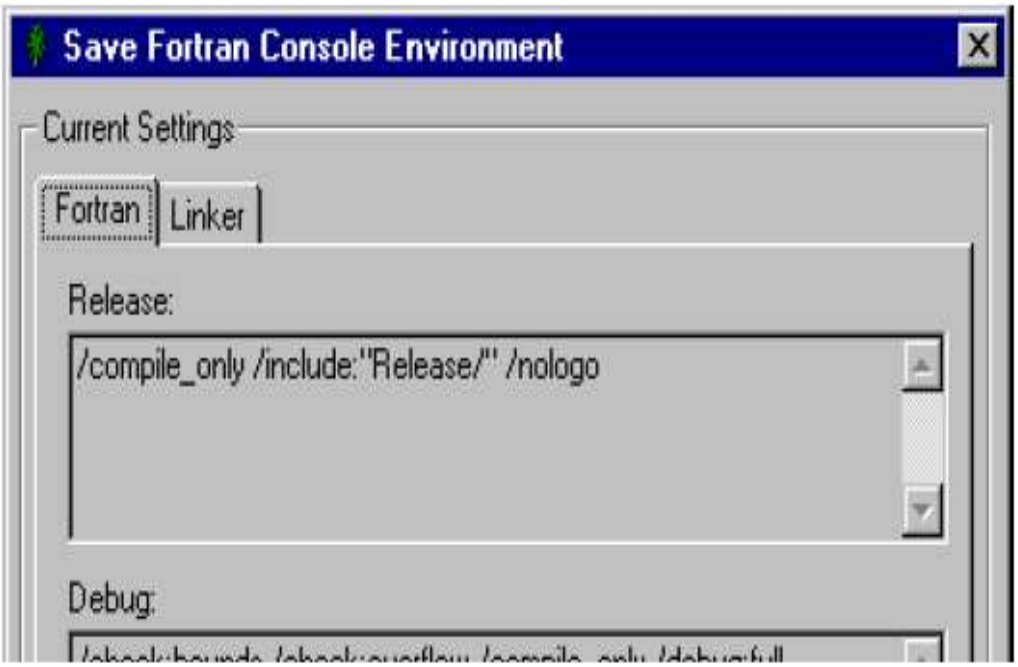

Figure 2.5: Project Settings Environment [143].

displayed tools (such as Linker). The Release and Debug configuration values are displayed for the selected tab. It is then verified if the displayed values are acceptable. The edit box titled Saved Fortran Console Environment allowed us to specify the name of the environment to be saved. And finally, a click on the save settings button saved the settings as a project settings environment.

To use an existing Fortran environment when creating a new project Figure 2.6, If the Fortran environment exists for the specified new Fortran project type, you will be asked whether you want to apply project settings options from a saved Fortran environment. If you click Yes, a window resembling the following dialog box will appear.

For the selected Fortran project type, a list of saved Fortran environments appears Figure 2.7. The Fortran environment is then selected. The selected environment is verified to be correct by viewing the Project Settings options. After selecting the appropriate Fortran environment for the Fortran project being created, we clicked to the Apply button to use the saved settings for the new project. Other tasks associated with creating a new project, such as adding source files, and so on is completed. To manage saved Fortran environments, in the Tools menu, we clicked on Managed Saved Fortran Environment or clicked the saw on the Fortran toolbar. A dialog box resembling the following appears.

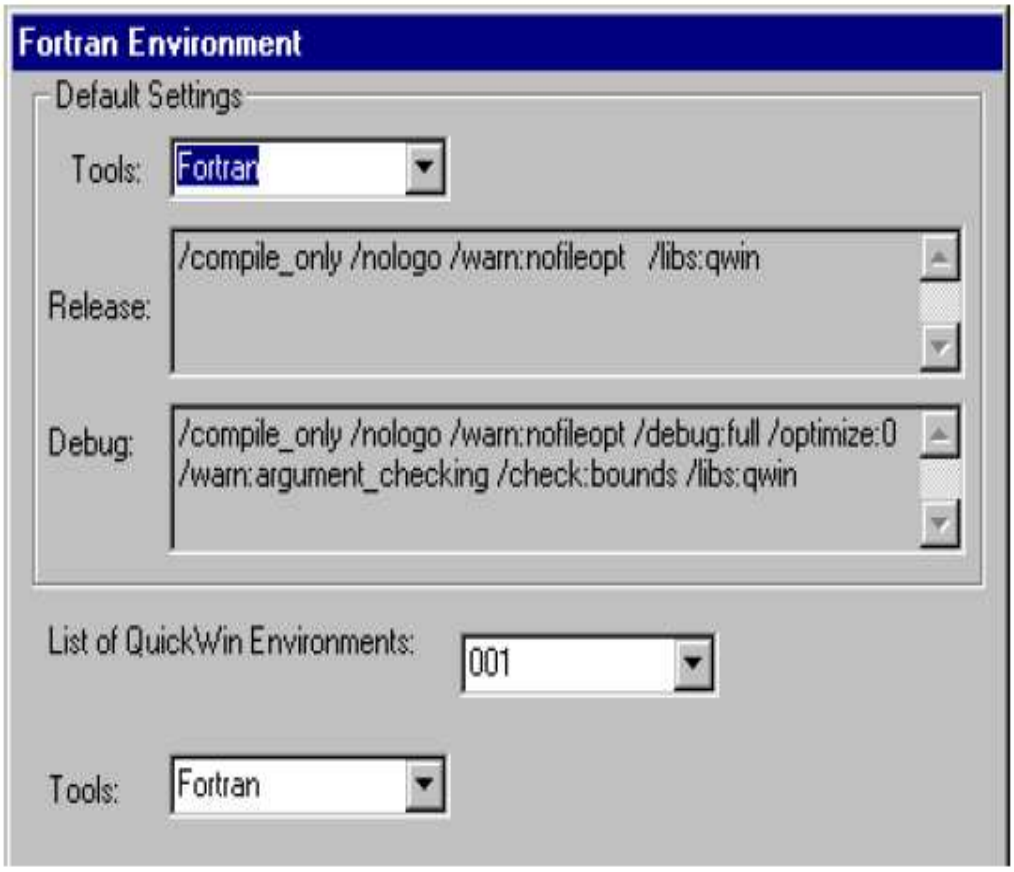

Figure 2.6: An Existing Fortran Project Settings Environment [143].

Initially, this dialog box displays the project types for which there are saved Fortran environments. We then double-click on the project type name to view the saved Fortran environments for that project type. This dialog box allows one to display the Fortran environments associated with each project type. to display the Fortran environments associated with that project type, double-click the name of a project type .

To display the project settings for a Fortran environment, we Click the name of a Fortran environment and View the project settings for the Fortran tab. Followed by Clicking other tool tab (such as Linker) and viewing the tool's project settings and If needed, we click (select) a different Fortran environment.

To determine whether a duplicates exist for a Fortran environment, we Click (select) the name of an environment or a project type and Click the Display Environments with Duplicate Settings button. If the Fortran environments have different project settings, No Duplicates Found is displayed. But if the Fortran environments have identical project settings, the duplicate environments are displayed.

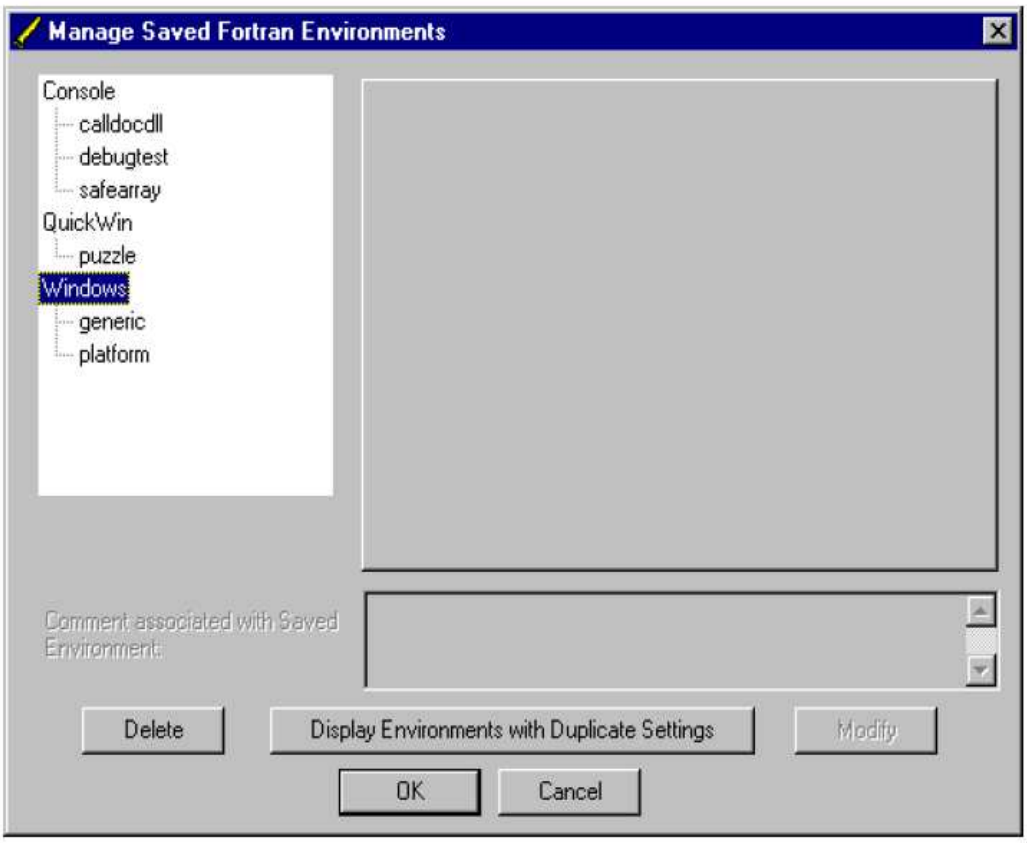

Figure 2.7: Saved Fortran Project Settings Environments [143].

To delete a Fortran environment, we Click (select) the name of an environment or the project type followed by Clicking the Delete button and finally Click OK to the delete confirmation box.

To set the browse option for the current configuration in the visual development environment, in the Project menu, we click on Settings. In the General category of the Fortran tab, we set the Generate Source Browse Information check box. Then Click the Browse Info tab and set the Build Browse info check box. We Click OK and Build our application. In the Tools menu, we click Source Browser and near the bottom on the Browse window, we locate the Case sensitive check box. Since Fortran is a case-insensitive language, we make sure the Case sensitive check box is clicked off. When we are done using the Browse window, we click OK. The Browse window allows us to view graphs of calling relationships between functions and view the symbols contained within the file, inother to perform other functions.

For the setting of projects Figure 2.8, If aiming at using the compiler and linker from the Microsoft visual development environment, we select the options needed by using the various

tabs in the Project menu Settings item.

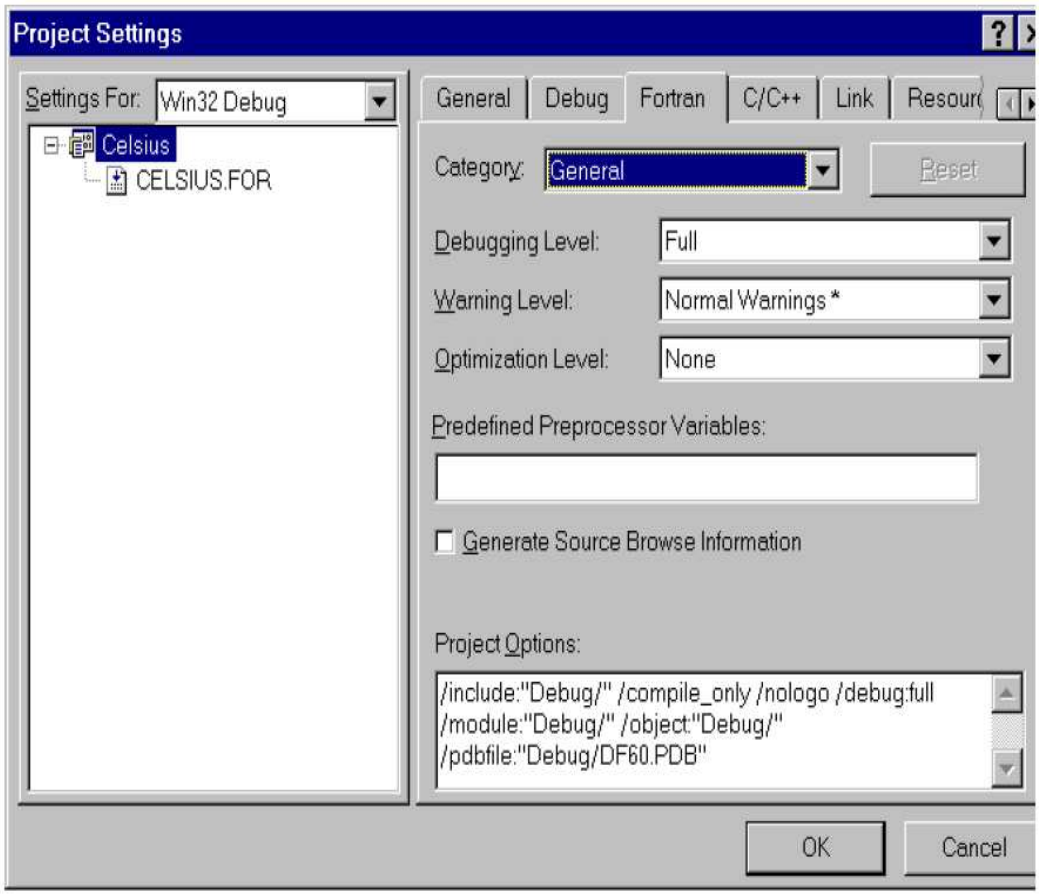

Figure 2.8: Project Settings, Fortran Tab [143].

The options are grouped under functional categories (the initial Category is General, as shown) to help locate the options needed for our application. From the Fortran tab, one can select one of the following categories from the Category drop-down list.

To prepare the program for debugging Figure 2.9, we start the visual development environment (click Developer Studio in the Compaq Visual Fortran program folder). And Open the appropriate Workspace (File menu, either Open Workspaces or Recent Workspaces). Click the FileView pane. To edit the source file to be debugged, we double-click on the file name and Click the Project name. The screen might appear as follows (the ClassView tab only appears if Visual C++ is also installed)

In the Build menu, we click Set Active Configuration and select the debug configuration. To check the project settings for compiling and linking, in the Project menu, we click Settings, then click the Fortran tab. Similarly, to check the debug options set for our program (such as program arguments or working directory), we click the Debug tab in the Project Settings

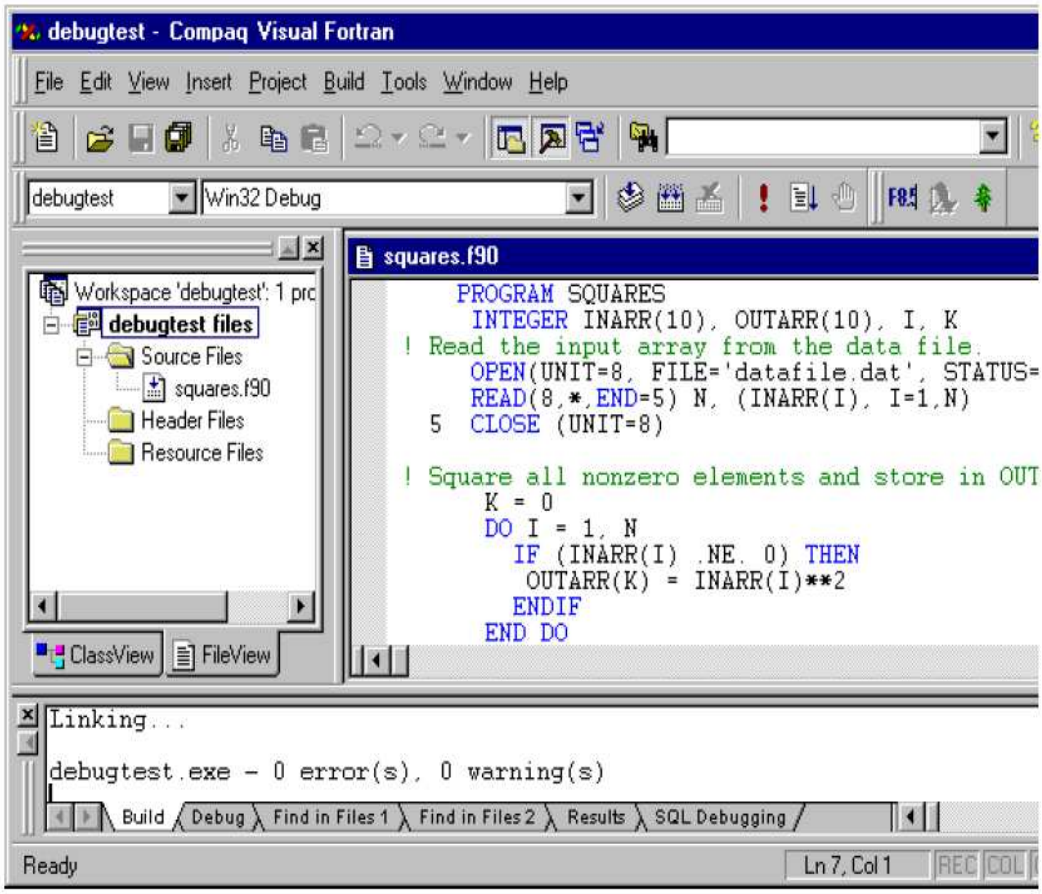

Figure 2.9: Debugging Fortran Programs [143].

dialog box.

To compile the program, we select the source file to be compiled and in the Build menu, we click Compile filename. One can eliminate any compiler diagnostic messages in the text editor and recompile if needed. To build our application, in the Build menu, we click Build file.EXE. Set breakpoints in the source file and debug the program.

To creat a Fortran COM Server Project Figure 2.10, The first step is to create a new project. We Start Developer Studio. In File menu, we click New. In the New Projects dialog box, we select (click) the Fortran COM Server project type, as shown below (if Microsoft Visual C++ is installed on your system, additional project types will appear).

We enter 'Adder' as the name of the project and accept or modify the project folder location. We click the OK button. (If you click Back, the previous screen appears, allowing you to change the name, location, or project type of the project being created). To define the initial attributes of the Fortran COM server project being created, additional information is requested. The following screen shows the Fortran COM Server AppWizard Figure 2.11. One can use the

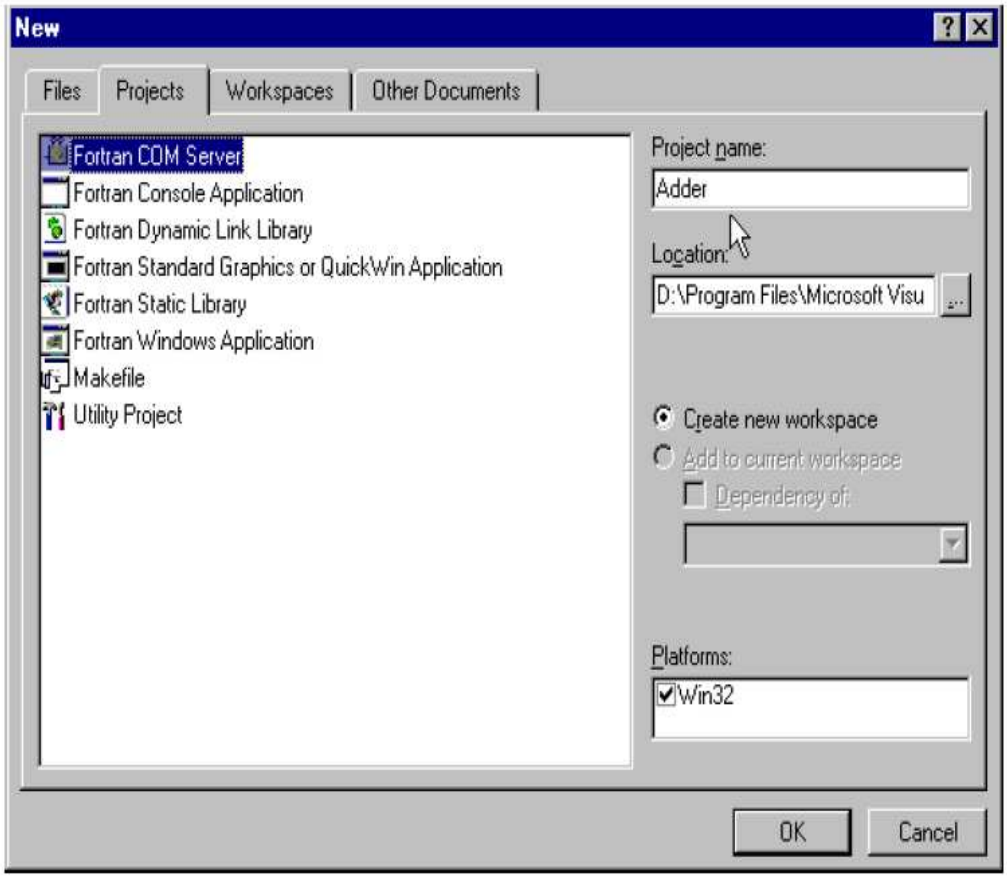

Figure 2.10: Creating a Fortran COM Server Project [143].

project AppWizard once per project to create the project files and skeleton template (as with other project types).

To Accept the default server type (DLL). Type the class name AddingMachine. Default text appears for the default interface name and class derived type name. To shorten the default interface name to IAdd and accept the default class derived type name, we Click the Finish button. (If you click Cancel, project creation is terminated). A summary screen appears Figure 2.12that summarizes the location and template information created for this project.

When we then click OK, the project is created and the Fortran COM Server Wizard appears.

2.5.2 Some important features when using Matlab (Matrix Laboratory) software that was used to plot the graphs in this work

To start MATLAB, the desktop appears with the default layout Figure 2.13, as shown in the figure below. The MATLAB desktop consists of the following parts, Command Window used to run MATLAB statements, Current Directory used to view, open, search for, and make

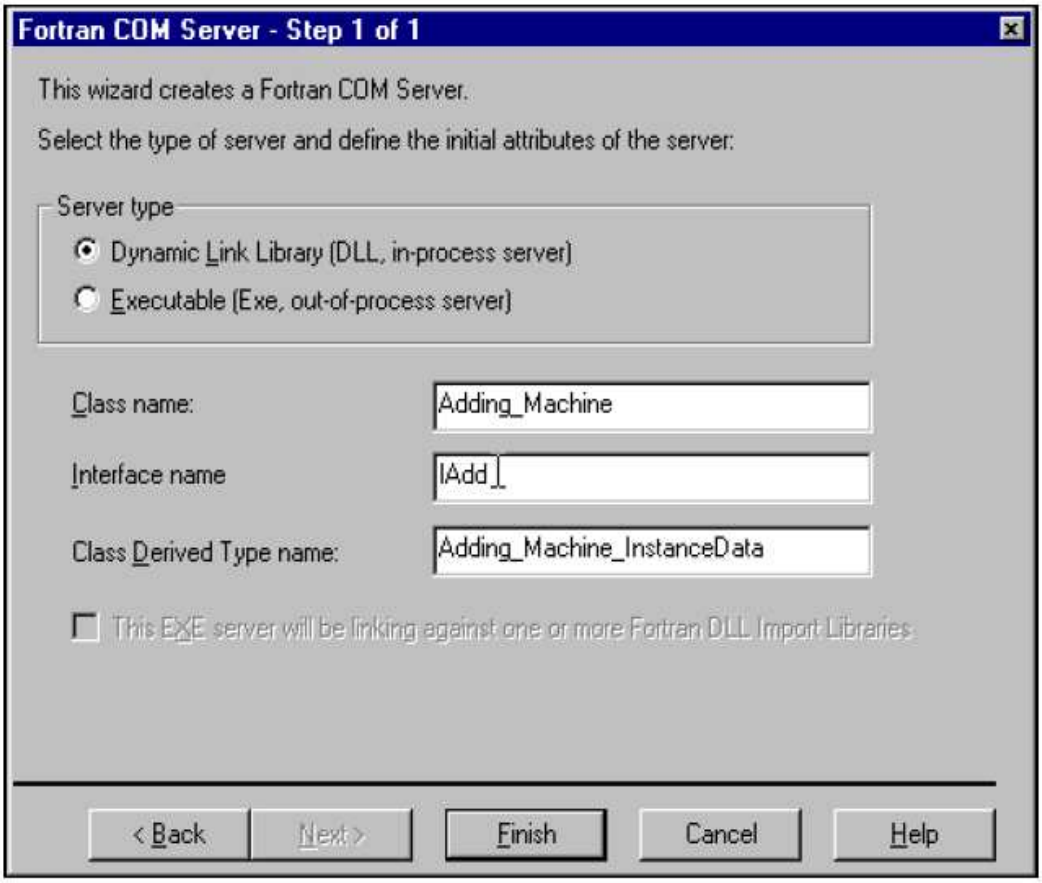

Figure 2.11: Fortran COM Server AppWizard [143].

changes to MATLAB related directories and files, Command History is used to display a log of the functions we have entered in the Command Window. One can copy them, execute them, and more Workspace which Shows the name of each variable, its value, and the Min and Max entry if the variable is a matrix.

In case where the desktop does not appear with the default layout, one can change it from the menu Desktop → Desktop Layout → Default.

The MATLAB editor can be used to create and edit M files, in which you can write and save MATLAB programs. An m-file can take the form of a script file or a function. A script file contains a sequence of MATLAB statements; the statements contained in a script file can be run in the specified order, in the MATLAB command window simply by typing the name of the file at the command prompt. M files are very useful when we use a sequence of commands over and over again, in many different MATLAB sessions and we will not want to manually type these commands at the command prompt every time we want to use them.

We can run a script, or a function that does not require an input argument, directly from

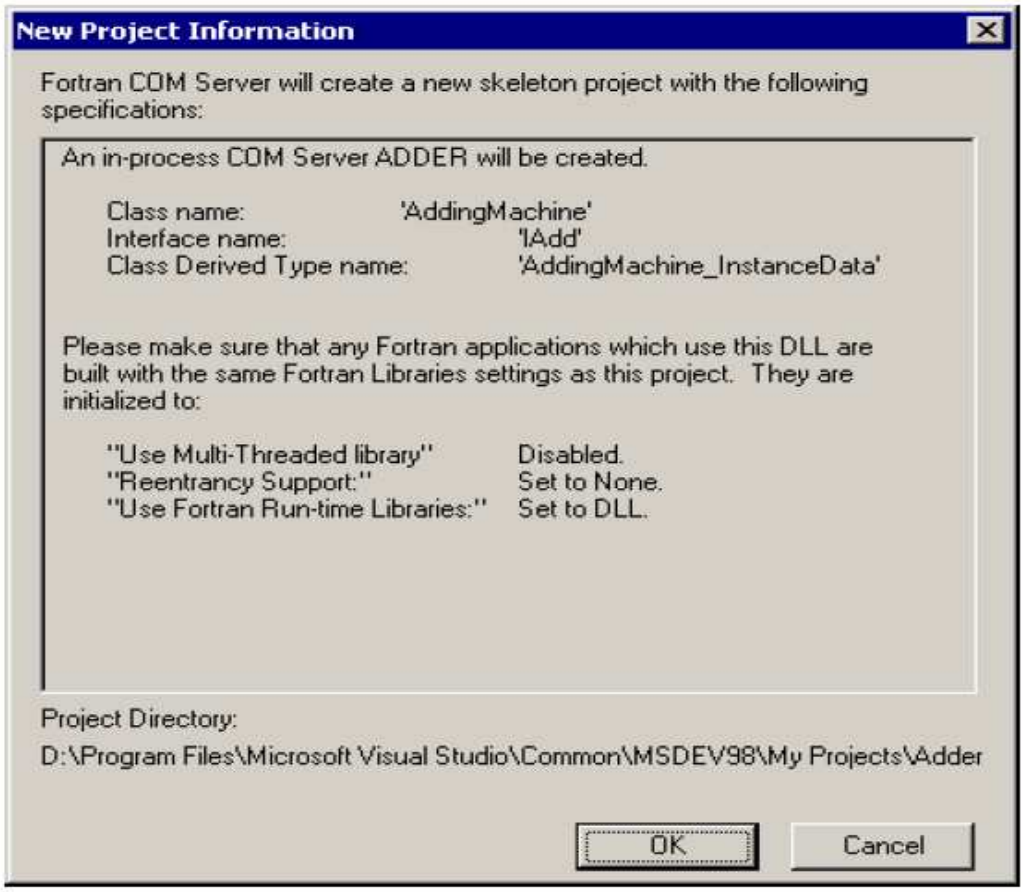

Figure 2.12: Creating a COM Server [143].

the Editor/Debugger Figure 2.14either by pressing F5 or selecting Save File and Run from the Debug menu. If we only want to run a part of a script, we can use the mouse to highlight the corresponding lines in the m-file and press F9. The results are shown in Command Window.

MATLAB has an extensive built-in help system, which contains detailed documentation for all of the commands and functions of MATLAB . There are different ways of asking for help when using MATLAB Command Line. HELP FUN displays a description of and syntax for the function FUN in the Command Window (e.g., help plot), DOC FUN displays the help browser for the MATLAB function FUN (e.g. doc help).

We can invoke the MATLAB help browser by typing "helpbrowser" at the MATLAB command prompt, clicking on the help button, or by selecting Start → MATLAB → Help from the MATLAB desktop.

To plot the graph of a function, we need to take the following steps:

• Define x, by specifying the range of values for the variable x, for which the function is to be plotted,

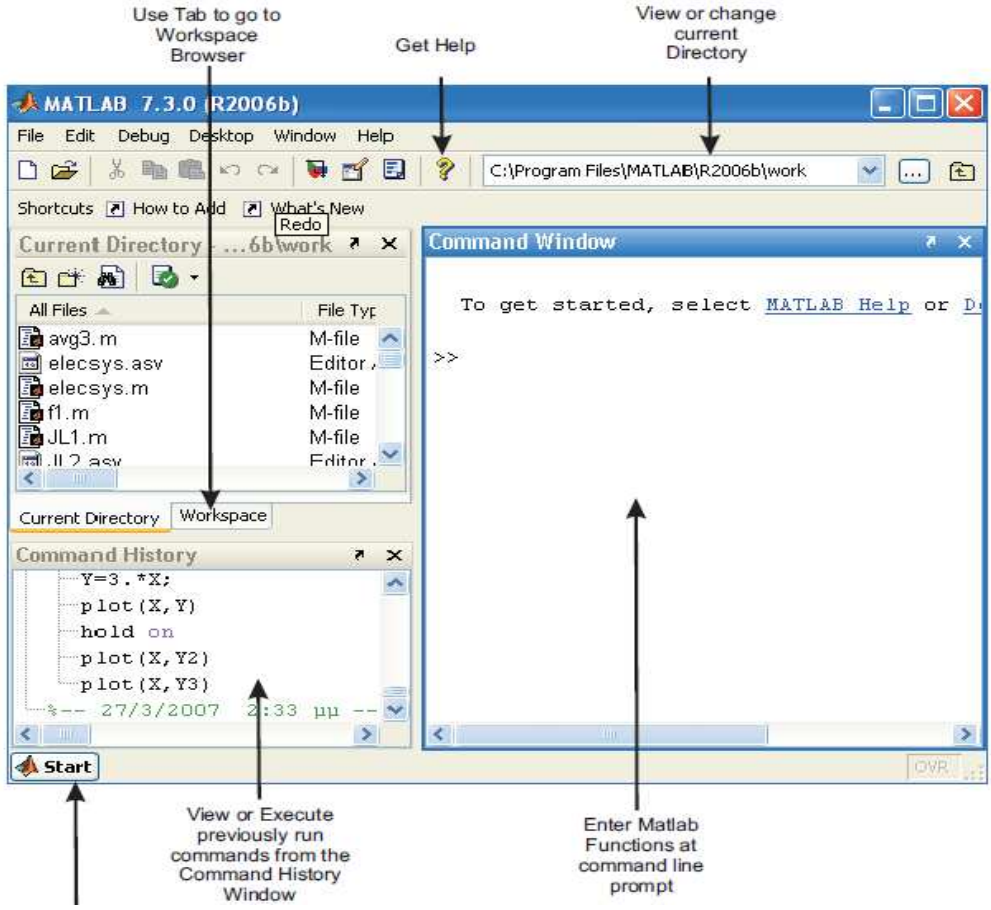

Figure 2.13: MATLAB Desktop(default layout) [144].

- Define the function, $y = f(x)$,
- Call the plot command, as plot(x, y).

Following example would demonstrate the concept. Let us plot the simple function y = x for the range of values for x from 0 to 100, with an increment of 5.

We create a script file and type the following code:

$x = [0 : 5 : 100];$

$y = x;$

$plot(x, y)$

When you run the file, MATLAB displays the plot.

MATLAB allows the addition of title, labels along the $x - axis$ and $y - axis$, grid lines and also to adjust the axes to spruce up the graph.

- The xlabel and ylabel commands generate labels along $x - axis$ and $y - axis$.
- The title command help to put a title on the graph.
- The grid on command allows us to put the grid lines on the graph.

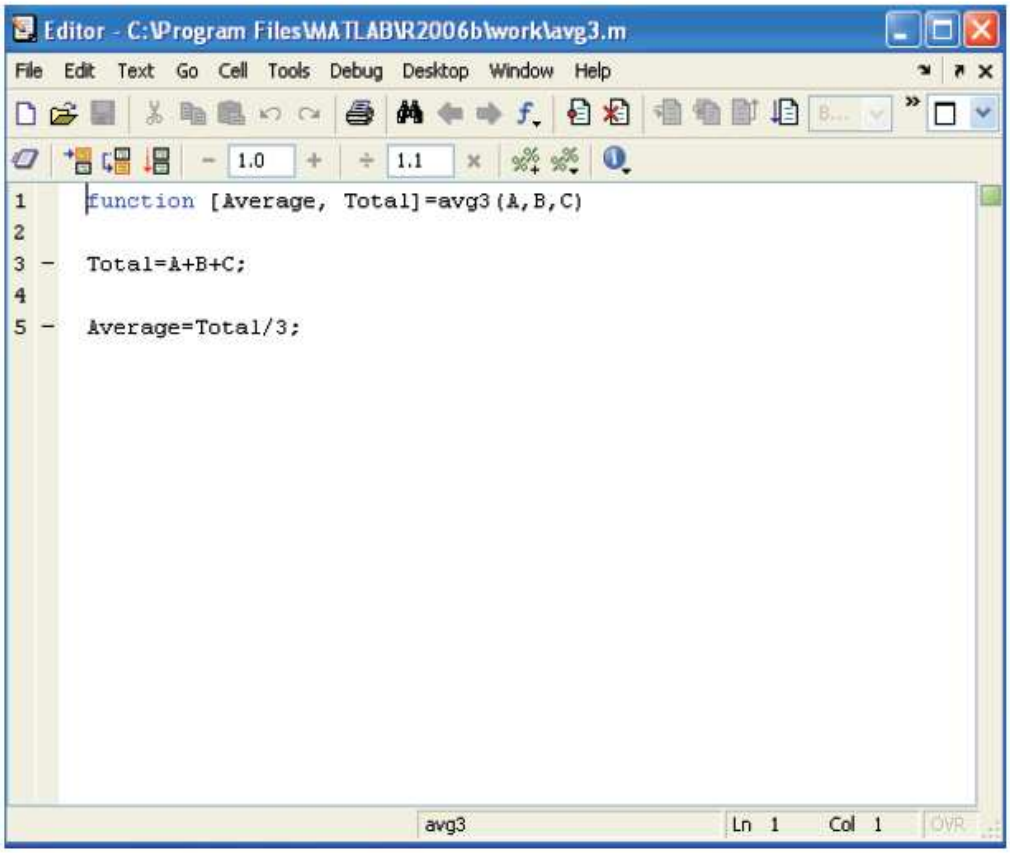

Figure 2.14: MATLAB Editor [144].

• The axis equal command allows generating the plot with the same scale factors and the spaces on both axes.

• The axis square command generates a square plot.

Example

Create a script file and type the following code:

$x = [0 : 0.01 : 10];$

$y = sin(x);$

$plot(x, y)$, $xlabel('x')$, $ylabel('Sin(x)')$, $title('Sin(x)Graph')$,

grid on, axis equal

MATLAB will generates the graph with all the above included.

The axis command allows us to set the axis scales. We can provide minimum and maximum values for x and y axes using the axis command in the following way:

axis ([xmin xmax ymin ymax])

When we create an array of plots in the same figure, each of these plots is called a subplot.

The subplot command is used for creating subplots and the syntax for the command is:

subplot($m, \quad n, \quad p$)

where, m and n are the number of rows and columns of the plot array and p specifies where to put a particular plot. Each plot created with the subplot command can have its own characteristics.

Conclusion

The non relativistic Schrödinger equation used to determine the ground state electronic properties of our system has been described. A dimensionless equation of motion have been established to represent the mathematical model of our system. Suitable reasons for using the Gupta potential here have been sorted. Detail steps for updating the position and velocities at a given time step in the verlet algorithm have clearly been made. In addition, the cubic and hexagonal unit cells used to generate our lattices for assigning our initial conditions have also been explained. The convergence criteria have been based on the multiple independent simulation of four different initial configurations and the system has been considered to be in equilibrium only when it remains below a certain pre-chosen threshold 10^{-2}. The verlet algorithm with the multiple independent simulation method have been summarized in a flow chart. Using the following steps in the Basin hopping method, angular move and random displacement, seeding, quasi Newton minimization algorithm and quenching, the local minima have been efficiently searched at reduced computing time with the assurance that the actual or final ground state is at thermal equilibrium and that any resulting potential energy surface does not change the global minimum of the local minima. The symmetry elements of each point group have been summarized. Lastly, the role played by each of these softwares in this work (Fortran 90, Chemcraft, Rastop and Matlab), have been summarized.

Chapter 3

RESULTS AND DISCUSSION

Introduction

In this chapter, we will explain how the Gupta parameters for the Aℓ clusters were obtained, proceeding by carrying out some verifications to show how these parameters are accurate. We shall then proceed to obtain the energies, geometries, point groups and bond lengths of all the Aℓ clusters within the range $3 \leq N \leq 170$ using these obtained parameters. A mathematical relation to analytically obtain the ground state energy of any cluster size will be of further obtained. In addition, their binding energies are to be obtained in other to study their structural stability. This stability behavior will be analyzed to distinguish those structures with enhance stability. The equilibrium distance of these clusters shall further be determined from the bond length and the total number of symmetries sorted from the optimized structures. Furthermore, comparison of the obtained results with the experimental works as well as other authors shall be made in detail. Still under this comparison, we are going to further show how accurate and efficient the Gupta potential is, using the Aℓ_9 cluster and the dimer. Lastly, through the octamer (Aℓ_8), we are to demonstrate how difficult it is to obtain all the global minima involved in a cluster as their nuclearity increases.

3.1 DETERMINATION OF THE GUPTA PARAMETERS AND VERIFICATION

3.1.1 Determination of the Gupta parameters

The first investigation was dedicated to the determination of the parameter values. Let r_2 and r_3 be the equilibrium separation distances in Aℓ_2 and Aℓ_3 respectively. Since the Aℓ_3 cluster had an equilateral triangle geometry with D_{3h} symmetry, from the Gupta potential given by the equation 2.6 and the force on the i^{th} particle given by the equation 2.8. Also,

knowing that the force $F_i = 0$ at equilibrium and taking F_2 and F_3 at equilibrium and solving them simultaneously, we expressed p and B as function of q and A as follows:

$$p = q + \frac{r_0 \ln\sqrt{2}}{r_3 - r_2}, \tag{3.1}$$

$$B = A\left(1 + \frac{r_0 \ln\sqrt{2}}{q\,(r_3 - r_2)}\right) \exp\left(\frac{r_2 - r_0}{r_2 - r_3} \ln\sqrt{2}\right). \tag{3.2}$$

Taking into account the experimental values of the cohesive energy and lattice parameters [124], the approximated values of q and A have been fitted. Under these considerations, the values of the parameters used in this work are given in Table 3.1.

Parameters	A	B	p	q
Values	$7.69 \cdot 10^{-2}$eV	1.1280eV	15.1194	1.930

Table 3.1: Gupta parameters for Aluminum clusters.

3.1.2 First verification of the Gupta parameters

For the first verification, the Gupta pair potential for $A\ell_2$ dimer and the corresponding force are displayed in Figure 3.1a) and Figure 3.1b) respectively.

The distance in the horizontal axis is in unit of r_0. As shown on the graph, the Gupta pair potential modeled to Aluminum decreases very rapidly to its minimum value as the distance increases from 0 to the equilibrium distance $0.9524r_0$. After the equilibrium distance, the potential increases slowly with the distance. According to the shape of the curve in Figure 3.1b), we can notice that the atoms repel each other when the distance between them is less than $0.9524r_0$ and attract each other otherwise. The smaller the distance between atoms becomes, the greater the intensity of the repulsive force. In the other hand, the attraction between the atoms reaches it maximum when $r_2 = 1.1085r_0$.

3.1.3 Second verification of the Gupta parameters

For the second verification of the many-body Gupta potential for Aluminum parameters listed in Table 3.1 above, we will determine the optimal configurations of $A\ell_3$, $A\ell_{50}$, $A\ell_{100}$ and $A\ell_{150}$ all presented in Figure 3.2 using different initial conditions. The obtained structures are then compared to the results presented by the authors of references [28, 29].

Starting with the $A\ell_3$ cluster, we obtained the total energy of -4.3498eV. Whatever the initial configuration, we ended up with the same stable configuration or lowest energy structure

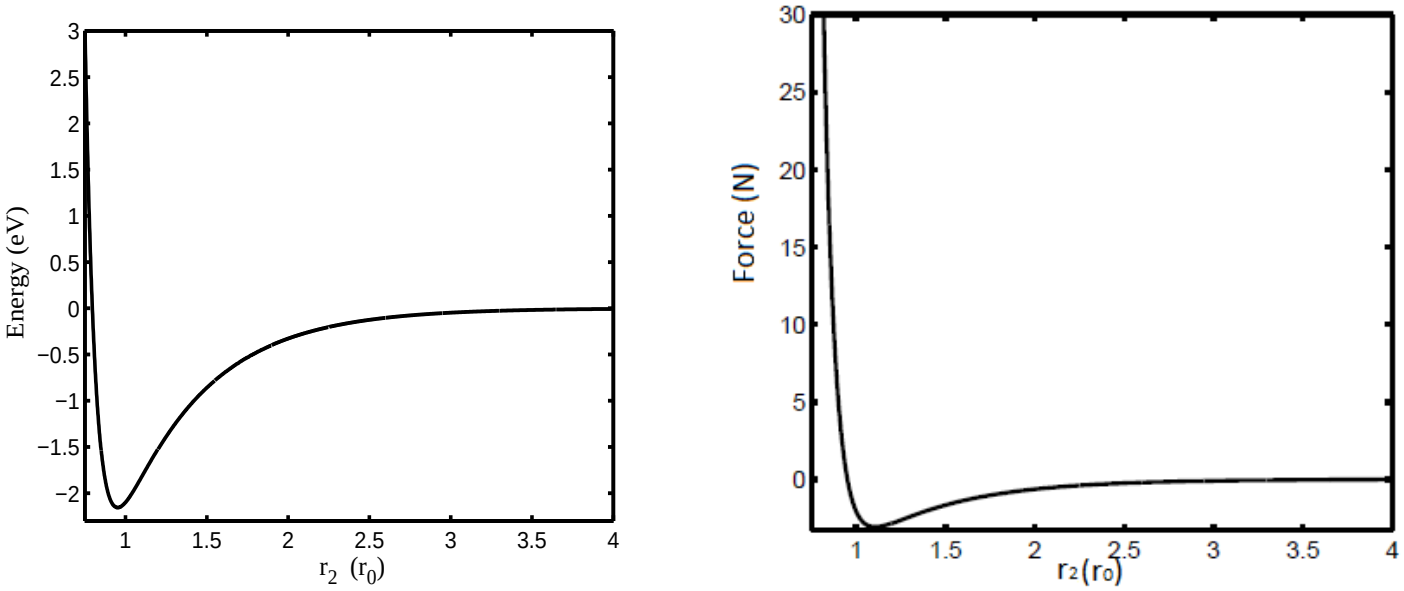

a) b)

Figure 3.1: a) The Gupta potential for the dimer of the Aluminum metal and b) The Gupta force acting on one atom in the dimer.

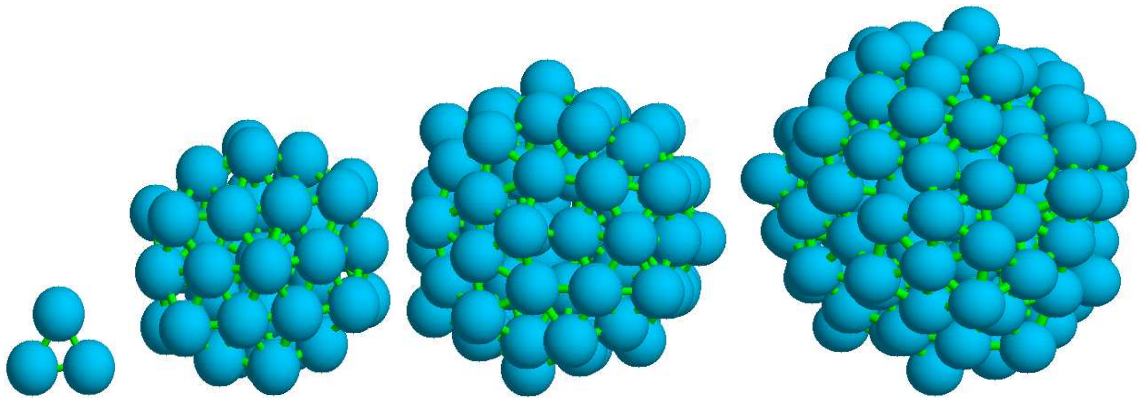

$A\ell_3$ $A\ell_{50}$ $A\ell_{100}$ $A\ell_{150}$

a) b) c) d)

Figure 3.2: Final configurations of: a)$A\ell_3$, b)$A\ell_{50}$, c)$A\ell_{100}$ and d)$A\ell_{150}$.

which was a D_{3h} with the only difference being the time taken to reach this final configuration. These results are in good agreement with those obtained by Doye [29]. We also obtained an $A\ell{-}A\ell$ bond of $0.9787r_0$. We tried several initial configurations and we noticed from our analysis that linear initialized coordinates were the ones that required more time to reach the optimized configuration. For illustration, Figure 3.3 shows the different optimization steps or paths for $A\ell_3$.

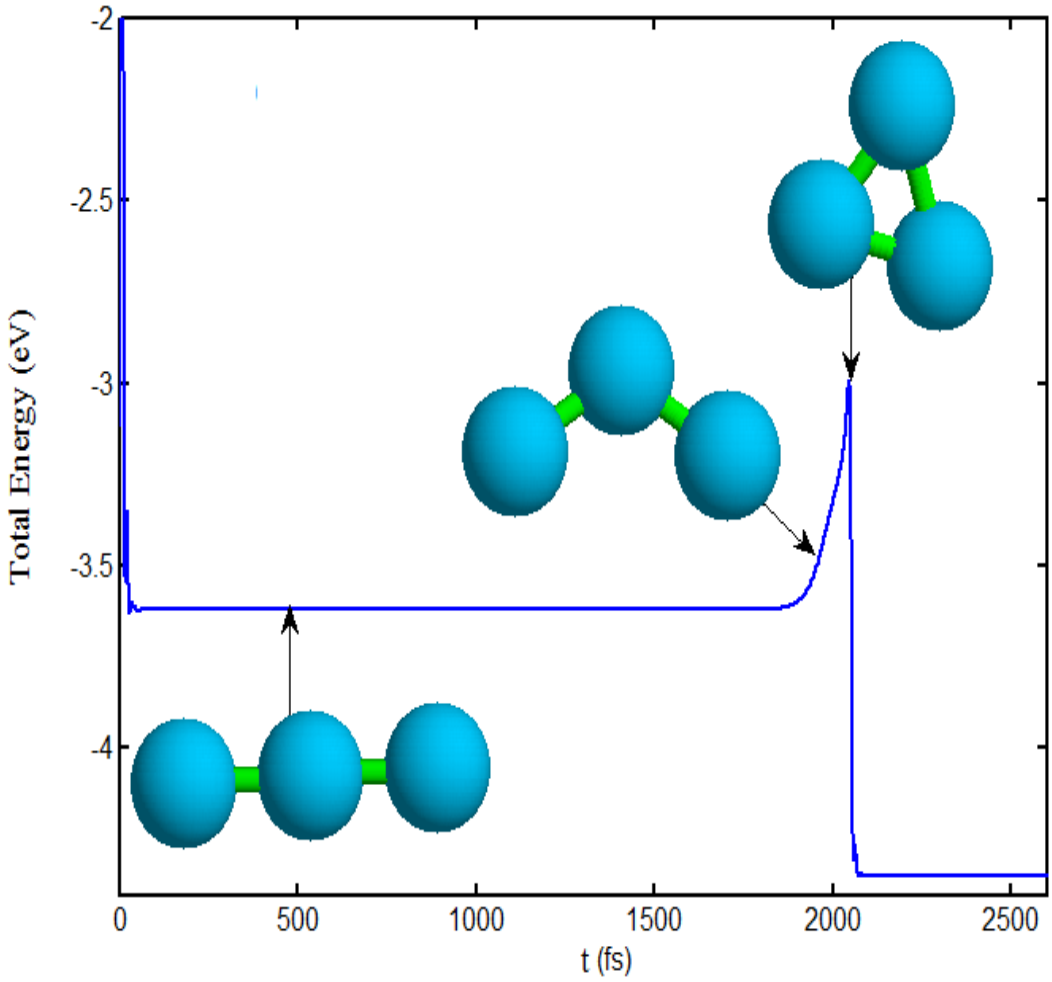

Figure 3.3: An illustration of the evolution of the lowest-energy $A\ell_3$ molecule with the Gupta potential starting from a linear initialized coordinates.

As shown in Figure 3.3, there are two stable configurations. The linear one was obtained after $t = 50$ and was maintained until $t = 1850$. During this phase, the kinetic energy of the molecule is approximately zero and the bond distance is $0.951068r_0$. After this phase, the molecule started a significant modification from the linear to the triangular form. The kinetic energy of the atoms increased to reach 0.5827 eV when $t = 2000$. At $t = 2050$, the kinetic energy was at its maximum (1.2177 eV) and then dropped abruptly to zero. The molecule then reached its most stable configuration at its lowest total energy.

Secondly, we considered $A\ell_{50}$ molecule and proceeded in the same manner as $A\ell_3$ molecule to have an energy of -139.1150eV. From different initial configurations, we obtained the same final optimized or stable configuration which is a (C_1). The initial configuration chosen here was a double ring of 25 atoms each and the minimization process for $A\ell_{50}$ is shown in Figure 3.4.

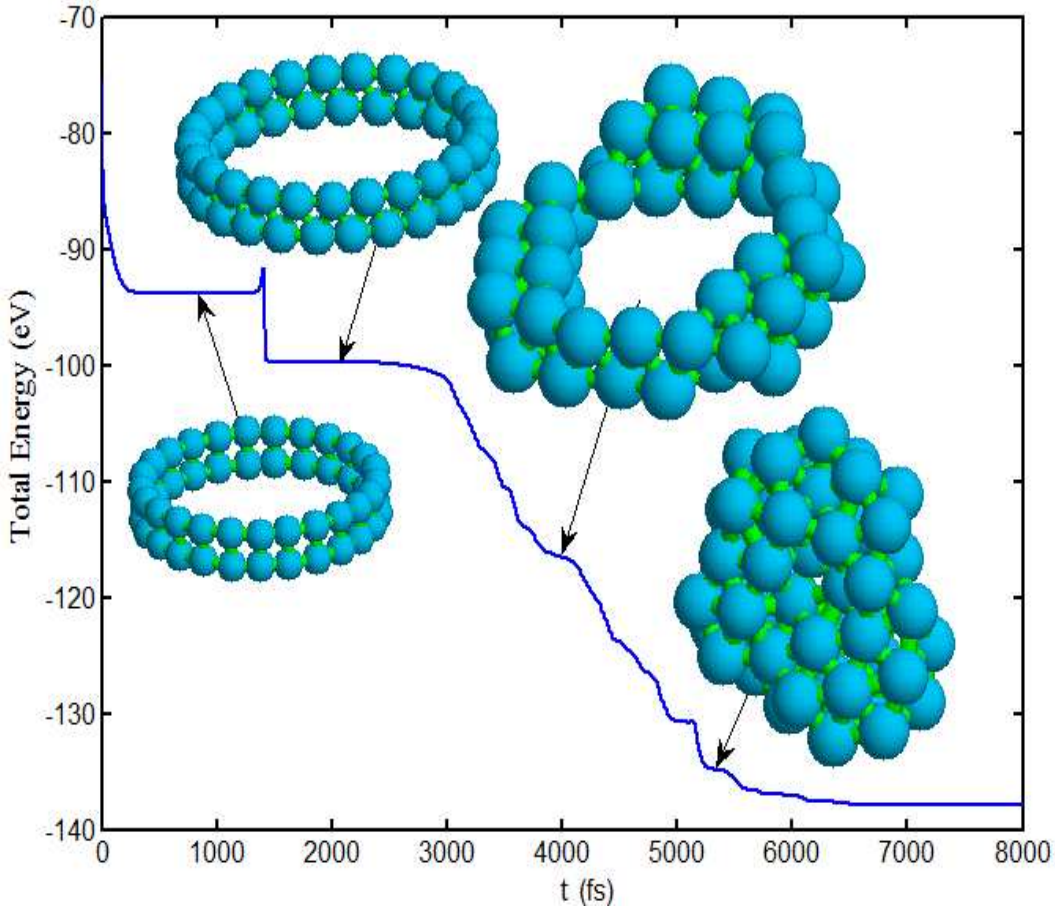

Figure 3.4: An illustration of the evolution of the lowest-energy $A\ell_{50}$ molecule with the Gupta potential starting from a cylinder initialized coordinates.

The minimum distance between $A\ell_{50}$ atoms is approximately constant and very close to $0.9446r_0$.

From our simulations, we have also observed that the structure remained almost constant until $t = 1250$. Between $t = 1250$ and $t = 3000$, one ring performed a rotation with angle $\frac{\pi}{25}$ around the rings axis. After $t = 3000$, the kinetic energy started to increase and reaches its maximum around $t = 4000$. As shown in the graph of Figure 3.4, important modifications of the structure were found after $t = 3000$. The optimized configuration was obtained for $t > 7000$ and is in good agreement with that obtained by the authors of reference [29].

Focusing on $A\ell_{100}$ and $A\ell_{150}$ molecules, we analyzed their optimizations starting from two different initial structures: the simple cubic lattice and the cylindrical configurations for each molecule. As illustrated in Figure 3.5 and Figure 3.6, we have shown some transformation steps for $A\ell_{100}$ and $A\ell_{150}$ respectively.

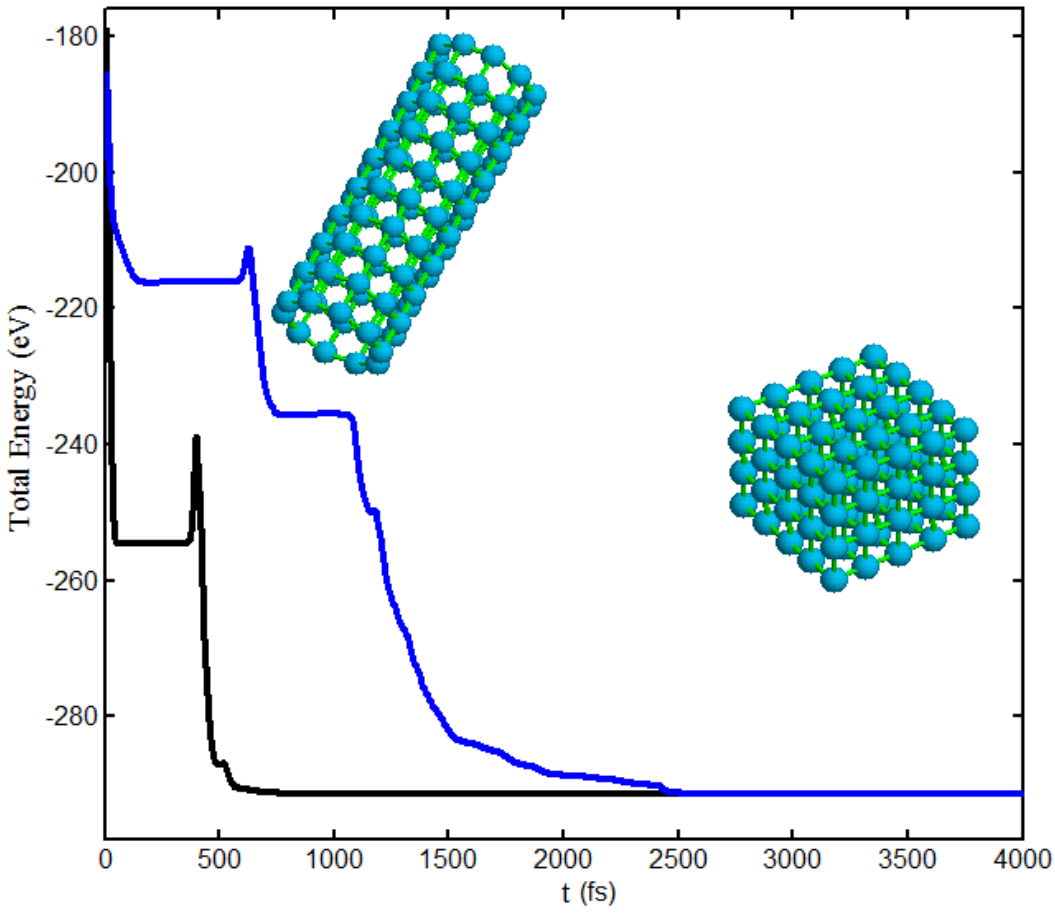

Figure 3.5: An illustration of the evolution of the lowest-energy Aℓ_{100} molecule starting from a simple cubic lattice (black curve) and from a cylinder initialized coordinates (blue curve).

For both figures, the black and the blue curves respectively correspond to the simple cubic lattice and cylindrical structures used as initial coordinates. From different initials configurations shown in Figures 3.5 and 3.6, we obtained the same final optimized configurations which are respectively (C_1) and (C_s). These structures are shown in Figure 3.2c) and Figure 3.2d) with energies -292.1767 eV and -447.9025 eV respectively which are in good agreement with those of Doye [29]. The minimum distance between Aℓ_{100} atoms is approximately constant and very close to $0.9444r_0$ and for Aℓ_{150} atoms, it is almost constant and very close to $0.9408r_0$. The peaks observed in the figures corresponded to some important modifications of the structures. We can notice from the two figures that, the simple cubic configurations stabilized first before the cylindrical configurations.

Our results for Aℓ_3, Aℓ_{50}, Aℓ_{100} and Aℓ_{150} molecules, using Gupta potential agrees well in terms of point groups and structures, with those found in the literature [28, 29]. According to the above results, we can notice that our Gupta parameters presented in Table 3.1 are well fitted.

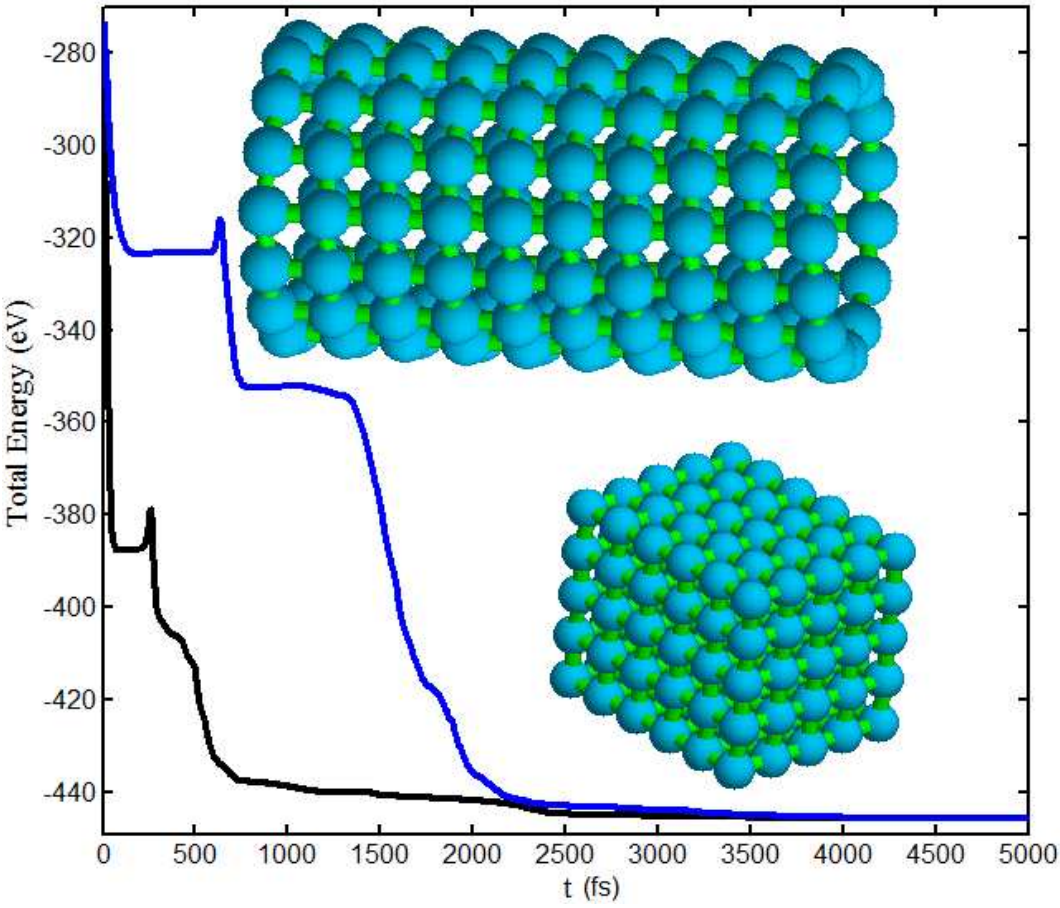

Figure 3.6: An illustration of the evolution of the lowest-energy $A\ell_{150}$ molecule starting from a simple cubic lattice (black curve) and from a cylinder initialized coordinates (blue curve).

3.2 OPTIMIZED STRUCTURES AND CORRESPONDING ENERGIES FOR $3 \leq N \leq 170$

3.2.1 Different energies and geometries

We then proceed to obtain all the global energy minimum structures of the clusters obtained using Gupta potential. The basin-hopping algorithm has proved to be particularly successful in locating putative global minima for a wide variety of cluster systems [17]. Anyway, there is no guarantee that we have located the true global minima, since the probability to miss a global minimum increases with cluster size.

However, according to the fact that the same lowest-energy minimum is obtained using different initial configurations, and also according to the good precision between our results and the given cohesive energy of aluminum, we are confident that our obtained global minima

are well estimated. Table 3.2 depicts the potential energy, point group and Aℓ−Aℓ bond of all the clusters for $3 \leq N \leq 170$.

The Structural assignment has been made in Table 3.2 where C stands for cyclic, D for decahedral, I for icosahedral, T for tetrahedral and O for octahedral. It should be noted that, of course, there is no guarantee that the simulations have been able to locate the true global minima, and the probability that a global minimum has been missed will increase with cluster size, as the size of the search space, and hence the number of minima, increases exponentially with N.

For each structure, the result obtained from the basin-hoping method is compared to that obtained from multiple independent simulations. For example, the lowest-energy structure found in a basin-hopping run for Aℓ_{147} is at −446.9617 eV while the same Mackay icosahedron structure obtained from multiple independent simulations has an energy of −446.9719 eV. However, this is the only example we found where reoptimization of a structure gives results with a difference 0.0102 eV greater than 0.00017 eV.

3.2.2 Mathematical relation between energies and number of atoms

We can notice from Table 3.2 that the ground state energy decreases with the number N of atoms. In order to go far in our analysis, we plotted on Figure 3.7 the ground state energy as function of N (curve in black color).

This curve brought out the following analysis: the shape of the curve is almost linear. Then, the cluster energies of geometric shell clusters are fitted to the following cubic expansion in $N^{1/3}$:

$$E(N) \simeq aN + bN^{2/3} + cN^{1/3} + d. \tag{3.3}$$

By using the cubic regression method we obtained the parameter values: $a = -3.40444$eV, $b = 2.17026$eV, $c = 0.12859$eV and $d = 1.03007$eV. To verify our assumption, we have plotted in Figure 3.7 (curve in blue) the above relation. A good agreement is obtained here between numerical result and semi-analytical one. The result obtained in equation (3.3) is an important outcome because this can help to predict the ground state energy of any cluster size knowing N and without the need for numerical simulation. As in the case of Nouemo et al [126], using the linear regression, showed that the ground state energy of iron could also be obtained analytically without numerical simulations with the relation $V_N \approx aN + b$, with $a = 8.54862$eV and $b = 25.55493$eV.

N	Energy(eV)	Bond(r_0)	PG	N	Energy(eV)	Bond(r_0)	PG
3	−4.34983	0.9787	D_{3h}	4	−6.8961	0.9941	T_d
5	−9.34712	0.9923	D_{3h}	6	−12.0278	1.0017	O_h
7	−14.5962	0.9949	D_{5h}	8	−17.0885	0.9983	C_{2v}
9	−19.7611	0.9954	C_{2v}	10	−22.4982	0.9854	C_{3v}
11	−25.2357	0.9798	C_{2v}	12	−28.2547	0.9739	C_{5v}
13	−31.6329	0.9829	I_h	14	−33.9797	0.9823	C_{3v}
15	−36.7320	0.9784	C_{2v}	16	−39.4368	0.9817	C_s
17	−42.1397	0.9847	C_2	18	−45.0494	0.9398	C_s
19	−48.3574	0.9304	D_{5h}	20	−51.0270	0.9288	C_{2v}
21	−53.6976	0.9318	C_1	22	−56.5141	0.9397	C_s
23	−59.7394	0.9456	D_{3h}	24	−62.3914	0.9411	C_{2v}
25	−65.1848	0.9498	C_s	26	−68.2925	0.9576	T_d
27	−71.0629	0.9441	C_{2v}	28	−73.8040	0.9447	C_s
29	−76.8017	0.9538	D_{3h}	30	−79.5915	0.9419	C_{2v}
31	−82.4369	0.9418	C_s	32	−85.2960	0.9478	C_{2v}
33	−88.0976	0.9493	C_{5v}	34	−90.8948	0.9453	D_{5h}
35	−94.3272	0.9255	C_{2v}	36	−97.2693	0.9299	C_s
37	−100.0447	0.9500	C_s	38	−103.0710	0.9262	D_{6h}
39	−106.1741	0.9285	C_{6v}	40	−109.0568	0.9260	D_{6h}
41	−111.9302	0.9296	C_{2v}	42	−115.0334	0.9311	C_1
43	−118.0820	0.9353	C_s	44	−120.9767	0.9222	C_{2v}
45	−124.0708	0.9386	C_1	46	−127.2073	0.9386	C_s
47	−130.3143	0.9363	C_{3v}	48	−133.3006	0.9373	C_s
49	−136.0027	0.9394	C_s	50	−139.1150	0.9446	C_1
51	−141.9827	0.9307	C_1	52	−145.1069	0.9345	C_s
53	−148.0852	0.9328	C_{5v}	54	−153.6278	0.9623	C_s
55	−156.9316	0.9643	I_h	56	−157.1739	0.9256	C_{3v}
57	−160.4398	0.9347	S_4	58	−163.3002	0.9255	C_s
59	−166.3712	0.9258	C_{2v}	60	−169.1812	0.9273	C_{3v}
61	−172.2358	0.9277	T_d	62	−175.2437	0.9283	C_s
63	−178.4397	0.9255	C_1	64	−181.3260	0.9225	C_{2v}

N	Energy(eV)	Bond(r_0)	PG	N	Energy(eV)	Bond(r_0)	PG
65	−184.5851	0.9321	C_1	66	−187.7525	0.9390	C_1
67	−190.7509	0.9319	C_1	68	−193.6235	0.9398	C_1
69	−196.6888	0.9376	C_3	70	−199.8774	0.9413	C_2
71	−202.7042	0.9245	C_s	72	−205.8481	0.9331	C_s
73	−208.7526	0.9237	C_s	74	−212.1544	0.9343	C_s
75	−215.4319	0.9360	C_s	76	−218.5124	0.9397	D_{3h}
77	−221.5578	0.9310	C_{3v}	78	−224.4132	0.9162	D_{3h}
79	−227.2243	0.9200	C_s	80	−230.6202	0.9295	C_s
81	−233.5749	0.9225	C_s	82	−236.6836	0.9320	C_2
83	−239.5451	0.9361	C_1	84	−242.7113	0.9378	C_s
85	−245.5700	0.9251	C_{2v}	86	−248.5707	0.9258	C_s
87	−252.1090	0.9284	C_1	88	−255.1910	0.9281	C_s
89	−258.3163	0.9280	C_s	90	−261.1174	0.9316	C_s
91	−264.4623	0.9545	D_{3h}	92	−267.3222	0.9383	C_2
93	−270.5029	0.9373	C_1	94	−273.5429	0.9295	C_{2v}
95	−276.6024	0.9307	C_s	96	−279.7527	0.9336	C_2
97	−282.7939	0.9478	C_1	98	−286.1358	0.9512	C_1
99	−289.2391	0.9493	C_1	100	−292.1767	0.9444	C_1
101	−295.3935	0.9416	C_1	102	−298.5960	0.9420	C_1
103	−301.4776	0.9471	C_1	104	−304.4115	0.9325	C_1
105	−307.5460	0.9382	C_s	106	−310.1656	0.9301	C_1
107	−313.0646	0.9277	C_s	108	−316.4403	0.9375	C_s
109	−320.1979	0.9396	C_1	110	−323.2767	0.9408	C_1
111	−326.3590	0.9353	C_1	112	−329.3589	0.9393	C_1
113	−332.4441	0.9339	C_1	114	−335.2425	0.9398	C_s
115	−338.8164	0.9451	C_1	116	−341.7280	0.9378	C_s
117	−344.8550	0.9386	C_1	118	−347.8365	0.9388	C_1
119	−350.9419	0.9359	C_1	120	−354.0818	0.9397	C_2
121	−356.9454	0.9413	C_1	122	−359.9576	0.9418	C_2
123	−363.4546	0.9366	C_1	124	−366.2721	0.9325	C_1
125	−369.4206	0.9312	C_1	126	−372.5688	0.9369	C_1
127	−376.0505	0.9312	C_1	128	−379.2189	0.9255	C_1

N	Energy(eV)	Bond(r_0)	PG	N	Energy(eV)	Bond(r_0)	PG
129	−381.9535	0.9356	C_3	130	−385.4508	0.9371	C_1
131	−388.1855	0.9338	C_1	132	−391.2332	0.9336	C_2
133	−394.2573	0.9384	C_s	134	−397.0438	0.9412	C_2
135	−400.4313	0.9401	C_s	136	−403.3256	0.9357	C_s
137	−406.7123	0.9367	C_s	138	−409.6199	0.9393	C_{2v}
139	−412.9599	0.9357	C_s	140	−416.0248	0.9387	C_s
141	−419.1856	0.9323	C_s	142	−422.5587	0.9394	C_{2v}
143	−425.7004	0.9331	C_s	144	−428.7183	0.9254	C_{2v}
145	−431.5097	0.9328	C_1	146	−434.5826	0.9286	C_1
147	−446.9617	0.9554	I_h	148	−441.0488	0.9265	C_s
149	−444.0072	0.9269	C_1	150	−447.9025	0.9408	C_s
151	−451.1330	0.9373	C_{2v}	152	−454.0891	0.9348	C_s
153	−457.3169	0.9249	C_{2v}	154	−459.5114	0.9310	C_s
155	−462.9513	0.9362	C_s	156	−465.8317	0.9363	C_{3v}
157	−469.3694	0.9391	C_1	158	−472.5375	0.9506	C_2
159	−475.7368	0.9519	C_s	160	−478.9933	0.9424	D_{3h}
161	−482.0470	0.9486	C_1	162	−485.2691	0.9395	C_s
163	−488.3247	0.9484	C_s	164	−491.5816	0.9476	C_2
165	−494.6451	0.9397	C_s	166	−497.7476	0.9451	C_s
167	−500.9590	0.9438	C_1	168	−503.9306	0.9436	C_2
169	−507.1065	0.9467	C_1	170	−510.1182	0.9463	C_s

Table 3.2: Potential energy, point group and Aℓ−Aℓ bond length of the lowest energy configurations.

3.2.3 The binding energy of the Aluminum cluster

To investigate the structural stabilities for Aℓ_N clusters, the average binding energy (E_b) for any Aℓ cluster is defined as

$$E_b = -\frac{E(N)}{N} \simeq 3.40444 - 2.17026N^{-\frac{1}{3}} - 0.12859N^{-\frac{2}{3}} - \frac{1.03007}{N} \tag{3.4}$$

where $E(N)$ is the total energy of the cluster containing N Aluminum atoms. Variation of the average binding-energies of the lowest-energy structures of Aℓ_N ($3 \leq N \leq 170$) clusters is given in Figure 3.8.

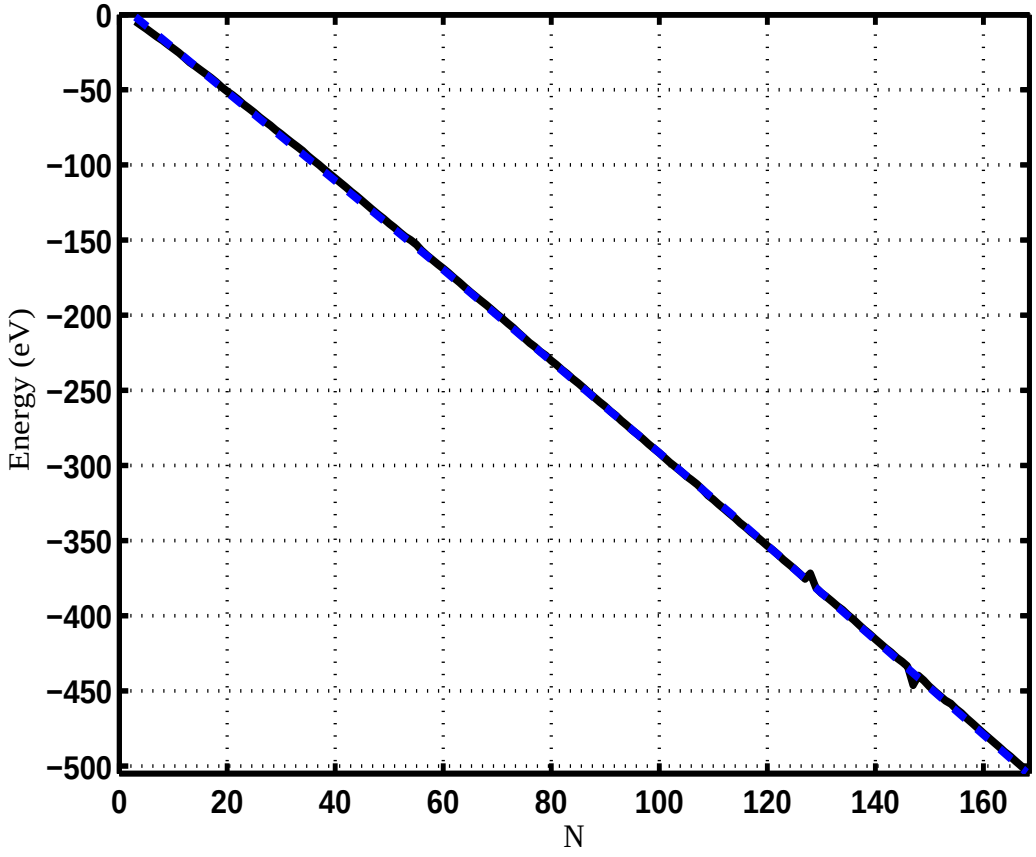

Figure 3.7: Ground state energy as function of the number of atoms. The curve with solid line (black) is our numerical result while curve with dashed line (blue) is our semi analytical result.

From Figure 3.8, one can see that the average binding energies increase overall but with little fluctuation around few cluster sizes (which are relevant to the magic-number clusters).

The origin of the magic-number clusters is related to the type of atoms. For noble gas atoms, the magic-number clusters correspond to filled electronic shells, thereby indicating the role of the total number of itinerant electrons on stability. Basing on the magic numbers in clusters that contain more than a few dozen atoms, it has been shown that the most stable species correspond to sizes with complete geometric shells in an icosahedral or cuboctahedral atomic arrangement [43]. Alkali metal clusters (s^1) conform to the Jellium model in that, certain nuclearities are relatively stable due to their filled electronic shells [42]. By contrast, clusters of alkaline earth elements (s^2), exhibit magic numbers which correspond to clusters consisting of concentric polyhedral shells of atoms where the relative stability of a given cluster is determined by the competition between packing and surface energy effects [45].

In the case of aluminum, due to the higher atomic valency (+3), the higher density of

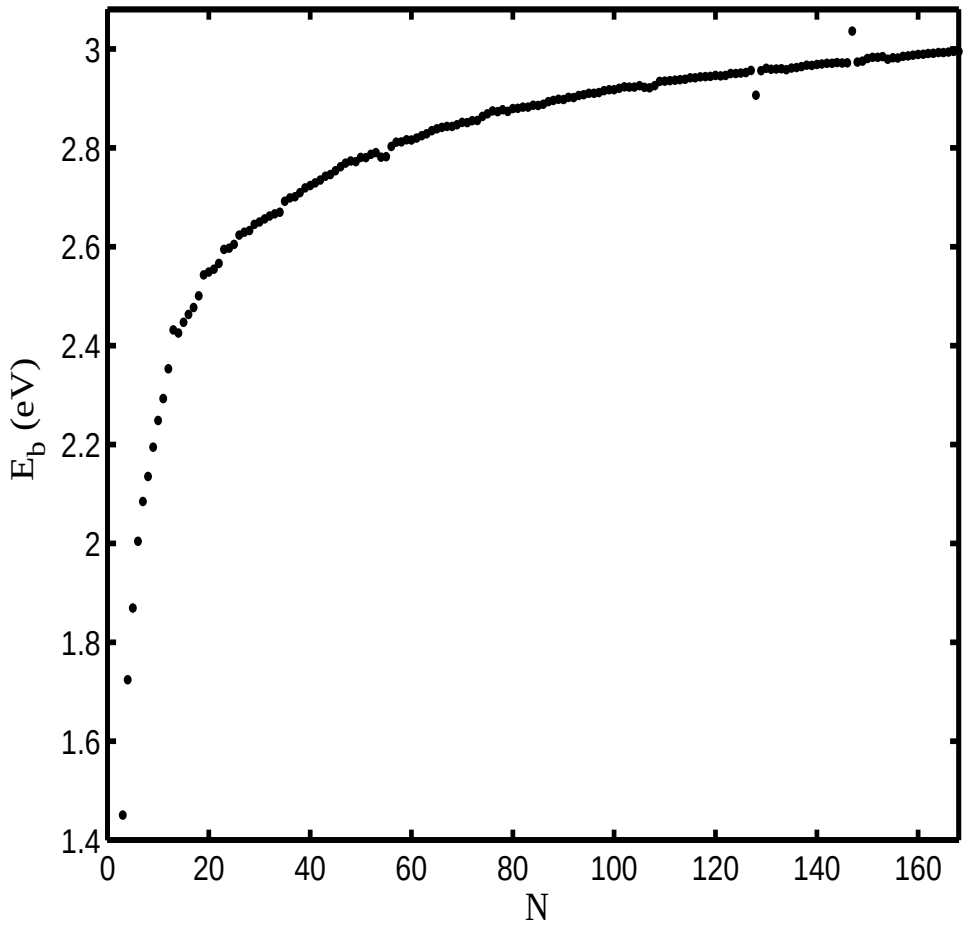

Figure 3.8: The average binding energy E_b as a function of cluster size.

electronic states and the involvement of $3p^1$, as well as $3s^2$ orbitals in bonding, the origin of these peaks is more complex [46]. It is believed that the crossover from the regime where electronic factors determine cluster stability to where packing and surface energy effects dominate, occurs at lower nuclearities than for the alkali metals [46, 47]. Variable temperature experiments by Baguenard et al. have shown, however, that Jellium effects can be seen at much higher nuclearities when the Aℓ clusters are generated at temperatures such that they are either molten or have molten surfaces [49].

The calculated average binding energy of the cluster with the largest-size (Aℓ_{170}) is about 3.4044 eV, and it is very closed to the cohesive energy of Aℓ crystal (3.3978 eV). This small relative error of 0.19% indicates that there is still a negligible discrepancy between properties of the aluminum clusters investigated and that of the bulk materials.

3.2.4 Stability analysis

An important feature of this graph (Figure 3.8)is the small peaks at $N = 13$, $N = 55$ and $N = 147$, corresponding to a region of enhanced stability for $3 \leq N \leq 170$. Such regions are more evident when the second difference in the binding energy D_2(N) defined as

$$D_2 = -E_b(N-1) + 2E_b(N) - E_b(N+1), \tag{3.5}$$

is plotted against N, as presented in Figure 3.9.

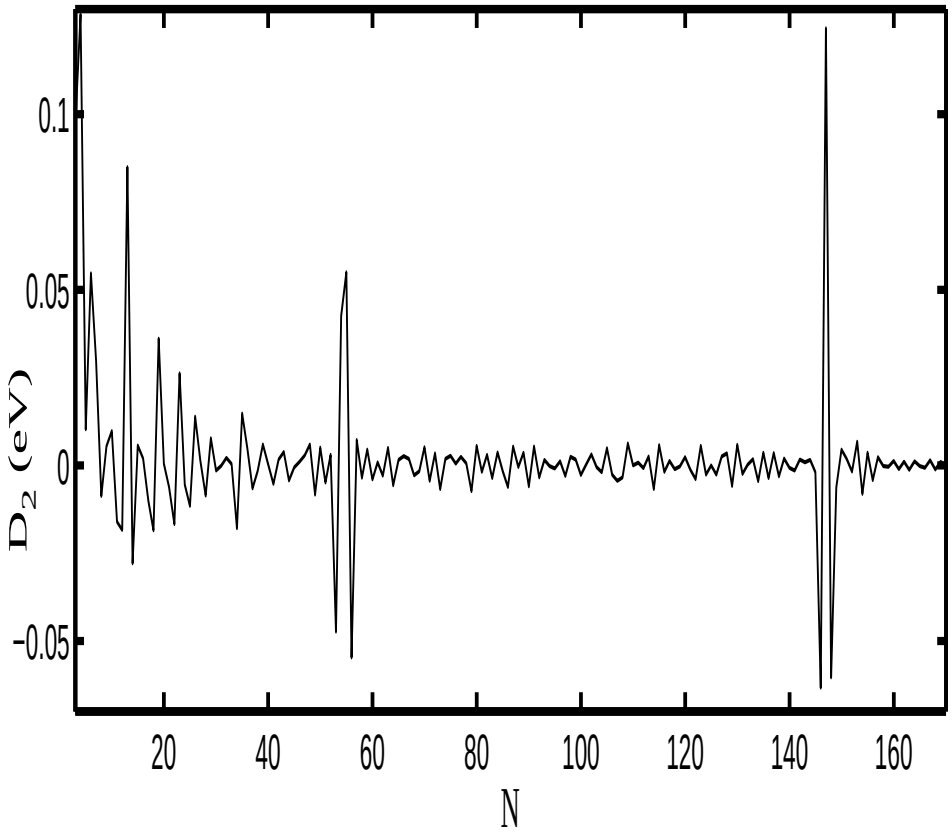

Figure 3.9: Second difference in the binding energy D_2 as a function of cluster size.

The second difference is related to the thermodynamic stability of a cluster with respect to disproportionality, assuming a quasi-equilibrium exist during cluster formation [145]. Figure 3.8 shows that there are pronounced peaks in D_2(N) at $N = 4$, 6, 13, 19, 53, 55, 56, 146, 147, and 148 and small peaks at 14, 23 and 35. Experimentally they do appear to be enhanced stability at around 4, 6, 13 and 19 atoms for small clusters with N $\leq$ 20 [146]. Jellium calculations by Chou and Cohen [147] predict peaks in D_2(N) at $N = 6$, 13 and 19, where the numbers of

valence electrons ($3N$ for neutral clusters) are close to Jellium shell closings [42]. Even here, our results are in good agreement with the experimental ones as well as with those obtained numerically by Chou and Cohen.

3.2.5 Bond length and the cluster size

On the other hand, the distances between the nearest Aℓ−Aℓ aluminum atoms remain almost constant as shown in Figure 3.10.

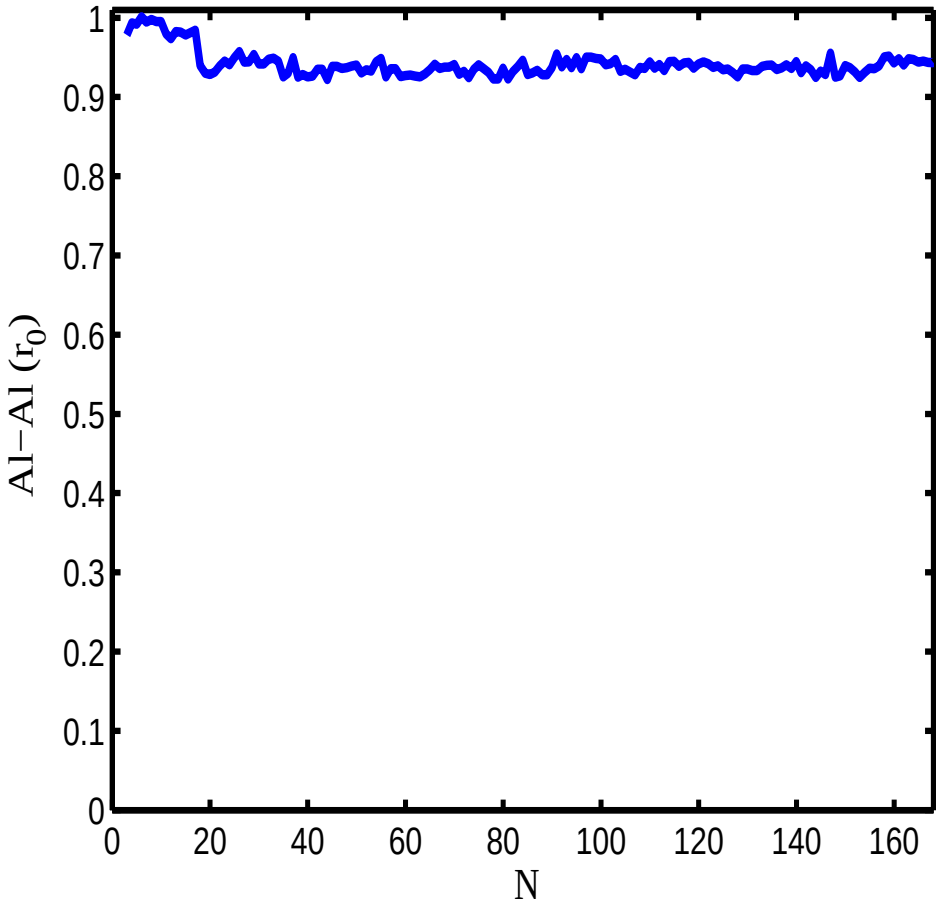

Figure 3.10: Aℓ−Aℓ bond length as function of the number of atoms.

The average Aℓ−Aℓ bond was found to be $0.9443r_0$ while the lower $0.9162r_0$ and higher $1.0017r_0$ distances were obtained in the case of Aℓ_{78} and Aℓ_6 clusters respectively. Taking into account the lattice constant of the aluminum crystal (404.95 pm), the value of r_0 can be determined as $r_0 = 303.2312$ pm.

3.2.6 Optimized structures

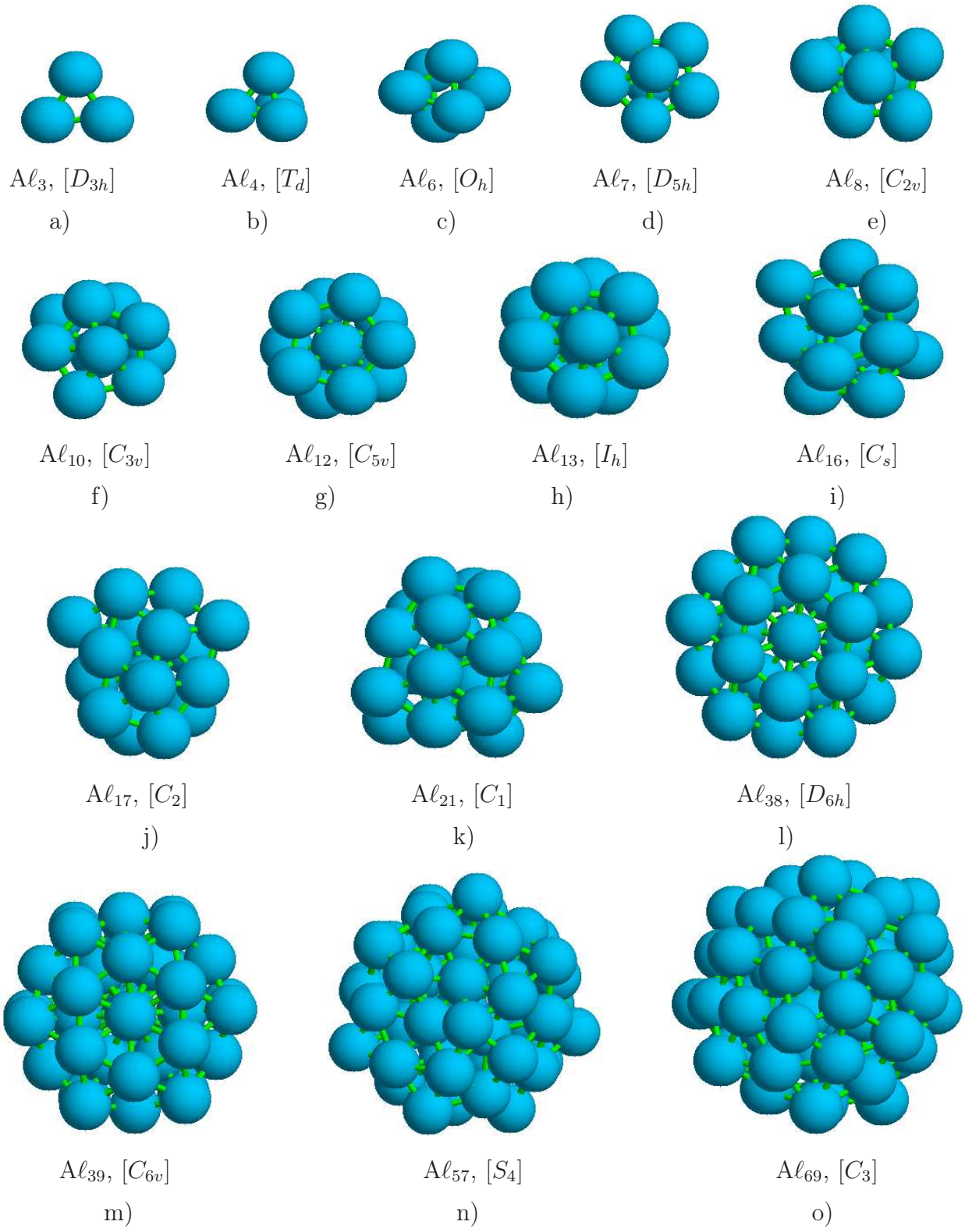

Figure 3.11: Ground-state structures for aluminum cluster geometries, as predicted by the Molecular Dynamics with the Gupta potential. The other optimized structures are presented in the index.

From our simulations, we came out with 15 symmetry groups: D_{3h}, T_d, O_h, D_{5h}, C_{2v}, C_{3v}, C_{5v}, I_h, C_s, C_2, C_1, D_{6h}, C_{6v}, S_4, and C_3. For each of these symmetry groups, one molecule was chosen together with its corresponding global minimum structure and was depicted in Figure 3.11. Following the order in which the symmetry groups are given above, structures of $A\ell_3$, $A\ell_4$, $A\ell_6$, $A\ell_7$, $A\ell_8$, $A\ell_{10}$, $A\ell_{12}$, $A\ell_{13}$, $A\ell_{16}$, $A\ell_{17}$, $A\ell_{21}$, $A\ell_{38}$, $A\ell_{39}$, $A\ell_{57}$ and $A\ell_{69}$ are plotted in Figures 3.11a), 3.11b), 3.11c), 3.11d), 3.11e), 3.11f), 3.11g), 3.11h), 3.11i), 3.11j), 3.11k), 3.11l), 3.11m), 3.11n) and 3.11o) respectively. The other optimized structures are presented in the index.

3.3 COMPARISON WITH OTHER WORKS

3.3.1 General comparison

The results obtained here using a Gupta potential agree well with those obtained by Doye [29] and by Noya et al. [148] using the glue potential and the monte-carlo simulations respectively. For more comparison, the values of energies and point groups of Aluminum clusters obtained by Doye using the Glue potential are presented in Table 3.3.

The comparison of Tables 3.2 and 3.3 shows that the point groups of the structures are identical with the exception of the following clusters: $A\ell_{47}$, $A\ell_{48}$, $A\ell_{50}$, $A\ell_{52}$, $A\ell_{53}$ and $A\ell_{54}$. For these clusters, the point groups obtained in this work (and with the Glue potential) are C_{3v} (C_s), C_s (C_{3v}), C_1 (C_s), C_s (C_1), C_{5v} (C_s) and C_s (C_{5v}) respectively. In addition, for a given cluster, the corresponding energy obtained in this thesis is slightly higher than that obtained with the Glue potential. Moreover, according to Table 3.3, the relationship between the energy and the number of atoms in the cluster is given as follows:

$$E_{\text{glue}} = -3.360N + 1.890N^{2/3} + 1.170N^{1/3} - 0.267. \tag{3.6}$$

Equation (3.6) shows that the binding energy of Aluminum cluster as predicted using the Glue potential is 3.360 eV. Consequently, our results have the best precision since the results obtained by Doye admit an error of 1.11%.

Andrés et al. demonstrated using Kohn sham Density Functional Theory that from $A\ell_{13}$ to $A\ell_{22}$, the icosahedral growth dominates global minima structures and this agrees with our work for $A\ell_{13}$ to $A\ell_{18}$ [149]. Also, Khanna et al. had earlier confirmed that from $A\ell_{13}$ to $A\ell_{18}$, icosahedral structures are more stable in all-electron PBE calculations [150].

N	Energy(eV)	PG	N	Energy(eV)	PG	N	Energy(eV)	PG
3	−4.099029	D_{3h}	4	−6.242292	T_d	5	−8.607257	D_{3h}
6	−11.257920	O_h	7	−13.860178	D_{5h}	8	−16.353276	C_{2v}
9	−19.063671	C_{2v}	10	−21.862051	C_{3v}	11	−24.616176	C_{2v}
12	−27.780117	C_{5v}	13	−31.278787	I_h	14	−33.585594	C_{3v}
15	−36.321872	C_{2v}	16	−39.039888	C_s	17	−41.750455	C_2
18	−44.777004	C_s	19	−48.182587	D_{5h}	20	−51.823659	C_{2v}
21	−53.470949	C_1	22	−56.404346	C_s	23	−59.732308	D_{3h}
24	−62.350544	C_{2v}	25	−65.195739	C_s	26	−68.459809	T_d
27	−71.162534	C_{2v}	28	−73.946989	C_s	29	−77.115629	D_{3h}
30	−79.792682	C_{2v}	31	−82.634873	C_s	32	−85.678623	C_{2v}
33	−88.453125	C_{5v}	34	−91.447319	D_{5h}	35	−94.464663	C_{2v}
36	−97.324975	C_s	37	−100.214276	C_s	38	−103.264168	D_{6h}
39	−106.437242	C_{6v}	40	−109.401628	D_{6h}	41	−112.178113	C_{2v}
42	−115.154425	C_1	43	−118.128134	C_s	44	−120.260703	C_{2v}
45	−124.074147	C_1	46	−127.238882	C_s	47	−130.228220	C_s
48	−133.418980	C_{3v}	49	−136.111570	C_s	50	−139.090832	C_s
51	−142.098016	C_1	52	−145.091286	C_1	53	−148.261944	C_s
54	−151.376943	C_{5v}	55	−154.612749	I_h	56	−157.245282	C_{3v}
57	−160.381251	S_4	58	−163.479187	C_s	59	−166.601625	C_{2v}
60	−169.702701	C_{3v}	61	−172.787060	T_d	62	−175.512306	C_s
63	−178.554122	C_1	64	−181.598713	C_{2v}	65	−184.466611	C_1
66	−187.498248	C_1	67	−190.610516	C_1	68	−193.508419	C_1
69	−196.696161	C_3	70	−199.701093	C_2	71	−202.700030	C_s
72	−205.819266	C_s	73	−208.794190	C_s	74	−211.818219	C_s
75	−215.088423	C_s	76	−218.367742	D_{3h}	77	−221.514884	C_{3v}
78	−224.595480	D_{3h}	79	−227.336269	C_s	80	−230.318346	C_s
81	−233.343636	C_s	82	−236.308999	C_2	83	−239.278725	C_1
84	−242.456890	C_s	85	−245.646464	C_{2v}	86	−248.606413	C_s
87	−251.592963	C_1	88	−254.736772	C_s	89	−257.685396	C_s
90	−260.675290	C_s	91	−263.877164	D_{3h}	92	−266.936839	C_2
93	−270.089293	C_1	94	−273.244125	C_{2v}	95	−276.204093	C_s
96	−279.154395	C_2	97	−282.115807	C_1	98	−285.257294	C_1
99	−288.206364	C_1	100	−291.309715	C_1	101	−294.334721	C_1

N	Energy(eV)	PG	N	Energy(eV)	PG	N	Energy(eV)	PG
102	−297.418136	C_1	103	−300.517946	C_1	104	−303.576439	C_1
105	−306.773455	C_s	106	−309.860784	C_1	107	−312.991830	C_s
108	−315.964908	C_s	109	−319.100302	C_1	110	−322.261377	C_1
111	−325.367188	C_1	112	−328.390553	C_1	113	−331.327112	C_1
114	−334.422411	C_s	115	−337.598496	C_1	116	−340.759024	C_s
117	−343.817038	C_1	118	−346.764630	C_1	119	−349.862568	C_1
120	−353.034842	C_2	121	−356.055763	C_1	122	−359.102294	C_2
123	−362.088084	C_1	124	−365.266998	C_1	125	−368.426994	C_1
126	−371.572700	C_1	127	−374.661505	C_1	128	−377.808061	C_1
129	−380.862378	C_3	130	−383.890586	C_1	131	−387.030763	C_1
132	−390.138328	C_2	133	−393.177026	C_s	134	−396.274720	C_2
135	−399.361340	C_s	136	−402.433300	C_s	137	−405.526322	C_s
138	−408.694151	C_{2v}	139	−411.773939	C_s	140	−414.942360	C_s
141	−418.022390	C_s	142	−421.159084	C_{2v}	143	−424.234289	C_s
144	−427.293974	C_{2v}	145	−430.398146	C_1	146	−433.528391	C_1
147	−436.702421	I_h	148	−439.807282	C_s	149	−442.741345	C_1
150	−445.909288	C_s	151	−449.086382	C_{2v}	152	−452.190934	C_s
153	−455.278091	C_{2v}	154	−458.319723	C_s	155	−461.506096	C_s
156	−464.682681	C_{3v}	157	−467.796799	C_1	158	−470.980712	C_2
159	−474.154929	C_s	160	−477.328706	D_{3h}	161	−480.408455	C_1
162	−483.573938	C_s	163	−486.653798	C_s	164	−489.818114	C_2
165	−492.896801	C_s	166	−496.054542	C_s	167	−499.123863	C_1
168	−502.260998	C_2	169	−505.328765	C_1	170	−508.459278	C_s

Table 3.3: Energies and point groups of the global minima of Aluminum clusters obtain by Doye using the Glue potential [29].

In general, the structures obtained in this manuscript are similar to those obtained by the authors of reference [30] who also used Gupta potential for their work. Nevertheless, we have noticed two differences between our results and theirs. Firstly, for $N = 9$ as an example, Gilles et *al* [30]. considered high symmetry structures and found the body-centered cubic to be lowest in energy, in disagreement with our present results. Although the body-centered cubic structure is stable, it is not the optimized structure. To verify this, we used their structure given in Figure 3.12a) as initial configuration, after a relatively long simulation time, the structure is transformed as shown in Figure 3.12c).

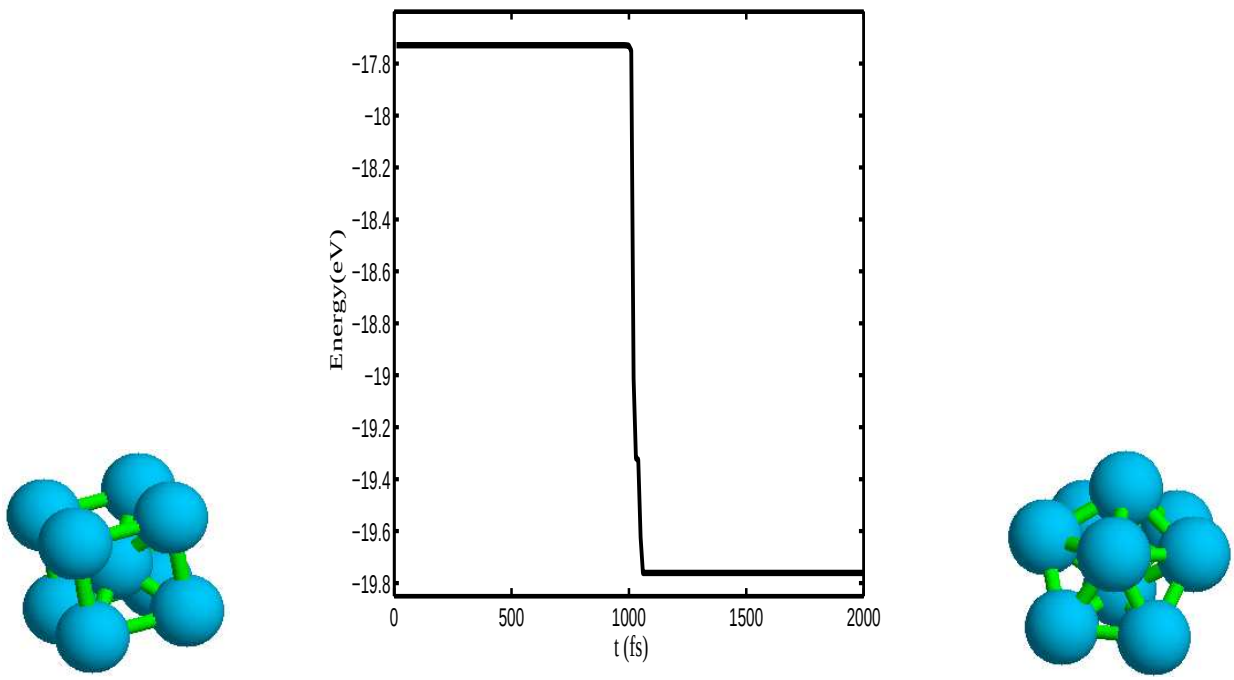

a) b) c)

Figure 3.12: a) Optimized Aℓ_9 according to Gilles et *al* [30]. b) An illustration of the evolution of the lowest-energy Aℓ_9 molecule with the Gupta potential starting from a body-centered cubic initialized coordinates. c) Optimized Aℓ_9 obtained here.

As shown in the curve of Figure 3.12b) their simulated body-centered cubic is a stable structure that is 2.0318 eV above the global minimum obtained in this manuscript, and which is, in fact, the second lowest-energy isomer. Secondly, the curve of the binding energy obtained in [30] is qualitatively similar to that obtained in this work. We believe that the quantitative differences that appear between the results are due to the values of the parameters of the potential.

In terms of absolute binding energies, our results are in good agreement with the experimental values. In comparison with some computed ones using Sutton-Chen potential, the Truhlar potential and the Cleri-Rosato potential as reported by Jasper et al. [31,32], the smallest error (0.19%) is found between our results and the experiment.

3.3.2 Aluminum Dimer Aℓ_2

Next we focus our attention on the performance of the potentials for the description of the Aℓ_2 dimer. The characterization of Aℓ_2 dimer has provided a challenge for both theory and experiment due to the closeness in energy of the singlet and triplet states. Table 3.4 shows the

equilibrium separation values for the Gupta potential, along with the values obtained using the other potentials or methods, as several ab initio and Density Functional Theory calculations, as well as experiment for comparison.

Potentials	r_2 (Å)	Precision
Sutton-Chen [151]	2.092	73.79%
Streitz-Mintmire [152]	2.207	77.85%
Cleri-Rosato [122]	2.325	82.01%
Truhlar potential (NP-B) [32]	2.523	88.99%
Gupta (this work)	2.888	98.13%
Experiment [124]	2.835	–

Table 3.4: $A\ell_2$ equilibrium separation values (r_2).

The $A\ell_2$ equilibrium separation distance as calculated using the Gupta potential agrees well with the experimental value with a precision of 98.13%. It is followed by the NP-B predicted value 82.01%, while the Sutton-Chen potential presents the lowest precision of 73.79%. This may be due to the Sutton-Chen being fitted to just structural data, which does not take into account the energetics data such as the vacancy formation energy and surface energies.

3.3.3 Aluminum Trimer $A\ell_3$

There have been several calculations of low-lying states of the Aluminum trimer. The most stable isomers have bond angles $\alpha \simeq 60^0$. Configuration interaction (CI) calculations lead either to (in C_{2v} notation) an $^2A_1$ ground state [153–155] or a near degeneracy between $^2A_1$ and $^4A_2$ states [156].

Electron spin resonance measurements of matrix isolated $A\ell_3$ shows a quartet ground state, [157] while magnetic deflection measurements shows a doublet. However, recent calculations have proven that the most stable form of $A\ell_3$ is an equilateral triangle ($^2A_1$ with the equilibrium bond length $r_e = 246.4500$ pm [158]. As presented in Figure 3.2a), our optimized configuration is also an equilateral triangle and the equilibrium bond length equals $0.9787r_0 = 296.7724$ pm ($r_0 = 303.2312$ pm).

3.3.4 Aluminum Tetramer $A\ell_4$

There have been several calculations of the aluminum tetramer, and they have led to different predictions shown in Figure 3.13.

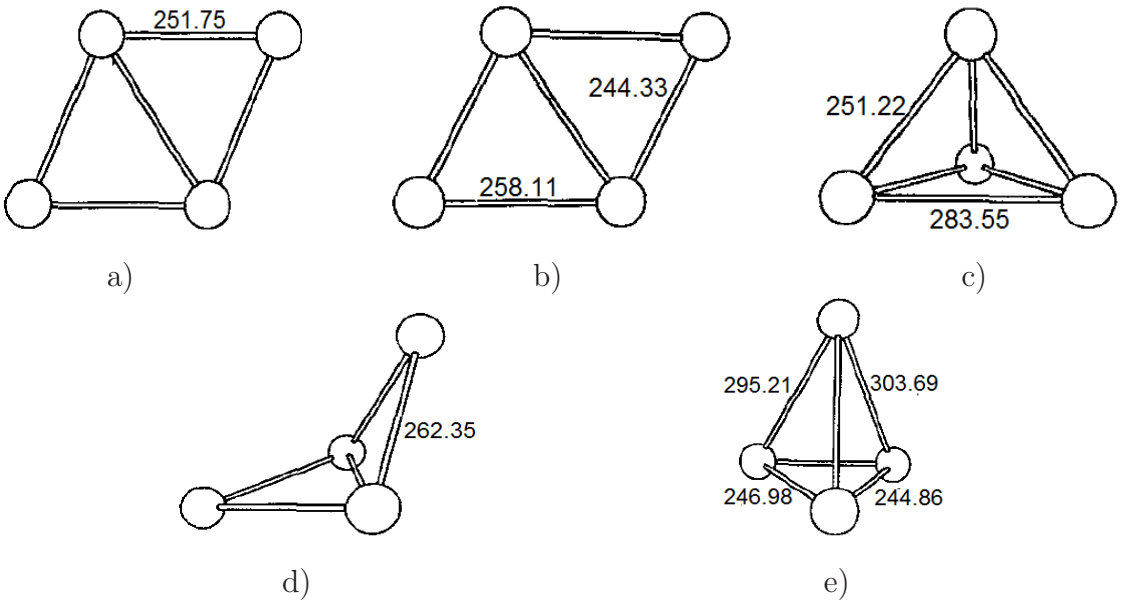

Figure 3.13: Structures of isomers of Aℓ_4. The internuclear separations are given in pm. The unmarked separations in e) are 295.21 pm and 246.98 pm [156].

- A planar rhombus structure with symmetry D_{2h} and energy -6.3851 eV has been obtained by Pettersson et al. as optimized configuration of Aℓ_4 cluster [157]. The corresponding structure is presented in Figure 3.13a) and is a planar rhombus with bond angle $\alpha = 56.5^0$.

- In the other hand, Upton predicted a three-dimensional deformed rhombus with C_{2v} symmetry as optimized configuration. Its energy equals -6.2649 eV and its structure is shown in Figure 3.13b) [156].

- Jug et al. have proposed a trigonal pyramid (C_{3v}) with the corresponding energy -5.9950 eV. Its structure presented in Figure 3.13c), is a Jahn-Teller distortion of a tetrahedron. The structure is somehow flattened from T_d symmetry [156].

- A quintet roof structure given in Figure 3.13d) with the energy -5.9338 eV and dihedral angle 122.7^0 (viewed as a distorted rhombus) has been obtained by Meier et al. [156].

- Pacchioni and Koutecky, [158] have predicted a square with symmetry D_{4h} and energy -6.1547 eV as optimized Aℓ_4 cluster.

- Finally, a singlet C_{2v} structure of Figure 3.13e) with -5.9149 eV has been presented [159]. This structure represents a tetrahedron with the opposite distortion and with the apex atom moved away from C_{3v} symmetry.

To verify this, we have done many simulations starting with different initial conditions. As shown in Figure 3.14, we have obtained three stable configurations of Aℓ_4 especially when the ring configuration is introduced as initial structure.

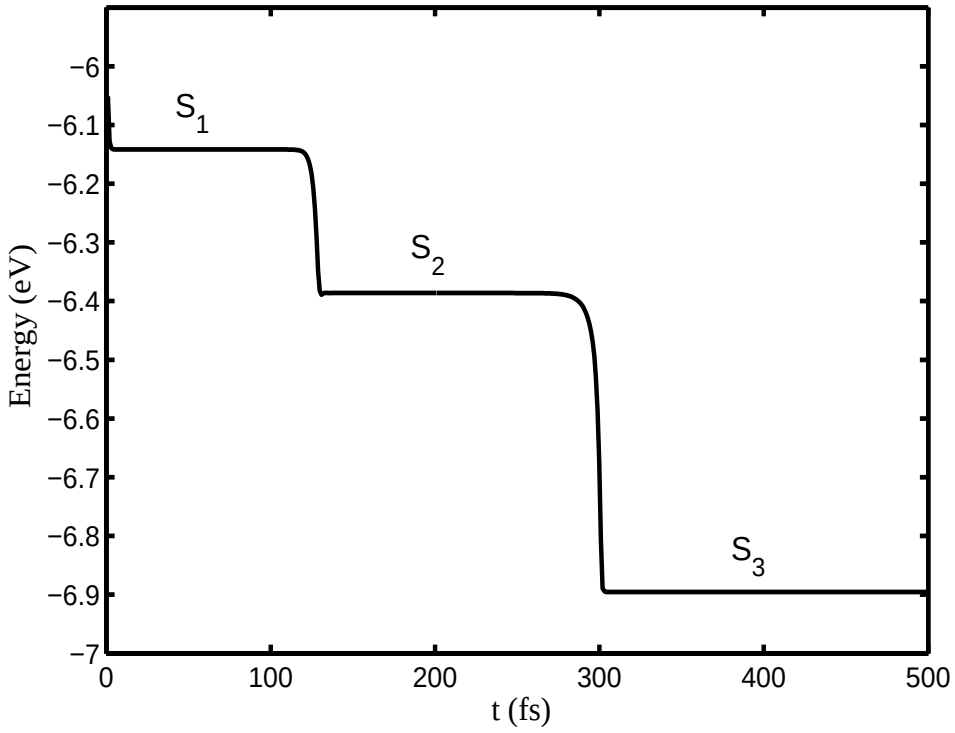

Figure 3.14: An illustration of the evolution of the lowest-energy Aℓ_4 molecule with the Gupta potential starting from a ring initialized coordinates.

In the graph, the parameters S_1, S_2 and S_3 represent the stable configurations obtained with the Gupta potential. After further investigations, we have found that a regular tetrahedron with symmetry T_d, bond length $r_4 = 301.4421$ pm and energy $E_4 = -6.8956$ eV is the most stable isomer of Aℓ_4 cluster. It is followed by a planar rhombus structure with symmetry D_{2h}, bond length $r_4 = 296.2568$ pm and energy $E_4 = -6.3863$ eV. The square structure with symmetry D_{4h}, bond length $r_4 = 294.7710$ pm and energy $E_4 = -6.1417$ eV appears to be the third isomer. The three stable isomers are depicted in Figure 3.15 with their corresponding point groups.

We can notice here that, our square and our planar rhombus structures are very closed to those obtained by Pettersson et al. and by Pacchioni and Koutecky respectively. As mentioned previously, the tetrahedral structure has been also obtained by the authors of references [29] and [30].

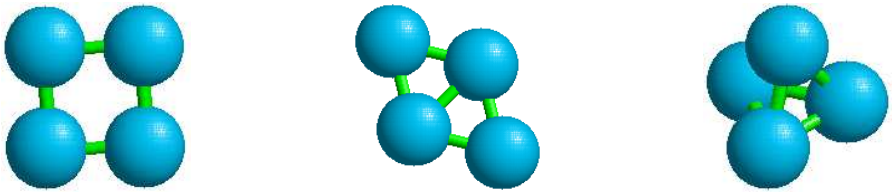

$[D_{4h}]$ a) $[D_{2h}]$ b) $[T_d]$ c)

Figure 3.15: Different isomers of Aℓ_4 obtained in this work. a) Square configuration, b) Rhombus configuration and c) Tetrahedral configuration.

3.3.5 Aluminum Pentamer $A\ell_5$.

Several studies have been carried out on Aluminum pentamer. Upton [153] found the Jahn-Teller distorted pyramidal structure (C_{2v}) to be the lowest in energy, Jug et al. [160] found that the pyramidal form (C_{4v}) was the most stable and Pettersson et al. found that a planar (C_{2v}) is more stable than the distorted pyramid which is also more stable than the regular pentagon (D_5). Similarly, Jones et al. have shown that the ideal pyramid (C_{4v}) is more stable than the planar structure but less stable than the triangular biprism D_{3h} [159].

To verify if we can obtain all these isomers with our model, we have performed different simulations starting from different initial configurations. An illustration of the evolution of the lowest-energy Aℓ_5 molecule starting from a linear initialized coordinates (black curve), from a ring initialized coordinates (blue curve) and from a pyramid coordinates (green curve) is presented in Figure 3.16.

From the graph of Figure 3.16, we can identify five different isomers named S_1, S_2, S_3, S_4 and S_5 as indicated on the curves. These isomers are presented with their point group respectively in Figures 3.17a), 3.17b), 3.17c), 3.17d) and 3.17e).

According to our simulations, the most stable isomer is the triangular biprism configuration (D_{3h}, $r_5 = 300.8963$ pm and $E_5 = -9.3471$ eV), followed by the regular pyramid (C_{4v}, $r_5 = 298.2582$ pm and $E_5 = -9.1115$ eV). After that, we have the three planar equilateral triangles (C_{2v}, $r_5 = 295.6201$ pm and $E_5 = -8.3860$ eV), the pentagon isomer (D_{5h}, $r_5 = 294.4678$ pm and $E_5 = -7.6492$ eV) and finally the linear structure ($r_5 = 288.0726$ pm and $E_5 = -6.5248$ eV). We can also notice here that, the equilibrium bond length r_5 increases with the stability of the isomer. Our obtained most stable isomer is in good agreement with the results obtained by the authors of references [29] and [30] as mentioned above.

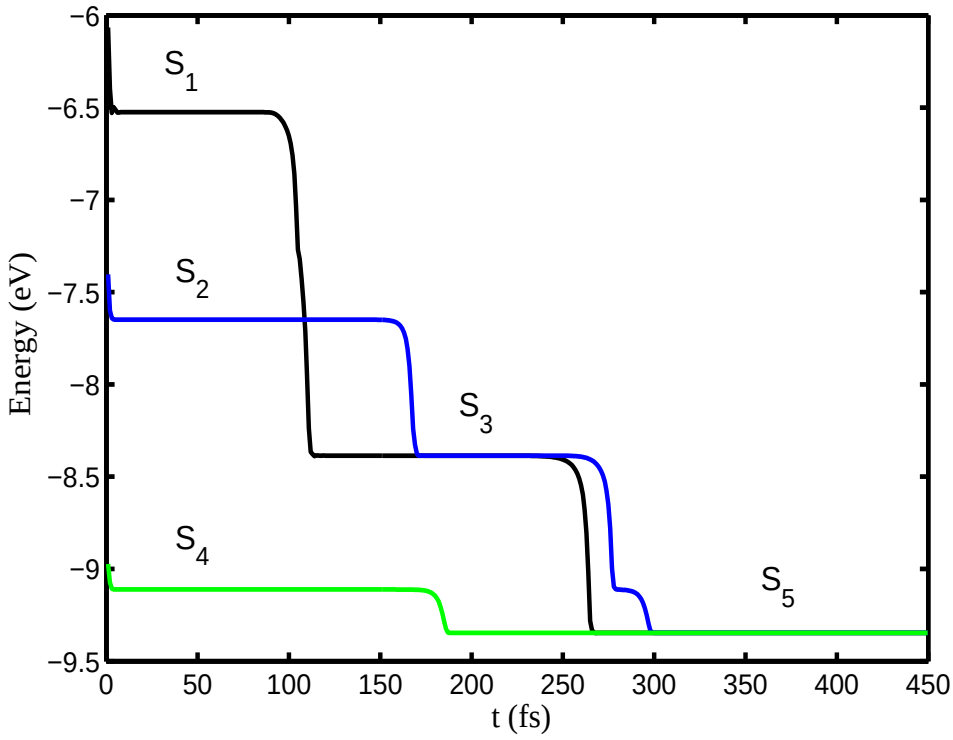

Figure 3.16: An illustration of the evolution of the lowest-energy Aℓ_5 molecule starting from a linear initialized coordinates (black curve), from a ring initialized coordinates (blue curve) and from a pyramid coordinates (green curve).

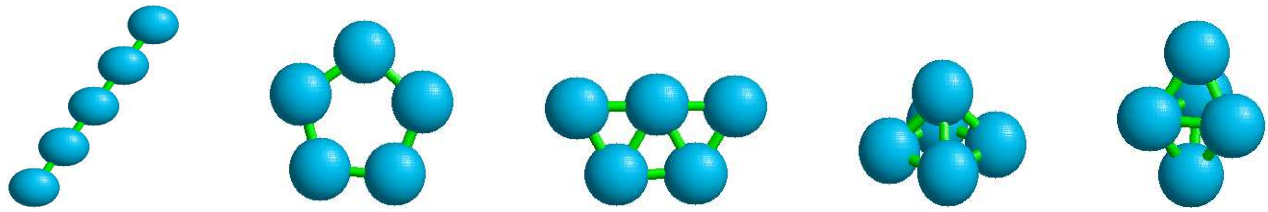

$[D_{16h}]$ $[D_{5h}]$ $[C_{2v}]$ $[C_{4v}]$ $[D_{3h}]$

a) b) c) d) e)

Figure 3.17: Different isomers of Aℓ_5 obtained in this work. a) linear configuration, b) pentagon configuration, c) three planar equilateral triangles configuration d) pyramidal structure and e) triangular biprism configuration.

3.3.6 Aluminum Hexamer $A\ell_6$.

The aluminum hexamer has been studied by a number of groups. The most stable form found by Upton [153] was a distorted octahedron, and Pettersson et al. [157] found that the octahedron was the most stable of the (symmetric) structures they studied.

The present study led to a large number of local minima, some of which and their corresponding point groups are shown in Figure 3.18.

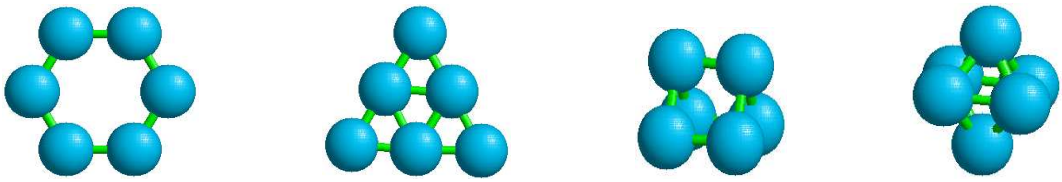

$[D_{6h}]$ a) $[D_{3h}]$ b) $[D_{3h}]$ c) $[O_h]$ d)

Figure 3.18: Different isomers of Aℓ_6 obtained in this work. a) planar hexagonal configuration, b) triangular configuration, c) prims configuration and d) octahedral configuration.

We also find that the octahedral (O_h) structure with the bond length $r_6 = 303.7467$ pm and energy $E_6 = -12.0278$ eV is the most stable isomer of Aℓ_6. The prism structure (D_{3h}) with the bond length $r_6 = 296.9240$ pm and energy $E_6 = -11.1372$ eV is our obtained second isomer. The planar triangular (D_{3h}, $r_6 = 296.0749$ pm and $E_6 = -10.3427$ eV) and hexagonal structures (D_{6h}, $r_6 = 294.7104$ pm and $E_6 = -9.0700$ eV) represent our third and fourth isomers respectively.

The first, the second and the fourth isomers are obtained when the ring is taken as initial configuration. In the other hand, if the cylinder is used as initial configuration, the third and the fourth isomers will be obtained. Also here, our results are in good agreement with those mentioned previously.

3.3.7 Aluminum Septamer $A\ell_7$

The most stable form of Aℓ_7 was predicted by Jug et al. [160] and by Raghavachari [161] to be a C_{3v} structure. Recently, a D_{5h} structure has been found to be the most stable isomer among the numerous local minima. It has been shown that the simulated C_{3v} structure is 0.4168 eV above the D_{5h} structure [162].

During our investigations, we have found that the D_{5h} structure with the bond length $r_7 = 301.6847$ pm and energy $E_7 = -14.5962$ eV is the most stable isomer of Aℓ_7. This structure is followed by two different C_{3v} structures: the first one is characterized by $r_7 = 300.6537$ pm and $E_7 = -14.4059$ eV while the second one has the following characteristics: $r_7 = 298.2582$ pm and $E_7 = -14.1794$ eV. The three isomers found in this work are shown in Figure 3.19 with their corresponding point group.

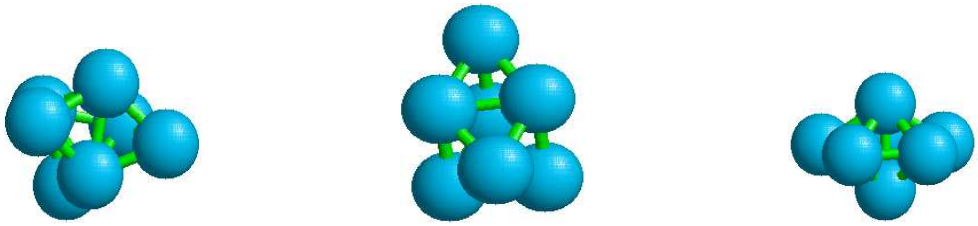

$[C_{3v}]$ a) $[C_{3v}]$ b) $[D_{5h}]$ c)

Figure 3.19: Different isomers of $A\ell_7$ obtained in this work. a) the less C_{3v} structure, b) the most C_{3v} structure and c) the D_{5h} structure.

Our D_{5h} structure shown in Figure 3.19c) is 0.4168 eV less than the structure C_{3v} shown in Figure 3.19a). Hence, our results are in good agreement with those obtained by the authors of references [160–162]. One local minimum also found between the two previously obtained is shown in Figure 3.19b) and is 0.1903 eV above the global minima.

3.3.8 Aluminum Octamer $A\ell_8$

Finally, we analyze the isomers of the octamer $A\ell_8$. For this purpose, we have done many simulations of $A\ell_8$ clusters starting from different initial configurations. An illustration of the evolution of the lowest-energy $A\ell_8$ molecule starting from a linear initialized coordinates (blue curve), from a simple cube initialized coordinates (black curve) and from a ring initialized coordinates (green curve) as shown in Figure 3.20.

The graph of Figure 3.20 reveals many isomers for $A\ell_8$ since we can identify many time intervals where the curves have constant behavior. We have selected seven isomers and their pictures are depicted in Figure 3.21.

The isomers shown in Figures 3.21a), 3.21b), 3.21c), 3.21d), 3.21e), 3.21f) and 3.21g) have the following energies -14.0131 eV, -14.2975 eV, -14.3460 eV, -15.5112 eV, -16.5919 eV, -16.9825 eV and -17.0885 eV respectively. Their corresponding bond lengths are given respectively as follows: 296.1659 pm, 294.5891 pm, 295.3169 pm, 297.3182 pm, 300.0473 pm, 298.4401 pm and 302.7157 pm. The large number of local minima in the energy surface for $A\ell_8$ indicates how difficult it would be to find the structures of all the stable isomers of larger clusters.

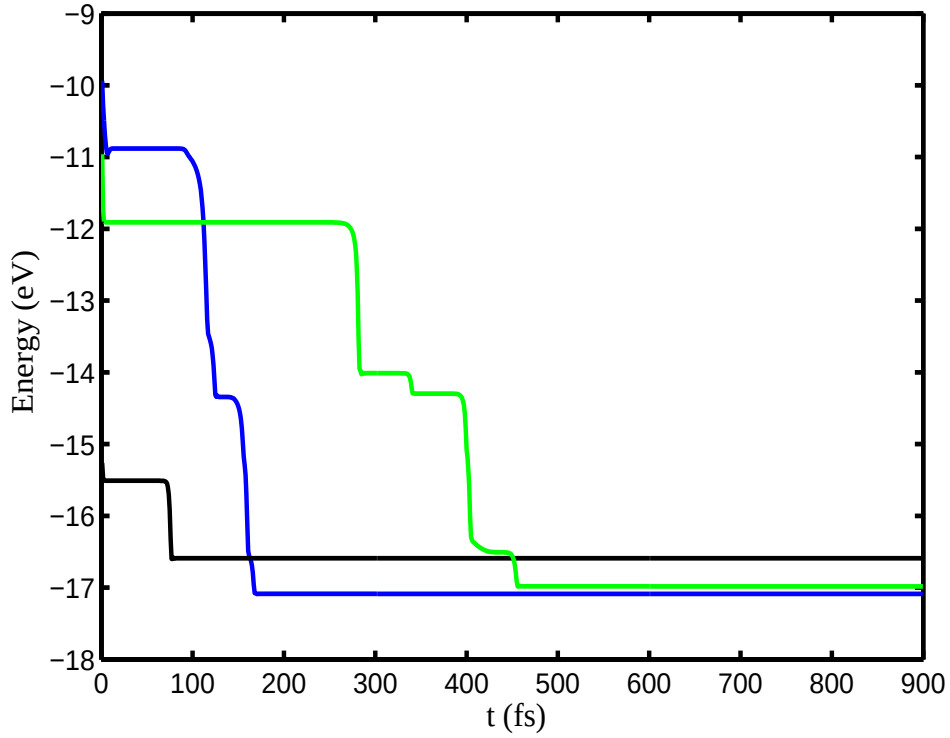

Figure 3.20: An illustration of the evolution of the lowest-energy Aℓ_8 molecule starting from a linear initialized coordinates (blue curve), from a simple cube initialized coordinates (black curve) and from a ring initialized coordinates (green curve).

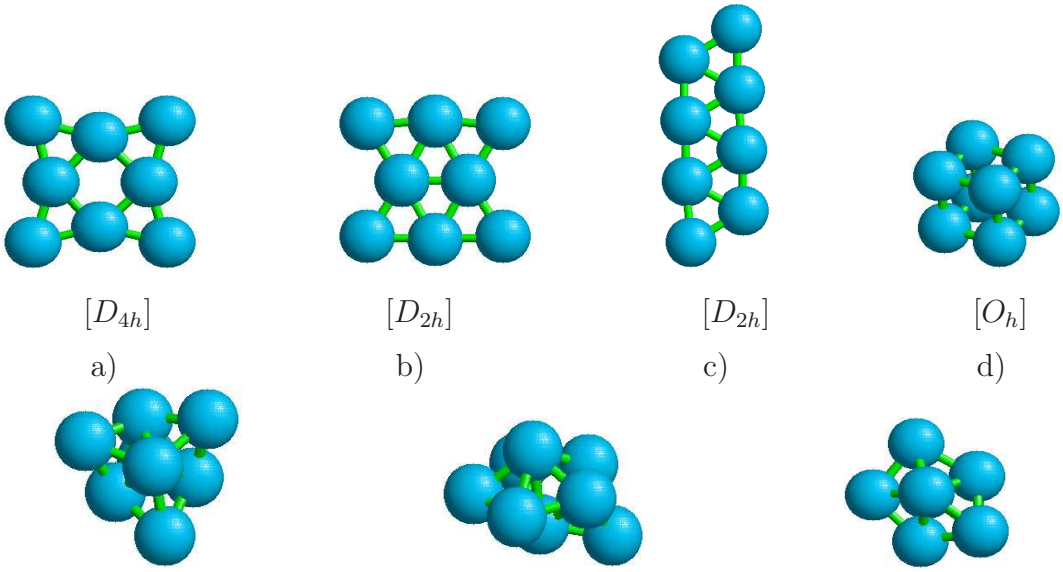

Figure 3.21: Different isomers of Aℓ_8 obtained in this work and listed according to their symmetry. a) [D_{4h}], b) [D_{2h}], c) [D_{2h}], d) [O_h], e) [O_h], d) [C_s] and e) [C_{2v}].

Conclusion

The dimer and trimer have been used to established a relation of P and B in terms of q and A, such that from the cohesive energy and lattice parameter of aluminium cluster, q and A would be obtained and hence P and B are fitted. The Gupta parameters have been used to plot the potential energy and force curves for the dimer, to show that for the potential energy curve, there exist an equilibrium position, $r_2 = 0.9524r_0$, below which the potential energy decreases rapidly and above which this energy increases slowly. For the force curve, $r_2 = 1.1085r_0$, is such that below this value, the force between the pair of atoms is repulsive and above this value, the force is attractive.

The $A\ell_3$, $A\ell_{50}$, $A\ell_{100}$ and $A\ell_{150}$ have further been optimized with the obtained Gupta parameters using different initial configurations in each case to obtain the same final configuration, with the linear initialized configuration taking the longest time to reach this stable configuration. From here, the Gupta parameter have then been used to obtain the ground state energy, geometry, point group and bond length of each $A\ell$ cluster in the range $3 \leq N \leq 170$. From these energies, a mathematical relation have been established to analytically calculate the ground state energy of any $A\ell$ size without need of any numerical simulation. Through the obtained average binding energy relations, the stability of $A\ell$ clusters have been analyzed. Some structures have shown extremely high stabilities at N = 4, 6, 13, 14, 19, 23, 35, 53, 55, 56, 146, 147 and 148 for $3 \leq N \leq 170$. From the lattice constant and the obtain bond length, the value of r_0 have been determined to be $r_0 = 303.2312pm$.

A total of 15 symmetry groups have been obtained namely: D_{3h}, T_d, O_h, D_{5h}, C_{2v}, C_{3v}, C_{5v}, I_h, C_s, C_2, C_1, D_{6h}, C_{6v}, S_4, and C_3. Furthermore, basing on the average binding energy of aluminum clusters, results obtained using the Gupta potential are slightly higher than those obtained with the Glue potential. In addition, these results with Gupta potential have shown an error of just 0.19% compared to the relatively large error of 1.11% shown by the Glue potential. Gupta potential together with these new parameters have proven that the high symmetry body centered cubic $A\ell_9$ cluster is not the most stable as mentioned by Gilles et *al* but that it is the second in terms of lowest energy. Furthermore, this Gupta potential have obtained the equilibrium separation of the dimer ($A\ell_2$) with the best precision (98.13%) compared to those obtained by Sutton-Chen (73.79%), Streitz-Mintmire (77.85%), Cleri-Rosato (82.01%) and Truhlar potential (88.99%). Lastly, the octamer ($A\ell_8$) have been used to show how difficult it is to locate all the local minima as the cluster size increases.

GENERAL CONCLUSION AND PERSPECTIVES

GENERAL CONCLUSION

This work has been based on the determination of the structures and the ground state energies of aluminum clusters ($3 \leq N \leq 170$) through the classical molecular dynamics method with the Gupta potential as the interatomic potential. As a result, the non relativistic Schrödinger equation used to determine the ground state electronic properties of our system have been described. A dimensionless equation of motion have been established to represent the mathematical model of our system. Suitable reasons for using the Gupta potential here have been sorted. Detail steps for updating the position and velocities for a given time step in the verlet algorithm have clearly been made. In addition, the cubic and hexagonal unit cells used to generate our lattices for assigning our initial conditions have also been explained. The convergence criteria have been based on the multiple independent simulation of four different initial configurations and the system has been considered to be in equilibrium only when it remains below a certain pre-chosen threshold. The verlet algorithm with the multiple independent simulation method have been summarized in a flow chart. Using the following steps in the Basin hopping method, angular move and random displacement, seeding, quasi Newton minimization algorithm and quenching, the local minima have been efficiently searched at reduced computing time with the assurance that the actual or final ground state is at thermal equilibrium and that any resulting potential energy surface does not change the global minimum of the local minima. The symmetry elements of each point group have been summarized. Lastly, the role played by each of these softwares in this work (Fortran 90, Chemcraft, Rastop and Matlab), has been summarized.

The dimer and the trimer have been used to established a relation of P and B in terms of q and A, such that from the cohesive energy and lattice parameter of aluminum cluster, q and A would be obtained and hence P and B are fitted. The Gupta parameters have been

used to plot the potential energy and force curves for the dimer, to show that for the potential energy curve, there exist an equilibrium position, $r_2 = 0.9524r_0$, below which the potential energy decreases rapidly and above which this energy increases slowly. For the force curve, $r_2 = 1.1085r_0$, is such that below this value, the force between the pair of atoms is repulsive and above this value, the force is attractive. The $A\ell_3$, $A\ell_{50}$, $A\ell_{100}$ and $A\ell_{150}$ have further been optimized with the obtained Gupta parameters using different initial configurations in each case to obtain the same final configuration, with the linear initialized configuration taking the longest time to reach this stable configuration. From here, the Gupta parameters have then been used to obtain the ground state energy, geometry, point group and bond length of each $A\ell$ cluster in the range $3 \leq N \leq 170$.

From these energies, a mathematical relation has been established to analytically calculate the ground state energy of any $A\ell$ cluster size without need of any numerical simulation. Through the obtained average binding energy relations, the stability of $A\ell$ clusters has been analyzed. Some structures have shown extremely high stabilities at $N = 4$, 6, 13, 14, 19, 23, 35, 53, 55, 56, 146, 147 and 148 for $3 \leq N \leq 170$. From the lattice constant and the obtain bond length, the value of r_0 has been determined to be $r_0 = 303.2312pm$. A total of 15 symmetry groups have been obtained namely: D_{3h}, T_d, O_h, D_{5h}, C_{2v}, C_{3v}, C_{5v}, I_h, C_s, C_2, C_1, D_{6h}, C_{6v}, S_4, and C_3. Furthermore, basing on the average binding energy of aluminum clusters, results obtained using the Gupta potential are slightly higher than those obtained with the Glue potential. In addition, these results with Gupta potential have shown an error of just 0.19% compared to the relatively large error of 1.11% shown by the Glue potential. Gupta potential together with these new parameters have proven that the high symmetry body centered cubic $A\ell_9$ cluster is not the most stable as mentioned by Gilles et *al* but that it is the second in terms of lowest energy. Furthermore, with this Gupta potential, we have obtained the equilibrium separation of the dimer ($A\ell_2$) with the best precision (98.13%) compared to those obtained by Sutton-Chen (73.79%), Streitz-Mintmire (77.85%), Cleri-Rosato (82.01%) and Truhlar potential (88.99%). Lastly, the octamer ($A\ell_8$) has been used to show how difficult it is to locate all the local minima as the cluster size increases. Finally, it is logical to conclude that the study of the structure and stability of aluminum clusters using the Gupta potential has permitted us to solve some among the many worries about clusters and those of aluminum in particular.

PERSPECTIVES

In our future plan of research, we shall include the following:

• Determination of the optimized configurations of other atoms and doped materials.

• The analysis of the physical properties of some clusters as well as the thermodynamic properties of pure $A\ell$ clusters and some $A\ell$ clusters.

Bibliography

[1] D. Altenpohl, Aluminum: Technology, Applications and Environment, the Aluminum Association Inc. and TMS, (1998) 86-93 .

[2] G. H. Wang, Cluster Physics. J. Shanghai Science and Technology Press, Shanghai, (2003).

[3] A. Aguado, J. M. Lt'opez, Phys. Rev. B 72 (2005) 205-420.

[4] W. A. Jesser, R. Z. Shneck, W. W. Gile, Phys. Rev. B 69 (2004) 144-121.

[5] Y. Feng, H. M. Duan, J. At. Mol. Phys. 28 (2011) 251.

[6] Z. M.Wu, L. Liu, X. Q. Wang, J. At. Mol. Phys. 27 (2010) 444.

[7] M. Schmidt, R. Kusche, T. Hippler et al, Phys. Rev. Lett. 86 (2001) 1191.

[8] G. A. Breaux, R. C. Benirschke, T. Sugai et al, Phys. Rev. Lett. 91 (2003) 215508.

[9] D.E. Bergeron, P.J. Roach, A.W. Castleman, N. Jones, S.N. Khanna, Science 307 (2005) 231.

[10] R. Moro, S. Yin, X. Xu, A.D.H. Walt, Phys. Rev. Lett. 93 (2004) 086803.

[11] F. Baletto, R. Ferrando, Rev. Mod. Phys. 77 (2005) 371.

[12] X. Li, H.B. Wu, X.B. Wang, L.S. Wang, Phys. Rev. Lett. 81 (1998) 1909.

[13] S.S. Kushvaha, Z. Yan, W. Xiao, M.J. Xu, Q.K. Xue, X.S. Wang, Nanotechnology 18 (2007) 145501.

[14] J. Kanzow, P.S. Horn, M. Kirschmann, V. Zaporojtchenko, K. Dolgner K F. Faupel, C. Wehlack, W. Possart, Appl. Surf. Sci. 239 (2005) 227.

[15] B.P. Cao, C. M. Neal, A.K. Starace, Y.N. Ovchinnikov, V.Z. Kresin, M.F. Jarrold, J. Supercond. Nov. Magn. 21 (2008) 163.

[16] D.G. Salinas, S. Gueron, D.C. Ralph, C.T. Black, M. Tinkham Phys. Rev. B 60 (1999) 6137.

[17] D.J. Wales, P.K.D. Jonathan, Phys. Chem. 101 (1997).

[18] S. Goedecker, W. Hellmann, T. Lenosky, Phys. Rev. Lett. 95 (2005) 55501.

[19] R.S. Berry, R.E. Kunz, T.P. Martin, Kluwer, Dordrecht (1996) pp. 299.

[20] P.K.D. Jonathan, Comput. Mater. Sci. 35 (2006) 227.

[21] P.K.D. Jonathan, C. Florent, Phys. Rev. Lett. 86 (2001) 3570.

[22] A. W. Castleman, Jr. and K. H. Bowen, J. Phys. Chem. 100 (1996) 12911.

[23] H. H. Anderson Springer, Journal of American Chemical society. 119 (1997) 3792-3796.

[24] K. Sattler, physical review letters. 77 (1996) 3573.

[25] H. W. Kroto, J. R. Heath, S. C. O Brien, R. F. Curl, and R. E. Smalley, Nature London. 318 (1985) 162.

[26] B. C. Guo, K. P. Kerns, A. W. Castleman, Science 255 (1992) 1411.

[27] S. N. Khanna, P. Jena, Phys. Rev. Lett. 69 (1992) 1664.

[28] D.L. Lesley, R.L. Johnston, Journal of Chemical physics. 122 (2005) 194308.

[29] P.K.D. Jonathan, University Chemical Laboratory, Lensfield Road, Cambridge CB2 1EW, United Kingdom, 2008.

[30] W.T. Giles, L.J. Roy, T.W. Nicholas, Chem. Phys. 112 (2000) 4773.

[31] A.W. Jasper, P. Staszewski, G. Staszewska, N.E. Schultz, D.G. Truhlar, Phys. Chem. B 108 (2004) 8996.

[32] A.W. Jasper, N.E. Schultz, D.G. Truhlar, Phys. Chem. B 109 (2005) 3915.

[33] D. E. Bergeron, A. W. Castleman, T. Morisato, and S. N. Khanna, Science 304 (2004) 84.

[34] D. E. Bergeron, A. W. Castleman, N. O. Jones, and S. N. Khanna, Nano Lett. 4 (2004) 261.

[35] M. Schmidt, R. Kusche, B. von Issendorff et al, Nature 393 (1998) 238.

[36] G. A. Breaux, B. Cao, and M. F. Jarrold, J. Phys. Chem. B 109 (2005) 16575.

[37] D. M. Cox, D. J. Trevor, R. L.Whetten et al, J. Chem. Phys. 84 (1986) 4561.

[38] X. G. Gong, V. Kumar, Phys. Rev. Lett. 70 (1993) 2078.

[39] F. S. Himojo, S. O. Hmura, R. K. Kalia et al, Phys. Rev. Lett. 104 (2010) 126102.

[40] C. M. Neal, A. K. Starace, M. F. Jarrold, Phys. Rev. B 76 (2007) 54113.

[41] A. K. Starace, B. Cao, O. H. Judd et al, J. Chem. Phys. 132 (2010) 34302.

[42] W. D. Knight, K. Clememger, W. A. de Heer, W. A. Saunders, M. Y. Chou, M. L. Cohen, Phys. Rev. Lett. 52 (1984) 2141.

[43] T. P. Martin, T. Bergmann, H. Gohlich, T. Lange, Chem. Phys. Lett. 172 (1990) 209.

[44] H. Hakkinen, M. Manninen, Phys. Rev. B 52 (1995) 1540.

[45] T. P. Martin, Phys. Rep. 273 (1996) 199.

[46] J. Lermé, M. Pellarin, B. Baguenard, C. Bordas, E. Cottancin, J. L. Vialle, M. Broyer, Large Clustrs of atoms and molecules, Springer (1996) 71-88.

[47] K. E. Schriver, J. L. Persson, E. C. Honea, R. L. Whetten, Phys. Rev. Lett. 64 (1990) 2539.

[48] P. Milani, W. de Heer, A. Châtelain, Z. Phys. D 19 (1991) 133.

[49] B. Baguenard, M. Pellarin, J. Lermé, J. L. Vialle, M. Broyer, J. Chem. Phys. 100 (1994) 754.

[50] T. P. Martin, U. Näher, H. Schaber, U. Zimmermann, J. Chem. Phys. 100 (1994) 2322.

[51] W. A. de Heer, W. D. Knight, M. Y. Chou, M. L. Cohen, Solid State Phys. 40 (1987) 93 .

[52] R. E. Leuchtner, A. C. Harms, A. W. Castleman, J. Chem. Phys. 91 (1989) 2753 .

[53] W. D. Schone, W. Ekardt, J. M. Pacheco, Phys. Rev. B 50 (1994) 11079 .

[54] L. D. Marks, Rep. Prog. Phys. 57 (1994) 603 .

[55] G. Schmid, V. Maihack, F. Lantermann, S. Peschel, J. Chem. Soc., Dalton Trans. (1996) 589.

[56] G. M. Francis, I. M. Goldby, L. Kuipers, B. von Issendorf, R. E. Palmer, J. Chem. Soc., Dalton Trans.(1996) 665.

[57] M. Faraday, Phil. Trans. R. Soc. Lond. 147 (1857) 145 .

[58] G. Schmid, Chem. Rev. 92 (1992) 1709 .

[59] T. S. Ahmadi, Z. L. Wang, T. C. Green, A. Henglein, M. A. El-Sayed, Science 272 (1996) 1924 .

[60] R. L. Whetten, J. T. Khoury, M. M. Alvarez, S. Murty, I. Vezmar, Z. L. Wang, P. W. Stephens, C. L. Cleveland, W. D. Luedtke, U. Landman, Adv. Mater. 8 (1996) 428 .

[61] Z. Y. Chen, A. W. Castleman, J. Chem. Phys. 98, 1 (1993) 231-235.

[62] Q. Sun, B. K. Rao, P. Jena, D. Stolcic, Y. D. Kim, G. Gantefor, A. W. Castleman, J. Chem. Phys. 121, 19 (2004) 9417-9422.

[63] B. v. Issendorff, O. Cheshnovsky, Ann. Rev. Phys. Chem. 56, 1 (2005) 549-580.

[64] J. Bowlan, A. Liang, W. A. de Heer, Phys. Rev. Lett. 106 (2011) 043401.

[65] B. K. Rao, P. Jena, J. Chem. Phys. 111, 5 (1999) 1890-1904.

[66] O. C. Thomas, W. Zheng, S. Xu, K. H. Bowen, Phys. Rev. Lett. 89 (2002) 213403.

[67] P. H. Acioli, Jellinek, J. Phys. Rev. Lett. 89 (2002) 213402.

[68] S. K. Nayak, S. N. Khanna, B. K. Rao, P. Jena, J. Phys. Chem. A 101, 6 (1997) 1072-1080.

[69] K. Selby, V. Kresin, J. Masui, M. Vollmer, W. A. de Heer, A. Scheidemann, W. D. Knight, Phys. Rev. B 43 (1991) 4565-4572.

[70] C. R. C. Wang, S. Pollack, D. Cameron, M. M. Kappes, J. Chem. Phys. 93, 6 (1990) 3787-3801.

[71] G. Pal, Y. Pavlyukh, W. Hübner, H. C. Schneider, J. Eur. Phys. B 79, 3 (2011) 327-334.

[72] I.Boustani, W. Pewestorf, P.Fantucci, V. B.Koutecký, Koutecký, J. Phys. Rev. B 35 (1987) 9437-9450.

[73] J. M. Pacheco, J. L. Martins, J. Chem. Phys. 106, 14 (1997) 6039-6044.

[74] R. Pandey, B.Rao, P. Jena, J. M. Newsam, Chem. Phys. Lett. 321, 1-2 (2000) 142-150.

[75] R. Pandey, B. K. Rao, P. Jena, M. A. Blanco, J. Am. Chem. Soc. 123, 16 (2001) 3799-3808.

[76] B. K. Rao, P. Jena, J. Chem. Phys. 116, 4 (2002) 1343-1349.

[77] T. Kurikawa, H. Takeda, M. Hirano, K. Judai, T. Arita, S. Nagao, A. Nakajima, K. Kaya, 18, 8 (1999) 1430 − 1438.

[78] M. Sodupe, C. W. Bauschlicher, J. Phys. Chem. 95, 22 (1991) 8640-8645.

[79] M.Sodupe, C. W. Bauschlicher, S. R. Langhoff, H. Partridge, J. Phys. Chem. 96, 5 (1992) 2118-2122.

[80] C. W. Bauschlicher, H. Partridge, S. R. Langhoff, J. Phys. Chem. 96, 8 (1992) 3273-3278.

[81] A. K. Kandalam, B. K. Rao, P. Jena, R. Pandey, J. Chem. Phys. 120, 22 (2004) 10414-10422.

[82] M. Walter, J. Akola, O. Lopez-Acevedo, P. D. Jadzinsky, G. Calero, C. J. Ackerson, R. L. Whetten, H. Gronbeck, H. Hakkinen, Proc. Nat. Acad. Sci. 105, 27 (2008) 9157-9162.

[83] J. W. Buchanan, J. E.Reddic, G. A. Grieves, M. A. Duncan, J. Phys. Chem. A 102, 32 (1998) 6390-6394.

[84] P. Jena, J. Phys. Chem. Lett. 4, 9 (2013) 1432-1442.

[85] S. Khanna, P. Jena, Chem. Phys. Lett. 219, 5 to 6 (1994) 479-483.

[86] W. J. Zheng, O. C. Thomas, T. P. Lippa, S. J. Xu, K. H. Bowen, J. Chem. Phys. 124 (2006) 14 .

[87] P. Lievens, P. Thoen, S. Bouckaert, W. Bouwen, F. Vanhoutte, H. Weidele, R. E. Silverans, A. Navarro Vázquez, P. Von Ragué Schleyer, J. Chem. Phys. 110, 21 (1999) 10316-10329.

[88] S. Freza, P. Skurski, Chem. Phys. Lett. 487, 1 to 3 (2010) 19-23.

[89] H. J. Zhai, B. Kiran, J. Li, L. S. Wang, Nature Mat. 2 (2003) 827.

[90] M. A. Tofanelli, C. J. Ackerson, J. Am. Chem. Soc. 134, 41 (2012) 16937-16940.

[91] A. N. Alexandrova, A. I. Boldyrev, H. J. Zhai, L. S. Wang, Coord. Chem. Rev. 250, 21-22 (2006) 2811.

[92] A. N. Alexandrova, H. J. Zhai, L. S. Wang, A. I. Boldyrev, Inorg. Chem. 43, 12 (2004) 3552-3554.

[93] H. J. Zhai, A. N. Alexandrova, K. A. Birch, A. I.Boldyrev, L. S.Wang, Angew. Chem. Int. Ed. 42 (2003) 6004.

[94] C. Romanescu, T. R. Galeev, W. L. Li, A. I. Boldyrev, L. S. Wang, Angew. Chem. Int. Ed. 50, 40 (2011) 9334.

[95] B. Kiran, S. Bulusu, H. J. Zhai, S. Yoo, X. C. Zeng, L. S. Wang, Proc. Nat. Acad. Sci. 102, 4 (2005) 961.

[96] D. E. Bean, P. W.Fowler, J. Phys. Chem. C 113, 35 (2009) 15569-15575.

[97] J. I. Aihara, H. Kanno, T. Ishida, J. Am. Chem. Soc. 127, 38 (2005) 13324-13330.

[98] S. Sahu, A. Shukla, Nano. Res. Lett 5, 4 (2010) 714-719.

[99] X. Li, A. E. Kuznetsov, H.F. Zhang, A. I. Boldyrev, L. S. Wang, Science 291, 5505 (2001) 859- 861.

[100] A. E. Kuznetsov, K. A. Birch, A. I. Boldyrev, X. Li, H. J. Zhai, L. S. Wang, Science 300, 5619 (2003) 622-625.

[101] G. Merino, T. Heine, Chem. Int. Ed. 51, 41 (2012) 10226-10227.

[102] J. Zhang, A. P. Sergeeva, M. Sparta, A. Alexandrova, Chem. Int. Ed. 51, 34 (2012) 8512-8515.

[103] N. D. Lang, Solid State Commun. 7, 15 (1969) 1047-1050.

[104] N. D. Lang, W. Kohn, Phys. Rev. B. 3(4) (1970) 1215-223.

[105] N. D. Lang, W. Kohn, Phys. Rev. B. 8(12) (1973) 6010-6012.

[106] D. M. Ceperley, B. J. Alder, Phys. Rev. Lett. 45 (7) (1980) 566-569.

[107] J. P. Perdew, E. R. McMullen, Zunger, Alex. Phys. Rev. A. 23 (6) (1981) 2785-2789.

[108] W. D. Knight, K. Clemenger, W. A. de Heer, W. A. Saunders, M. Y. Chou, M. L. Cohen, Phys. Rev. Lett. 52 (1984) 2141.

[109] K. Clemenger, Phys. Rev. B 32 (1985) 1359 .

[110] T. P. Martin, T. Bergmann, H. Göhlich, T. Lange, Chem. Phys. Lett. 172 (1990) 209.

[111] T. P. Martin, U. Näher, H. Schaber, U. Zimmermann, J. Chem. Phys. 100 (1994) 2322.

[112] J. Pedersen, S. Bjørnholm, J. Borggreen, K. Hansen, T. P. Martin, H. D. Rasmussen, Nature 353 (1991) 733.

[113] T. P. Martin, U. Näher, H. Schaber, Chem. Phys. Lett. 199 (1992) 470.

[114] B. Baguenard, M. Pellarin, J. Lermé, J. L. Vialle, M. Broyer, J. Chem. Phys. 100 (1994) 754.

[115] D. Rayane, P. Melinon, B. Cabaud, A. Horeau, B. Tribolet, M. Broyer, Phys. Rev. A 39 (1989) 6056.

[116] T. P. Martin, T. Bergmann, H. Gohlich, T. Lange, Chem. Phys. Lett. 176 (1991) 343.

[117] T. P. Martin, U. Näher, T. Bergmann, H. Göhlich, T. Lange, Chem. Phys. Lett. 183 (1991) 119.

[118] Cruz, J.A.L. Fernando, Lopes, N. José Canongia, Calado, C.G. Jorge. Fluid Phase Equilibria. 241 1-2 (2006) 51-58.

[119] Jump up to:a b Justo, J. F. Bazant, M. Z. Kaxiras, E. Bulatov, V. V. Yip, S. Phys. Rev. B. 58 5 (1998) 2539-2550.

[120] Tersoff, J. Physical Review B. 39 8 (1989) 5566-5568.

[121] M. S. Daw, S. Murray Foiles, M. Stephen Baskes, I. Michael, Materials Science Reports. 9 7-8 (1993) 251-310.

[122] F. Cleri, V. Rosato, Physical Review B. 48 1 (1993) 22-33.

[123] I. A. Solov'yov et al, Springer International Publishing AG (2017).

[124] S.R. Langhoff, J.C.W. Bauschlicher, Chem. Phys. 92 (1990) 1879.

[125] R.P. Gupta, Phys. Rev. B 23 (1981) 6265-70.

[126] S. Nouemo, F. Tchoffo, J.M.B. Ndjaka, S. Domngang, Journal of Taibah University for Science 10 (2016) 430.

[127] A. E. Carlsson Solid State Physics vol 43 New York Academic (1990).

[128] M. S. Daw, M. I. Baskes, Phys. Rev. Lett. 50 (1983) 1285-8.

[129] M. W. Finnis, J. E. Sinclair, Phil. Mag. A 50 (1984) 45-55.

[130] F. Ercolessi, E. Tosatti, M. Parrinello, Phys. Rev. Lett. 57 (1986) 719-22.

[131] J. H. Li, X. D. Dai, S. H. Liang, K .P. Tai, Y. Kong, B. X. Liu, Phys. Rep. 455 (2008) 1-134.

[132] C. Rey, L. J. Gallego, J. GarcýaRodeja, J. A. Alonso, M. P. niguez, Phys. Rev. B 48 (1993) 8253-62.

[133] K. Michaelian, N. Rendón, I.L. Garzón, Phys. Rev. B 60 (1999) 2000.

[134] J. Guevara, A. M. Llois, M. Weissmann, Phys. Rev. B 52 (1995) 11509-16.

[135] F. Willaime, C. Massobrio, Phys. Rev. B 43 (1991) 11653-65.

[136] D. Frenkel, B. Smith, Academic Press. New York, 1996.

[137] L. Zhigilei, University of Virginia, MSE 4270-6270.

[138] B. Knapp, S. Frantal, M. Cibena, W. Schreiner, P. Bauer, Journal of Computational biology 18 (2011) 8.

[139] D. J. Wales, J. P. K. Doye, J. Phys. Chem. A 101 (1997) 5111.

[140] Z. Li, H. A. Scheraga, Proc. Natl. Acad. Sci. U.S.A. 84 (1987) 6611.

[141] D. Liu, J. Nocedal, Math. Program. B 45 (1989) 503.

[142] P.W. Atkins, M.S. Child, C.S.G. Phillips, Oxford University Press, Oxford 1970.

[143] Guide, Compaq Visual Fortran programmer, Houston, Texas. August (2000).

[144] Jorio, Ado and Kasperczyk, Nano letters. 14 (2014) 5687-5692.

[145] W.A. de Heer, Rev. Mod. Phys. 65 (1993) 611.

[146] M.F. Jarrold, D.H. Russell, Plenum, New York, 1989.

[147] M.Y. Chou, M.L. Cohen, Phys. Lett. A 113 (1986) 420.

[148] E.G. Noya, J.P.K. Doye. Physical Review B73 (2006) 125-407.

[149] A. Aguadoa, J. M. Lpez. Journal of Chemical Physics 130 (2009) 064-704.

[150] S.N. Khanna, B.K. Rao, P. Jena, Phys. Rev. B 65, (2002) 125105.

[151] A.P. Sutton, J. Chen, Phil. Mag. Let. 61 (1990) 139.

[152] F.H. Streitz, J.W. Mintmire, Phys. Rev. B 50 (1994) 11996.

[153] T. H. Upton, J. Chern. Phys. 86 (1987) 7054 .

[154] H. Basch, Chern. Phys. Lett. 136 (1987) 289.

[155] J. S. Tse, J. Mol. Struct. Theochem 165 (1988) 21.

[156] U. Meier, S. D. Peyerimhoff, F. Grein, Z. Phys. D 17 (1990) 209.

[157] L. G. M. Petterson, C. W. Bauschlicher, T. Halicioglu, J. Chern. Phys. 87 (1987) 2205 .

[158] J. A. Howard, R. Sutcliffe, J. S. Tse, H. Dahmane, B. Mile, J. Phys. Chern. 89 (1985) 3595.

[159] R. O. Jones, J. Chern. Phys. 99 (1993) 15.

[160] K. Jug, H. P. Schluff, H. Kupka, R. Iffert, J. Comput. Chern. 9 (1988) 803.

[161] K. Raghavachari, Bull. Am. Phys. Soc. 35 (1990) 606 .

[162] G. Pacchioni, J. Koutecky, B. Bunsenges. Phys. Chern. 88 (1984) 242.

Below are the optimized structures of all the aluminium clusters with their point groups obtained using Molecular dynamics with Gupta potential, ranging from 3 to 170, with exception of those already presented in chapter3.

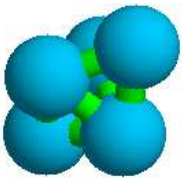

$A\ell_5$, $[D_{3h}]$

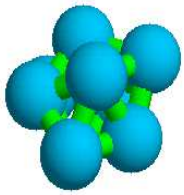

$A\ell_9$, $[C_{2v}]$

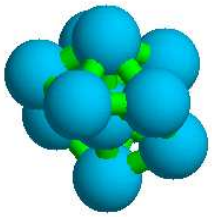

$A\ell_{11}$, $[C_{2v}]$

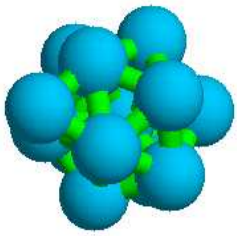

$A\ell_{14}$, $[C_s]$

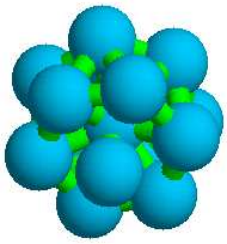

$A\ell_{15}$, $[C_{2v}]$

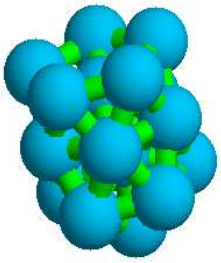

$A\ell_{18}$, $[C_s]$

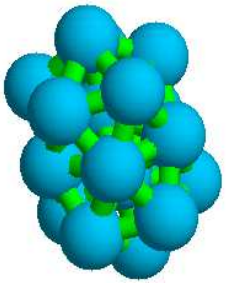

$A\ell_{19}$, $[D_{5h}]$

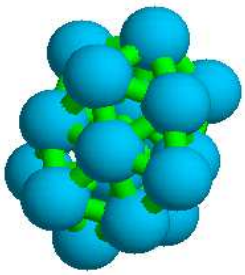

$A\ell_{20}$, $[C_s]$

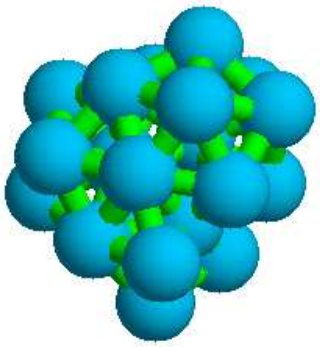

$A\ell_{22}$, $[C_s]$

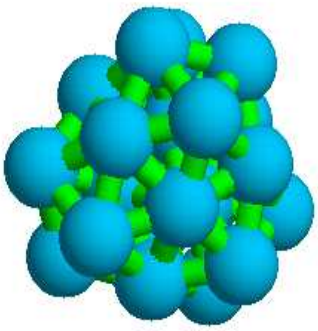

$A\ell_{23}$, $[D_{3h}]$

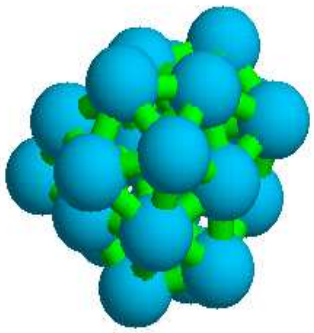

$A\ell_{24}$, $[C_{2v}]$

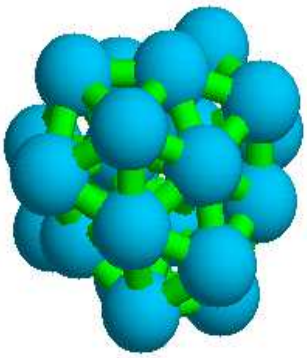

$A\ell_{25}$, $[C_s]$

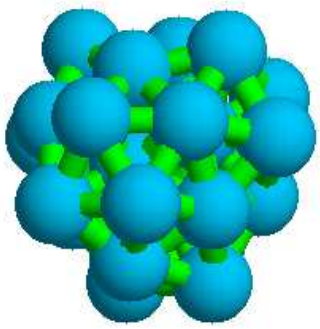

$A\ell_{26}$, $[T_d]$

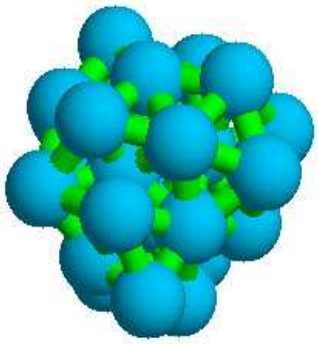

$A\ell_{27}$, $[C_{2v}]$

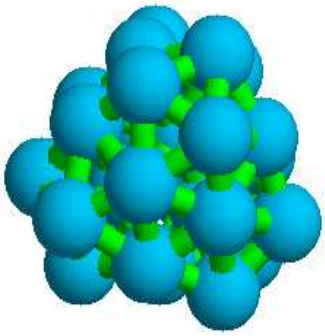

$A\ell_{28}$, $[C_s]$

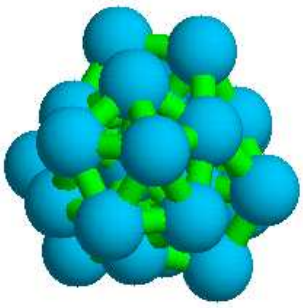

$A\ell_{29}$, $[D_{3h}]$

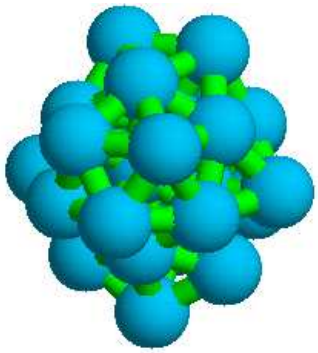

$A\ell_{30}$, $[C_{2v}]$

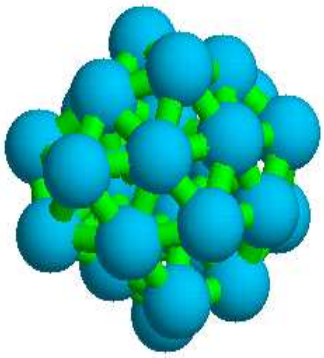

$A\ell_{31}$, $[C_s]$

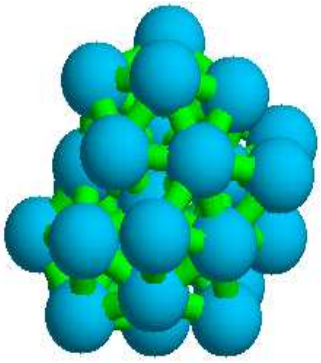

$A\ell_{32}$, $[C_{2v}]$

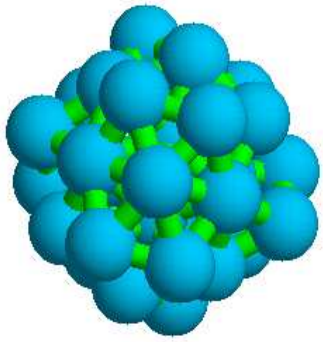

$A\ell_{33}$, $[C_{5v}]$

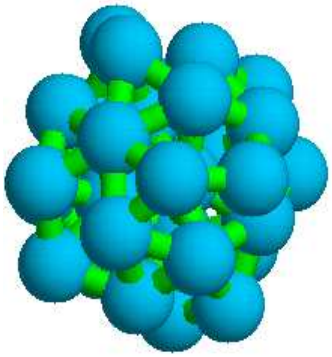

$A\ell_{34}$, $[D_{5h}]$

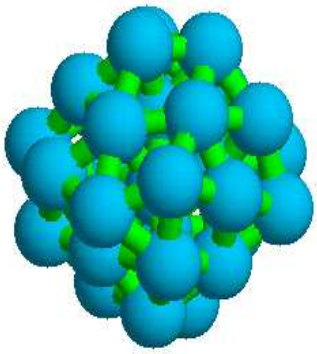

$A\ell_{35}$, $[C_{2v}]$

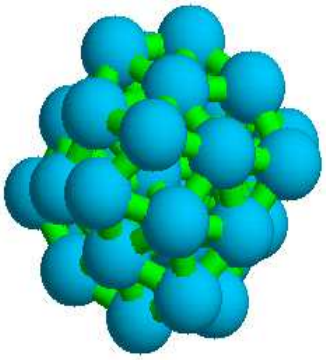

$A\ell_{36}$, $[C_s]$

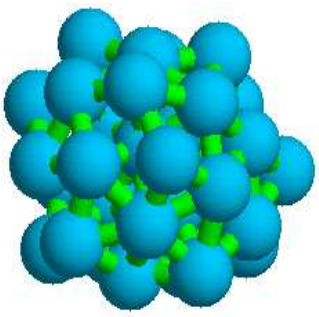

$A\ell_{37}$, $[C_s]$

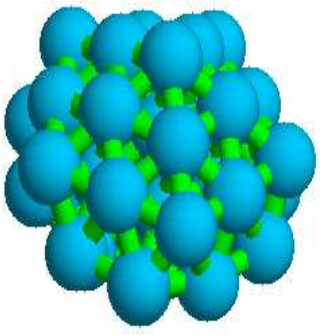

$A\ell_{40}$, $[D_{6h}]$

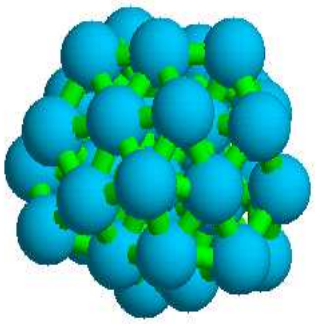

$A\ell_{41}$, $[C_{2v}]$

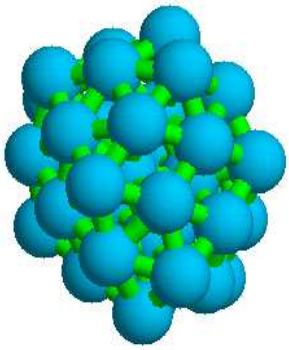

$A\ell_{42}$, $[C_1]$

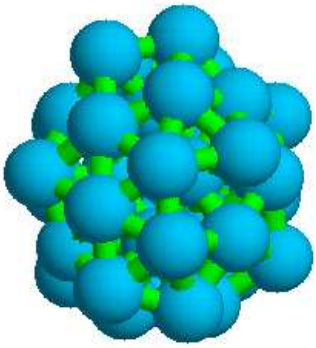

$A\ell_{43}$, $[C_s]$

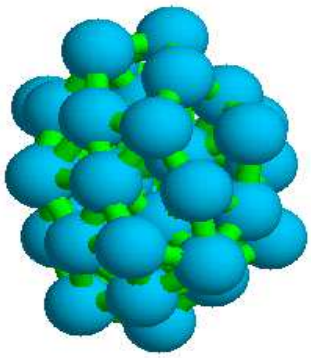

$A\ell_{44}$, $[C_{2v}]$

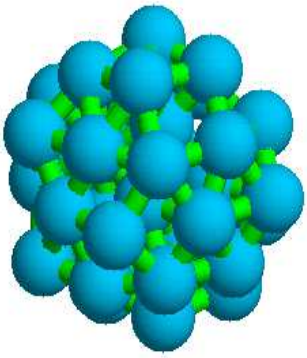

$A\ell_{45}$, $[C_1]$

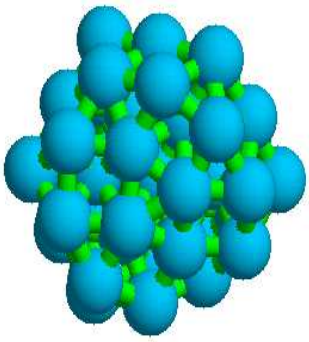

$A\ell_{46}$, $[C_s]$

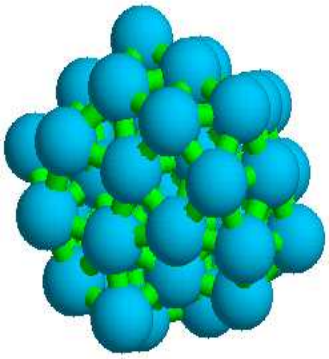

$A\ell_{47}$, $[C_{3v}]$

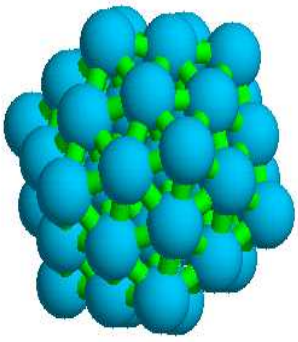

$A\ell_{48}$, $[C_s]$

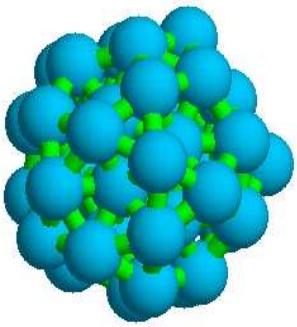

$A\ell_{49}$, $[C_s]$

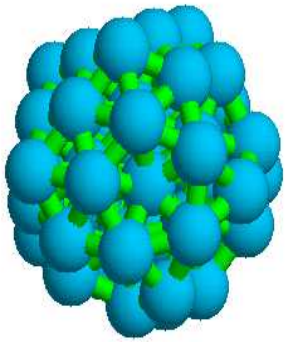

$A\ell_{51}$, $[C_1]$

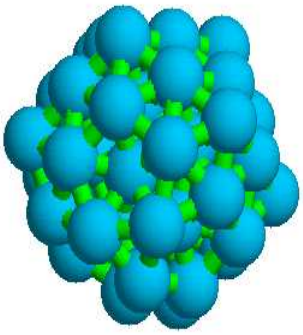

$A\ell_{52}$, $[C_s]$

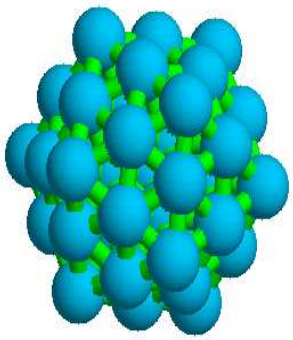

$A\ell_{53}$, $[C_{5V}]$

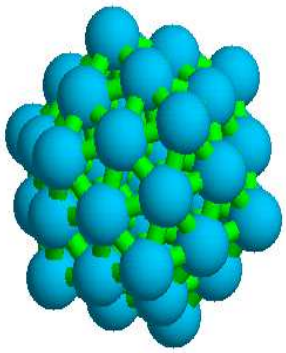

$A\ell_{54}$, $[C_S]$

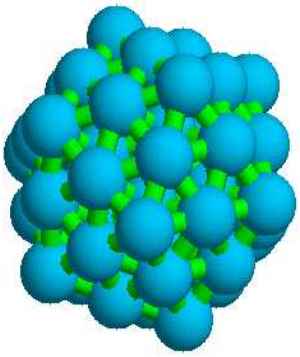

$A\ell_{55}$, $[I_h]$

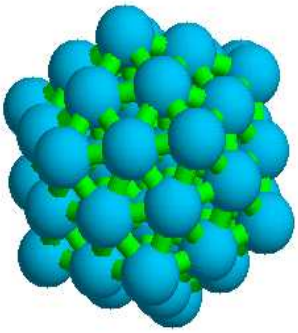

$A\ell_{56}$, $[C_{3v}]$

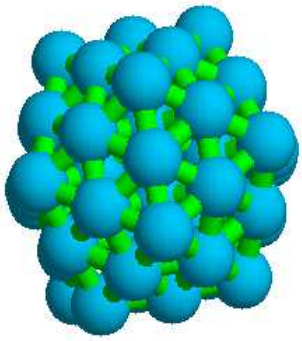

$A\ell_{57}$, $[S_4]$

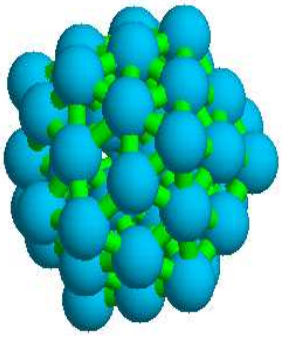

$A\ell_{58}$, $[C_s]$

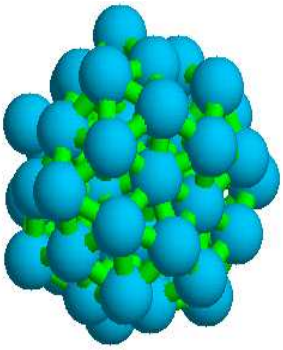

$A\ell_{59}$, $[C_{2v}]$

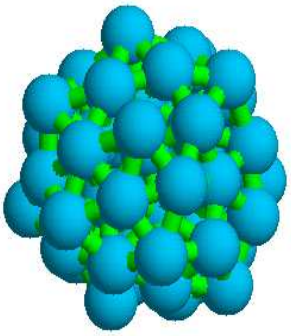

$A\ell_{60}$, $[C_{3v}]$

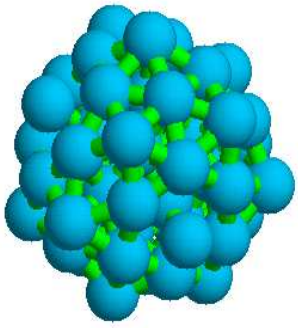

$A\ell_{61}$, $[T_d]$

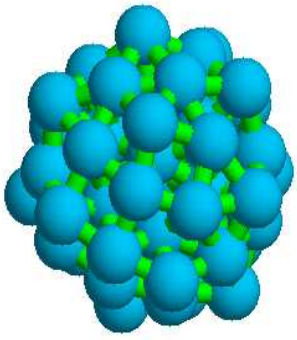

$A\ell_{62}$, $[C_s]$

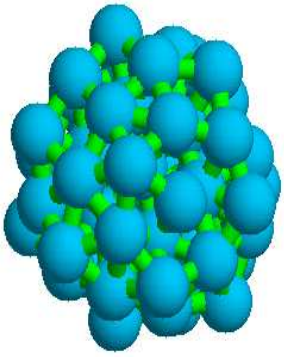

$A\ell_{63}$, $[C_1]$

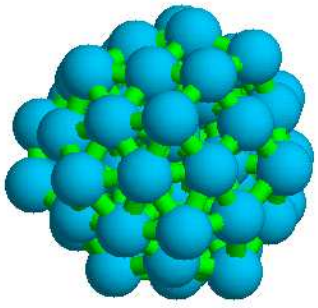

$A\ell_{64}$, $[C_{2v}]$

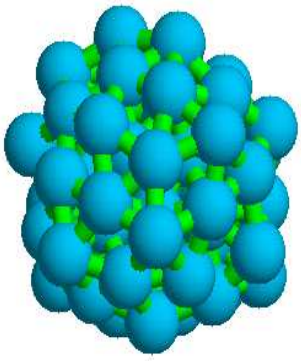

$A\ell_{65}$, $[C_1]$

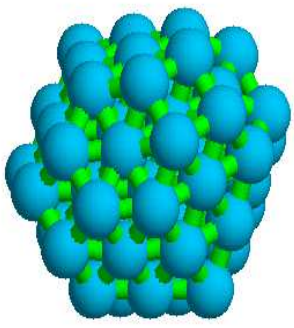

$A\ell_{66}$, $[C_1]$

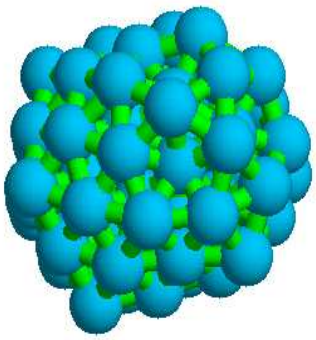

$A\ell_{67}$, $[C_1]$

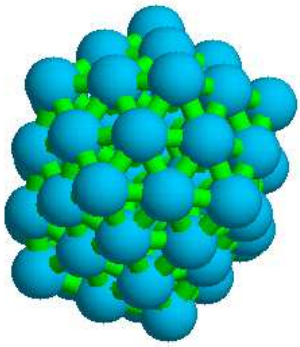

$A\ell_{68}$, $[C_1]$

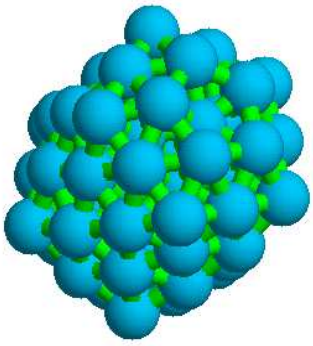

$A\ell_{69}$, $[C_3]$

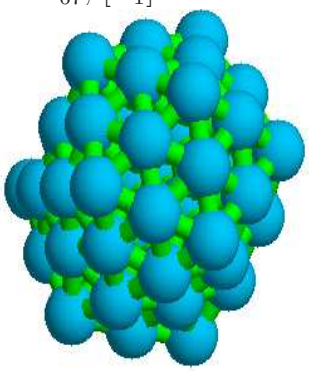

$A\ell_{70}$, $[C_2]$

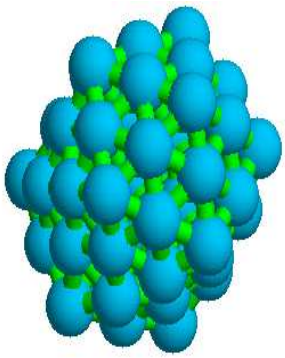

$A\ell_{71}$, $[C_s]$

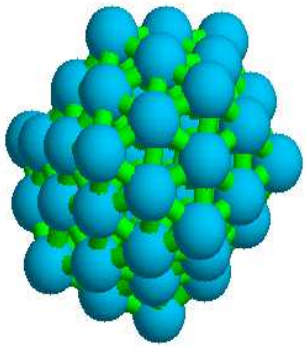

$A\ell_{72}$, $[C_s]$

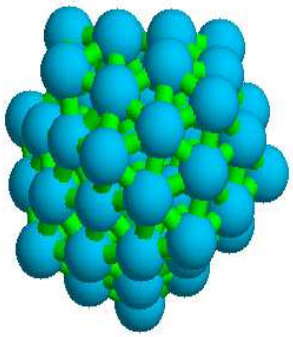

$A\ell_{73}$, $[C_s]$

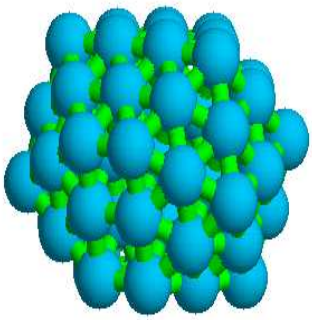

$A\ell_{74}$, $[C_s]$

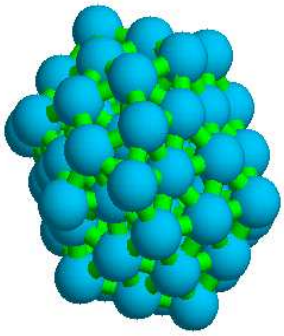

$A\ell_{75}$, $[C_s]$

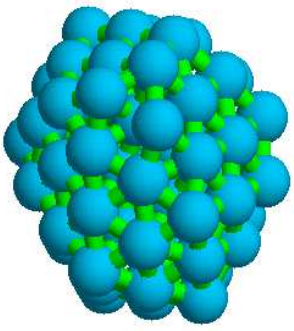

$A\ell_{76}$, $[D_{3h}]$

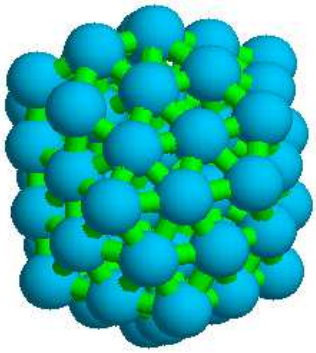

$A\ell_{77}$, $[C_{3v}]$

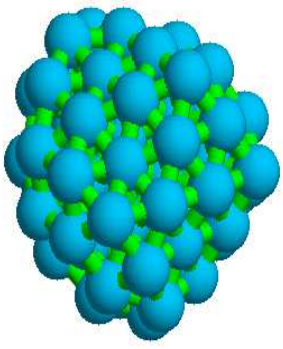

$A\ell_{78}$, $[D_{3h}]$

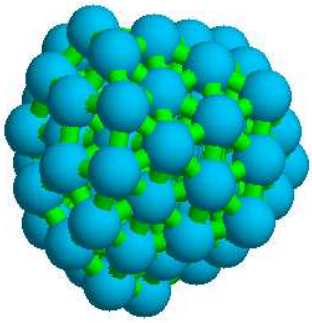

$A\ell_{79}$, $[C_s]$

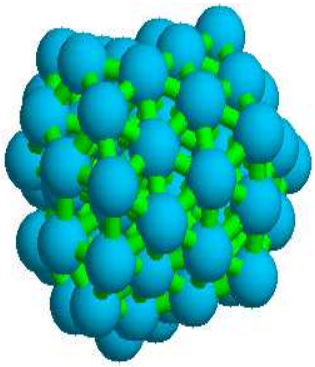

$A\ell_{80}$, $[C_s]$

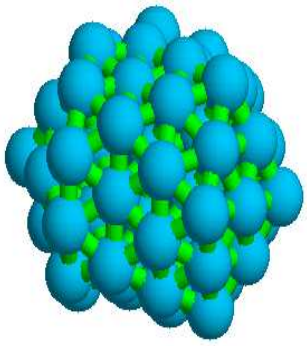

$A\ell_{81}$, $[C_s]$

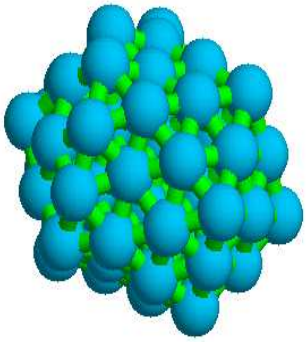

$A\ell_{82}$, $[C_2]$

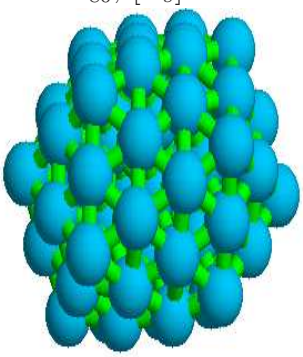

$A\ell_{83}$, $[C_1]$

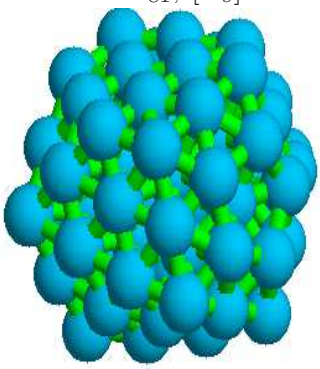

$A\ell_{84}$, $[C_s]$

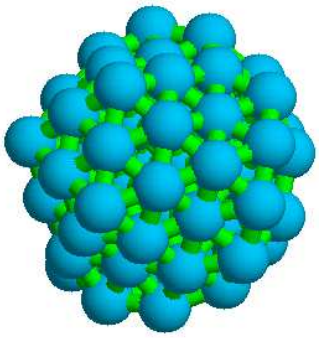

$A\ell_{85}$, $[C_{2v}]$

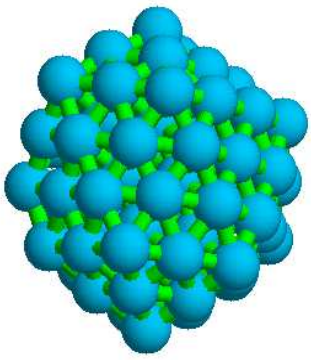

$A\ell_{86}$, $[C_s]$

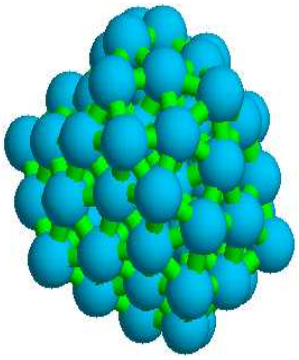

$A\ell_{87}$, $[C_1]$

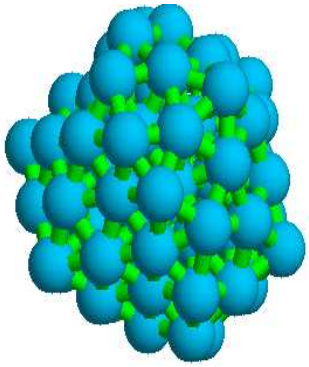

$A\ell_{88}$, $[C_s]$

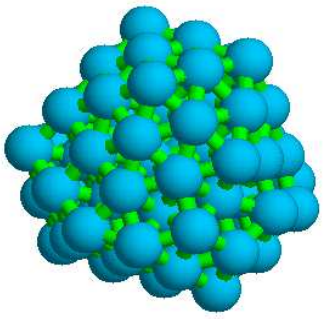

$A\ell_{89}$, $[C_s]$

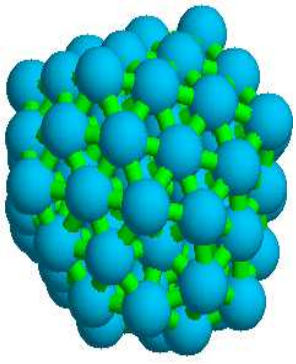

$A\ell_{90}$, $[C_s]$

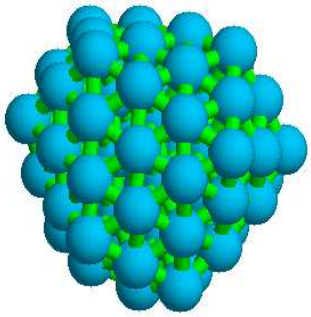

$A\ell_{91}$, $[D_{3h}]$

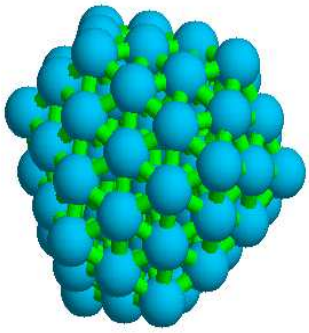

$A\ell_{92}$, $[C_2]$

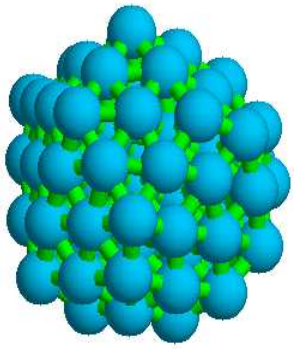

$A\ell_{93}$, $[C_1]$

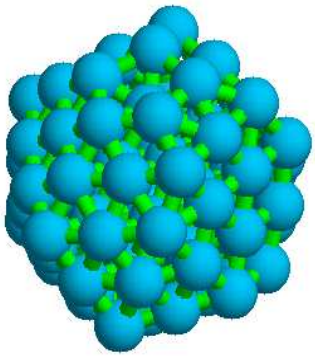

$A\ell_{94}$, $[C_{2v}]$

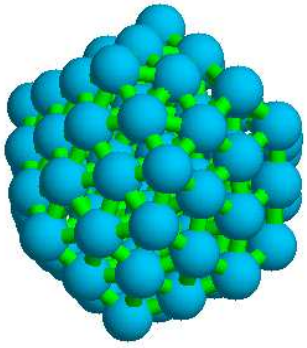

$A\ell_{95}$, $[C_s]$

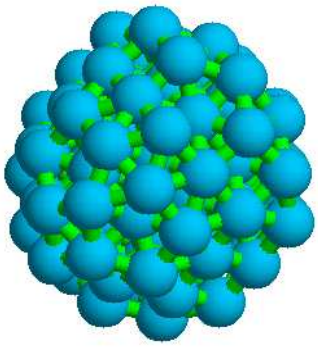

$A\ell_{96}$, $[C_2]$

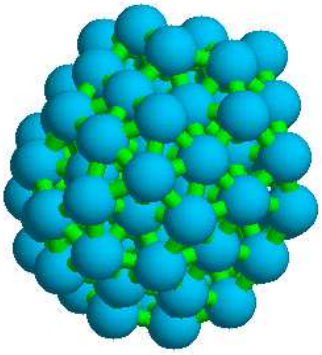

$A\ell_{97}$, $[C_1]$

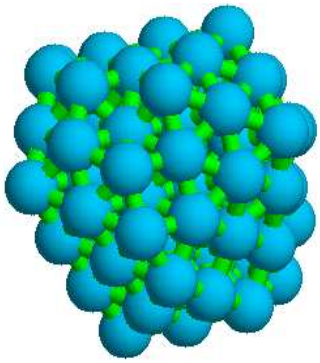

$A\ell_{98}$, $[C_1]$

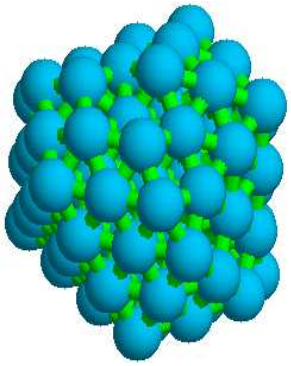

$A\ell_{99}$, $[C_1]$

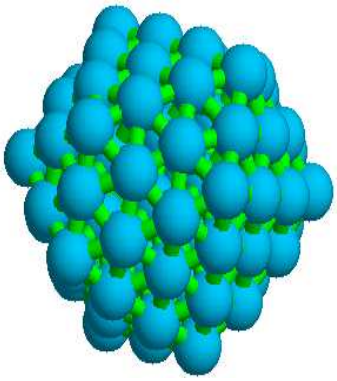

$A\ell_{101}$, $[C_1]$

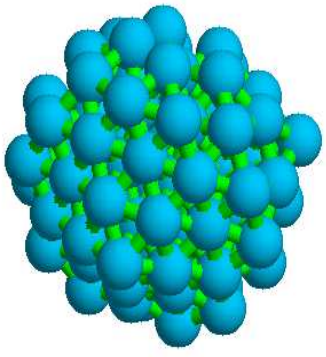

$A\ell_{102}$, $[C_1]$

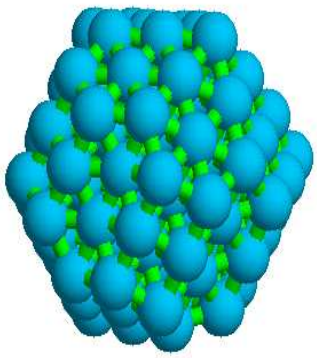

$A\ell_{103}$, $[C_1]$

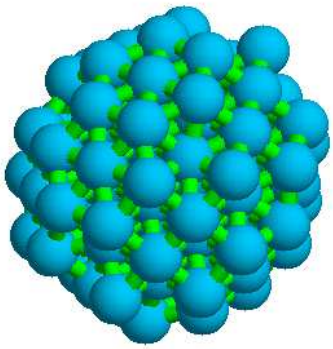

$A\ell_{104}$, $[C_1]$

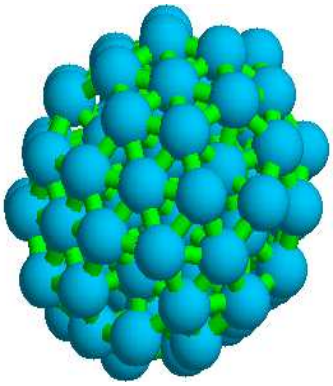

$A\ell_{105}$, $[C_s]$

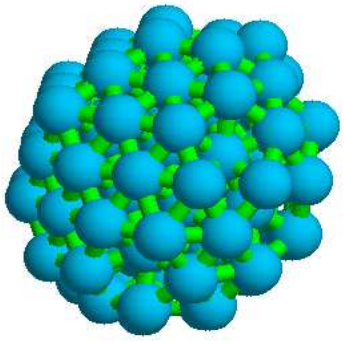

$A\ell_{106}$, $[C_1]$

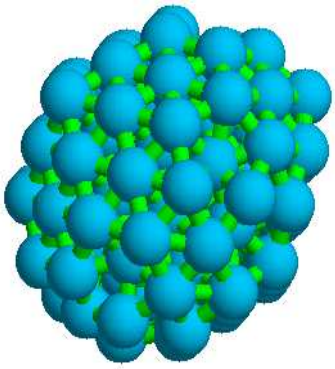

$A\ell_{107}$, $[C_s]$

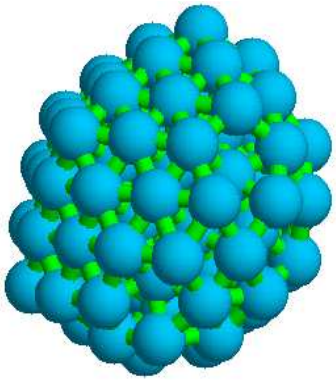

$A\ell_{108}$, $[C_s]$

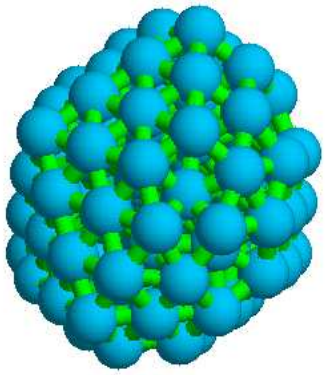

$A\ell_{109}$, $[C_1]$

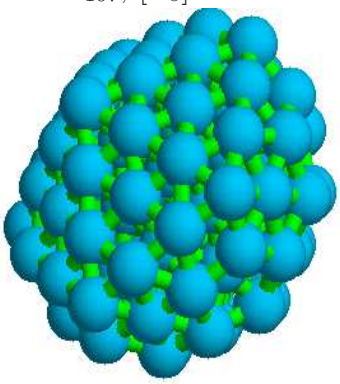

$A\ell_{110}$, $[C_1]$

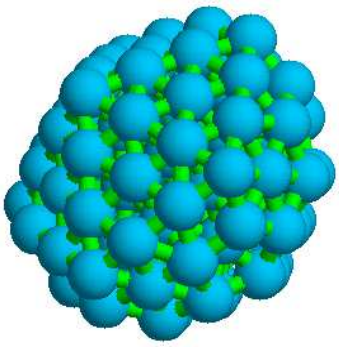

$A\ell_{111}$, $[C_1]$

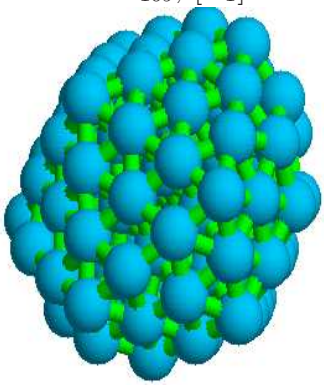

$A\ell_{112}$, $[C_1]$

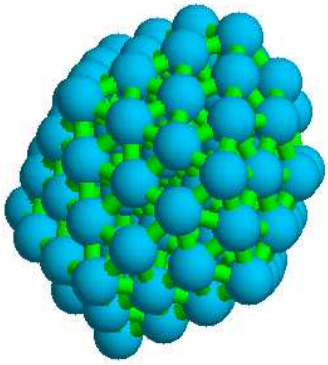

$A\ell_{113}$, $[C_1]$

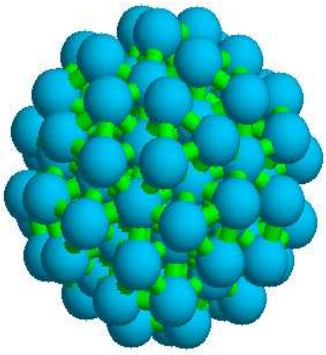

$A\ell_{114}$, $[C_s]$

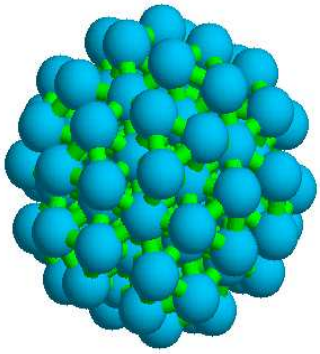

$A\ell_{115}$, $[C_1]$

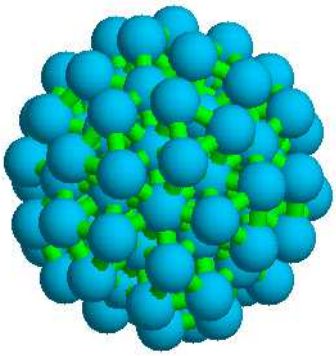

$A\ell_{116}$, $[C_s]$

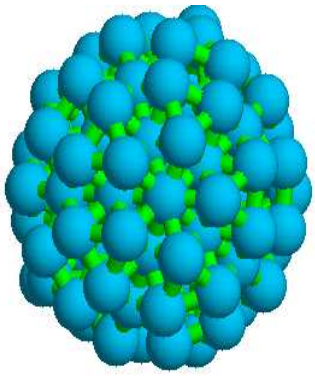

$A\ell_{117}$, $[C_1]$

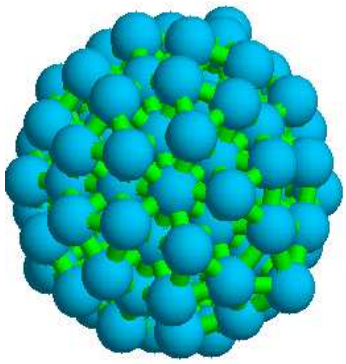

$A\ell_{118}$, $[C_1]$

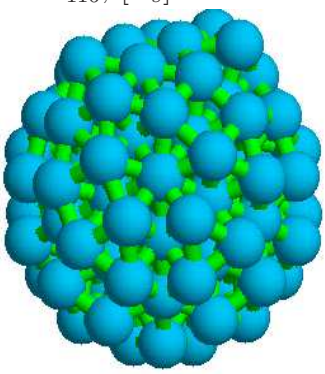

$A\ell_{119}$, $[C_1]$

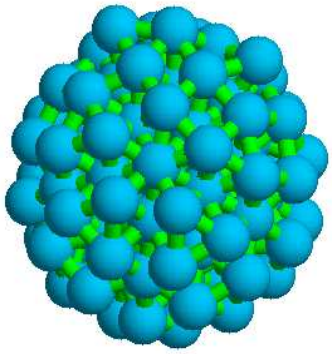

$A\ell_{120}$, $[C_2]$

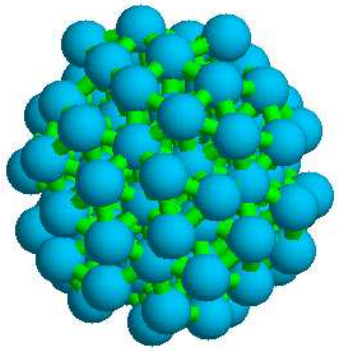

$A\ell_{121}$, $[C_1]$

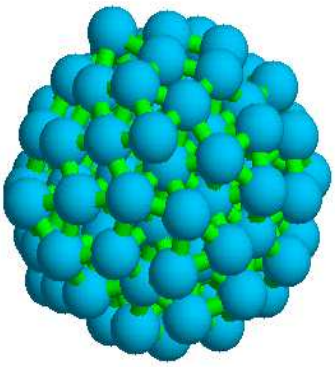

$A\ell_{122}$, $[C_2]$

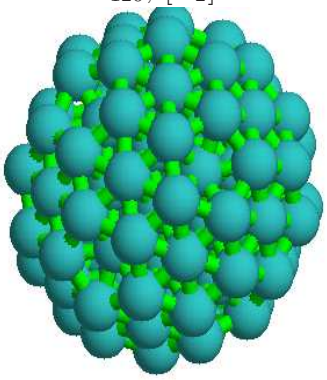

$A\ell_{123}$, $[C_1]$

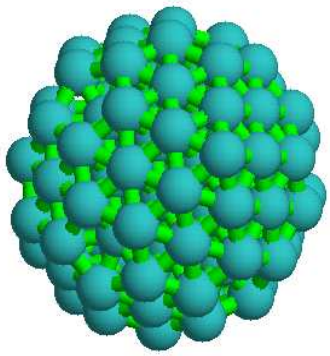

$A\ell_{124}$, $[C_1]$

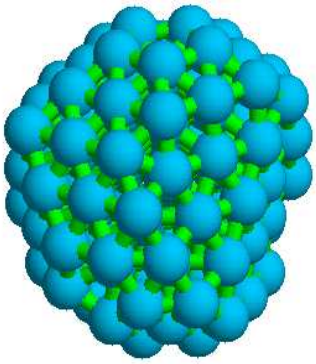

$A\ell_{125}$, $[C_1]$

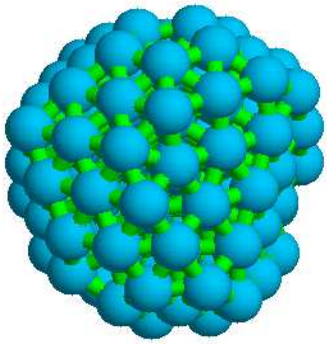

$A\ell_{126}$, $[C_1]$

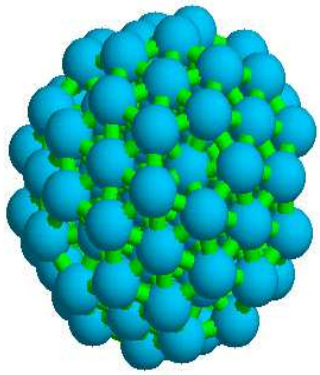

$A\ell_{127}$, $[C_1]$

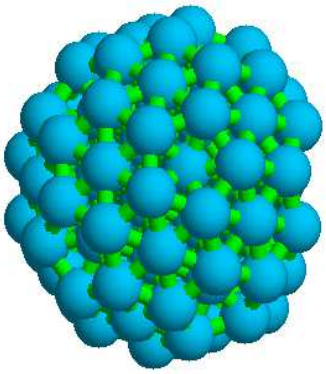

$A\ell_{128}$, $[C_1]$

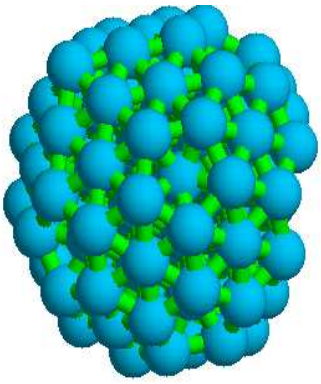

$A\ell_{129}$, $[C_3]$

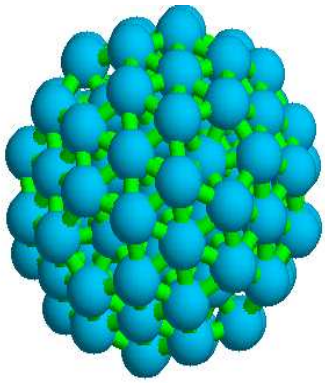

$A\ell_{130}$, $[C_1]$

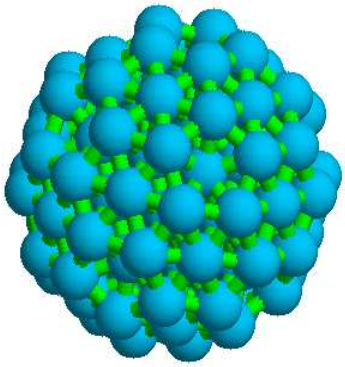

$A\ell_{131}$, $[C_1]$

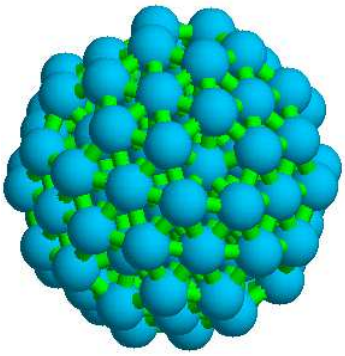

$A\ell_{132}$, $[C_2]$

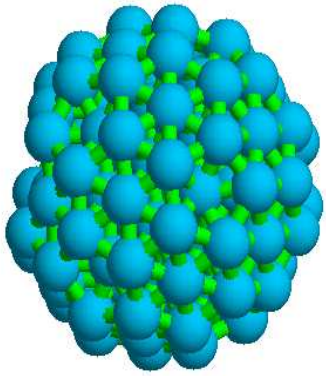

$A\ell_{133}$, $[C_s]$

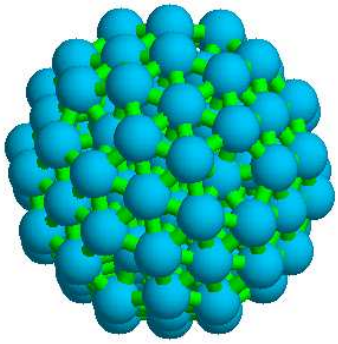

$A\ell_{134}$, $[C_2]$

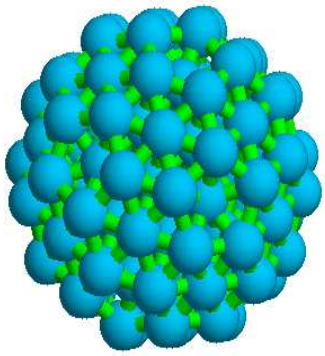

$A\ell_{135}$, $[C_s]$

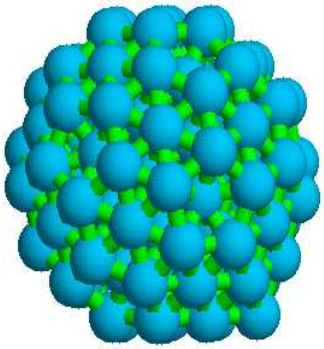

$A\ell_{136}$, $[C_s]$

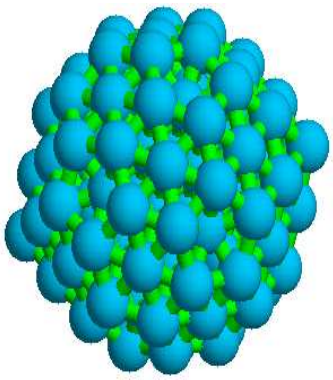

$A\ell_{137}$, $[C_s]$

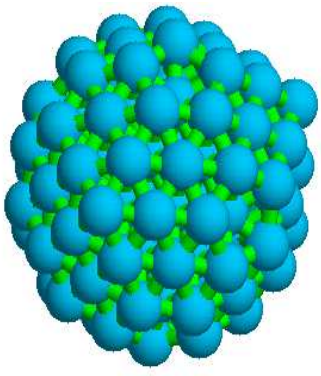

$A\ell_{138}$, $[C_{2v}]$

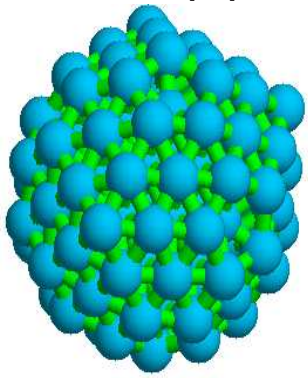

$A\ell_{139}$, $[C_s]$

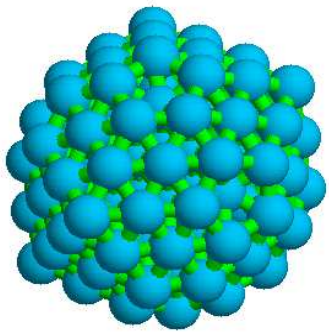

$A\ell_{140}$, $[C_s]$

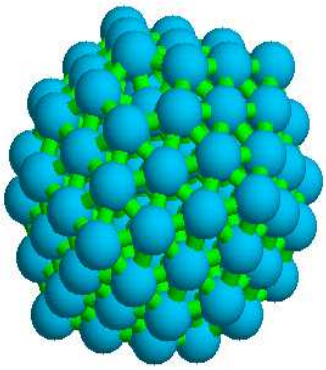

$A\ell_{141}$, $[C_s]$

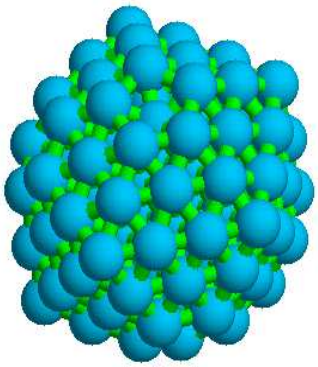

$A\ell_{142}$, $[C_{2v}]$

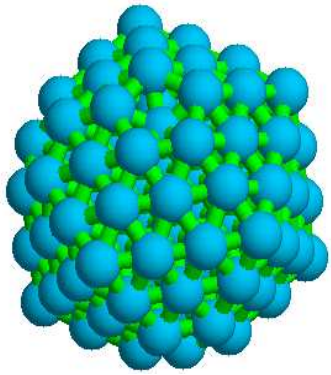

$A\ell_{143}$, $[C_s]$

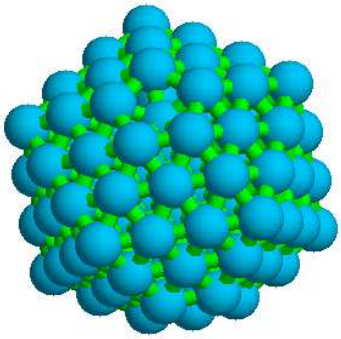

$A\ell_{144}$, $[C_{2v}]$

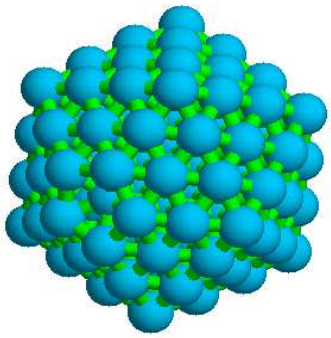

$A\ell_{145}$, $[C_1]$

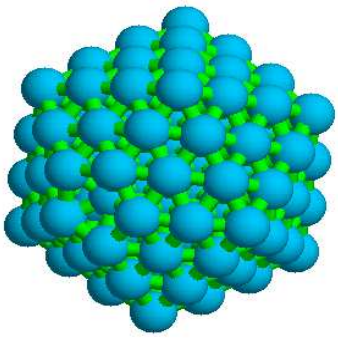

$A\ell_{146}$, $[C_1]$

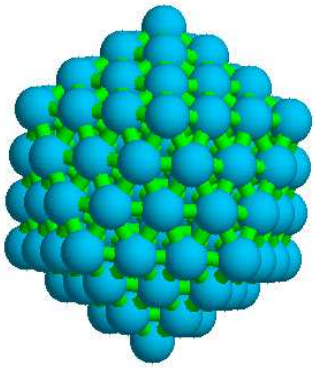

$A\ell_{147}$, $[I_h]$

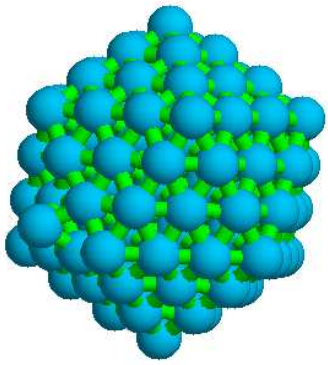

$A\ell_{148}$, $[C_s]$

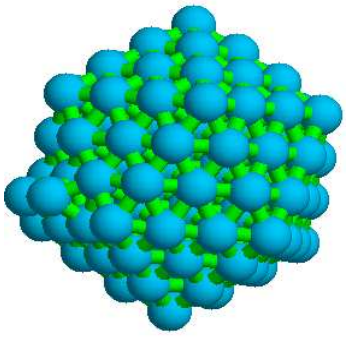

$A\ell_{149}$, $[C_1]$

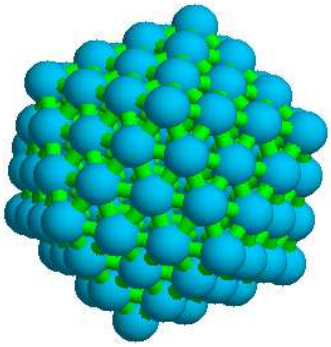

$A\ell_{151}$, $[C_{2v}]$

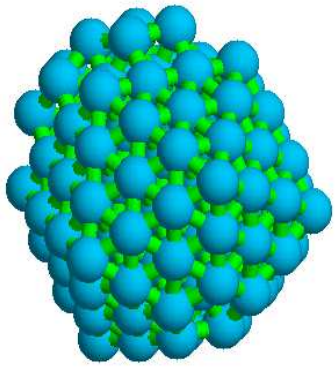

$A\ell_{152}$, $[C_s]$

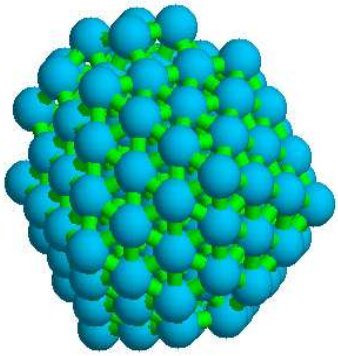

$A\ell_{153}$, $[C_{2v}]$

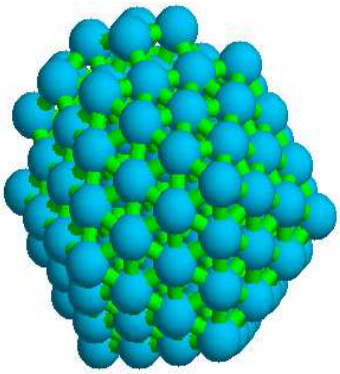

$A\ell_{154}$, $[C_s]$

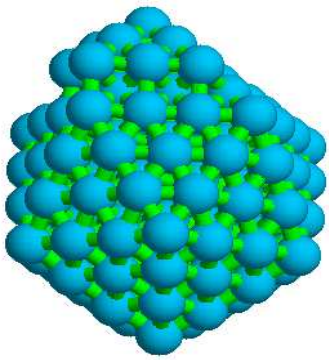

$A\ell_{155}$, $[C_s]$

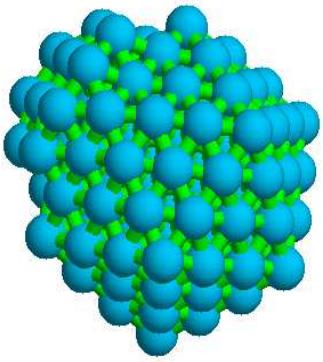

$A\ell_{156}$, $[C_{3v}]$

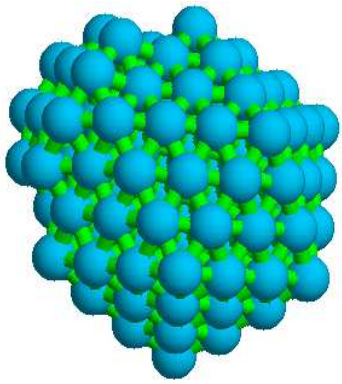

$A\ell_{157}$, $[C_1]$

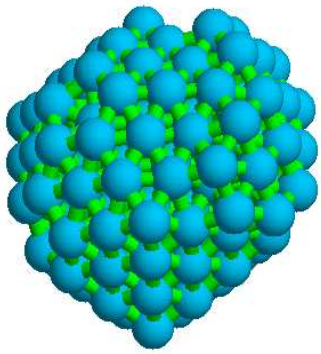

$A\ell_{158}$, $[C_2]$

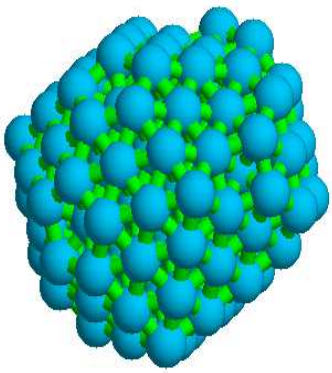

$A\ell_{159}$, $[C_s]$

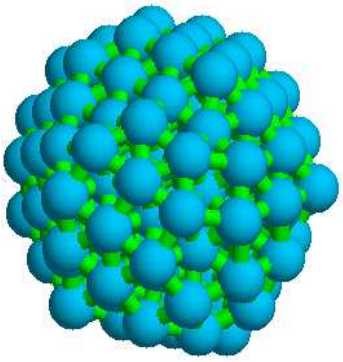

$A\ell_{160}$, $[D_{3h}]$

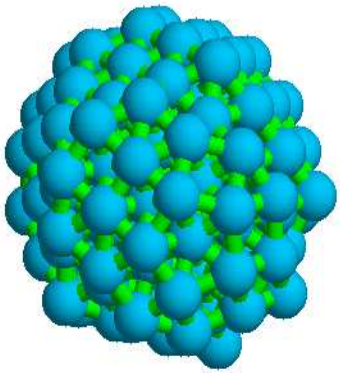

$A\ell_{161}$, $[C_1]$

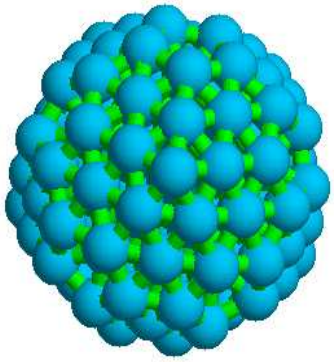

$A\ell_{162}$, $[C_s]$

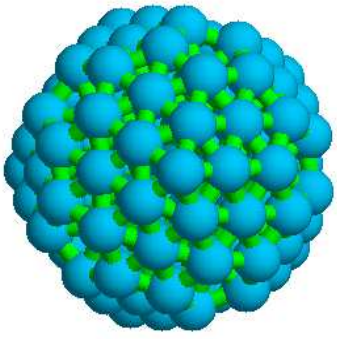

$A\ell_{163}$, $[C_s]$

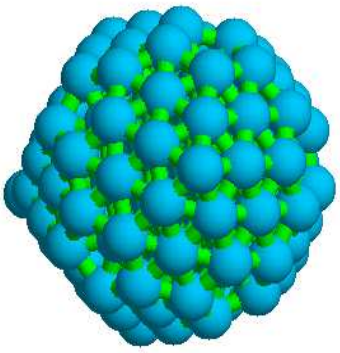

$A\ell_{164}$, $[C_2]$

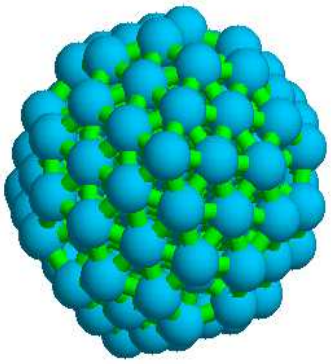

$A\ell_{165}$, $[C_s]$

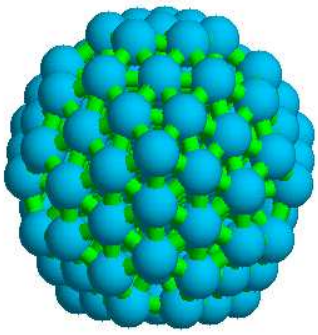

$A\ell_{166}$, $[C_s]$

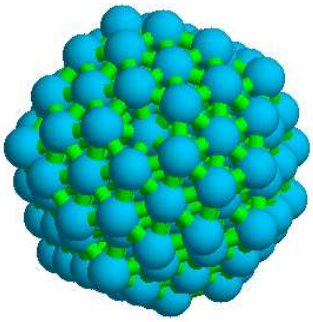

$A\ell_{167}$, $[C_1]$

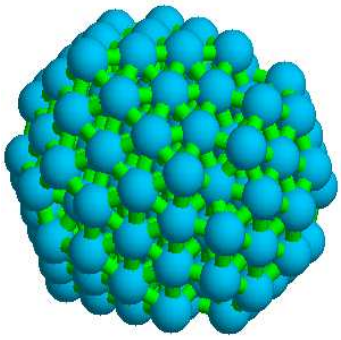

$A\ell_{168}$, $[C_2]$

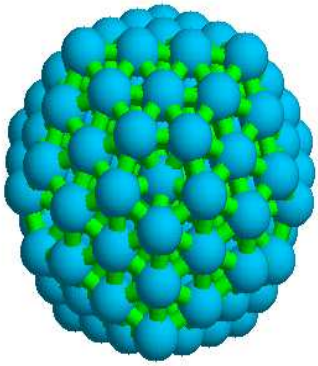

$A\ell_{169}$, $[C_1]$

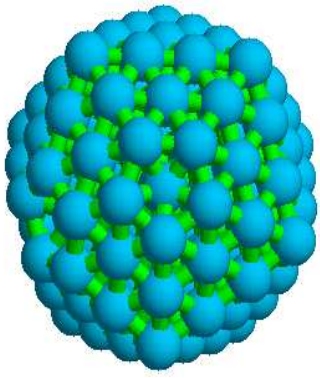

$A\ell_{170}$, $[C_s]$

PUBLICATION ISSUED IN THIS THESES

W.M. Keyampi, T.S. Tsasse, B. Nana, S. Zekeng. Global minimization of aluminum clusters using Gupta potential. Chemical Physics Letters 754 (2020) 137635. Impact factor 1.901, https://doi.org/10.1016/j.cplett.2020.137635.

Chemical Physics Letters 754 (2020) 137635

Contents lists available at ScienceDirect

Chemical Physics Letters

journal homepage: www.elsevier.com/locate/cplett

Research paper

Global minimization of aluminum clusters using Gupta potential

W.M. Keyampi[a], T.S. Tsasse[a], B. Nana[b,*], S. Zekeng[a]

[a] Laboratory of Materials Science, Department of Physics, Faculty of Sciences, University of Yaounde I, PO Box 812, Yaounde, Cameroon
[b] Department of Physics, Higher Teacher Training College, University of Bamenda, PO Box 39, Bamenda, Cameroon

ARTICLE INFO

Keywords:
Aluminum cluster
Ground state
Gupta potential

ABSTRACT

In this paper, the ground-state geometries and energies of $A\ell_N (N \leqslant 170)$ clusters have been investigated using the Gupta potential combined with the molecular dynamics simulation quenching method. The Gupta parameters have been fixed according to the experimental values of the cohesive energy and lattice parameters. For each minimum, the energy and point group (PG) have been obtained. Our optimized structures are in agreement with previous ones obtained using Murrell-Mottram potential as well as those obtained using the Glue potential. A simple relation between the ground state energy and the number of atoms has been proposed which can permit one to predict the ground state for any Aluminum cluster with a known number of atoms.

1. Introduction

In physical chemistry, clusters refer to stable aggregates made of several atoms (molecules) bonding in certain physical or chemical forces that exist in microscopic states [1]. Studying metals in cluster form is of great interest due to the following reasons: development of bulk properties with increasing cluster size, the central position of clusters between molecules and condensed matter and thirdly their nature of phase transitions in finite systems [2]. Understanding clusters have become a new and important field of research with a focus on the dynamics of its formation, structures and other properties [3–8]. It has become a new and significant field to study the formation, structures, evolutional behavior and other properties of clusters. Due to their small size, nanoclusters can remain in a “liquid-like” state at temperatures below the melting point [9,10], and their magnetic moments can exceed large values of up to cluster sizes of several hundred atoms [11].

In general, the geometric structures of clusters do not resemble those of bulk metals since there are no constraints on rotational symmetry from the crystallographic restriction theorem. Due to their rich and interesting basic physical problems and possible applications, Aluminum nanoclusters have attracted much attention [12]. Aluminum in many research fields and technological applications such as catalysis, cluster deposition [13], microelectronics [14], and superconductivity [15], atomic distribution on their surfaces play a fundamental role, where the surface structure and its quality are of primary importance.

In the hope of understanding the properties of molecules in terms of their structures and of the microscopic interactions between them, simulations are generally carried out. Simulations results need to be compared to experimental ones for confirmation. The isolation of large species of fullerene and the determination of their geometries have been carried out successfully through experiment. In other to find their lowest energy configurations, sophisticated minimization techniques have been put in place [16,17]. It is clearly known that finding the global minimum on a cluster is a difficult problem [18]. This is because the number of structurally distinct minima increases almost exponentially with increasing nuclearity, due to the high dimensionality of configuration space.

Ab-initio electronic structure methods are often used to determine the lowest energy structure. However, a very long time for convergence is needed when the number of atoms making up the cluster increases, which is a drawback. As such, many empirical potentials which adequately describe interactions between atoms in clusters have been developed [19]. For more accuracy in the determination of the energy, the potential should incorporate well modeled different external surface twin planes, different crystal structures, and the response to strain. Furthermore, vibrational properties need to be well described so as to model the potential temperature dependence of the structure [20]. Therefore, the prediction of the correct structure of a cluster represents a tough challenge for potential in use.

The first objective of this work is to fixe the Gupta parameters taking into account the experimental values of the cohesive energy and lattice parameters of the Aluminum clusters. The second objective is to use the many body Gupta potential to obtain the lowest energy, which corresponds to the global minima (stable configuration), for each Aluminum cluster with sizes ranging from 3 to 170 atoms. We then compared our results to those obtained using the Murrell-Mottram

* Corresponding author.
E-mail address: na1bo@yahoo.fr (B. Nana).

https://doi.org/10.1016/j.cplett.2020.137635
Received 13 January 2020; Received in revised form 21 May 2020; Accepted 21 May 2020
Available online 01 June 2020

potential, Glue potential, Sutton-Chen potential, Truhlar potential and the Cleri-Rosato potential [21–25]. Gupta potential has been extensively used in metallic cluster simulations [26], which leads to results that are in good agreement to those generated from first-principle methods [27]. One of the most important aspects with the Gupta potential is that for an adequate time, corresponding to each structure, the structure converges directly to its stable configuration irrespective of the initial configuration. Additionally, this method can permit one to simulate much larger clusters than previously accessible thus enlarging the range of materials science issues that could be addressed. Gupta potential allows one to perform simulations involving more than three hundred atoms on small work stations.

This work has been organized as follows: in the second section, we describe the many-body Gupta potential model and provide details on the simulation method. In section three, we present our optimized structures, their respective energies and some global minima cluster structures obtained from our calculations. Our structures are then compared to those obtained using different potentials. Finally, in Section four we conclude the work.

2. Gupta potential and methodology

2.1. Gupta-type potential

The many-body Gupta potential was originally proposed to study relaxation near surfaces and impurities in bulk transition metals [28]. The principal part of the many-body Gupta potential rests on the tight-binding model originally proposed by Ducastelle [29] and Friedel [30]. The main idea consists of constructing a functional within the second momentum approximation [31,32] which takes into account the essential band character of the metallic bond. The cohesive energy of the system depends on five parameters. It is written in terms of repulsive pair and attractive many-body terms which are obtained by summing over all atoms. Its expression is given in Eq. (1) and results from the summation of the total bonding energy between N atoms.

$$V = \sum_{i=1}^{N} \left[\sum_{j>i}^{N} V_{ij}^{r}(r_{ij}) - \sqrt{\sum_{j>i}^{N} V_{ij}^{a}(r_{ij})} \right], \tag{1}$$

with

$$V_{ij}^{r} = Ae^{-p\left(\frac{r_{ij}}{r_0}-1\right)} \text{ and } V_{ij}^{a} = B^2 e^{-2q\left(\frac{r_{ij}}{r_0}-1\right)}. \tag{2}$$

A is the index to measure the interatomic repulsive strength, and B is an effective jump integral only related to the type of atoms. p and q are adjustable parameters, V_{ij}^{r} and V_{ij}^{a} are respectively the repulsive potential and the attractive potential. r_0 is the equilibrium distance between atoms and $r_{ij} = \|\vec{r_j} - \vec{r_i}\|$ represents the distance between the i^{th} and j^{th} atoms. N is the total number of atoms with equal mass.

The choice of these potentials is motivated by the need for computational efficiency in order that global optimization is feasible for the sizes we consider in this work and by our intention to compare with previous results.

2.2. Methodology

All the global optimization calculations in this work were performed using a numerical code based on the molecular dynamics method (Which is a computer simulation method for studying the physical movements of atoms and molecules). Molecular dynamics was used here for determination of the possible spatial structures. It is based on numerical integration of Newton's equations:

$$m_i \frac{d^2\vec{r_i}}{dt^2} = \overrightarrow{F_i} = -\frac{dV_i}{dr_i}\frac{\vec{r_i}}{r_i}. \tag{3}$$

where m_i and $\vec{r_i}$ are the mass and the position of the i^{th} particle, respectively. $\overrightarrow{F_i}$ is the total force exerted on the i^{th} particle by all other particles and V_i is the potential energy created on the i^{th} particle by all other particles.

We have calculated the structural changes as a function of the cluster energy. Newton's equations of motion for each atom within the cluster were treated using the Verlet algorithm. To define the cluster configurations that are local and global minima, one must construct an initial geometry from which to start the molecular dynamics. While it is possible that the intuitively chosen initial geometry could be close to a local minimum, this is unlikely. The initial velocities of each atom were chosen randomly and the time step of $h = 5{\cdot}10^{-3}$ fs was used. The velocity and the position of the i^{th} particle at $t + h$ are given as

$$\begin{aligned} \vec{v_i}(t+h) &= \vec{v_i}(t) + h\vec{a_i}(t), \\ \vec{r_i}(t+h) &= \vec{r_i}(t) + h\vec{v_i}(t) + \tfrac{1}{2}h^2\vec{a_i}(t). \end{aligned} \tag{4}$$

Following this path, the atomic positions and velocities as a function of time were obtained and were used to calculate time-averages of physical quantities characterizing the cluster structure and dynamics. The global optimization of the aluminum clusters was performed using the basin-hopping method. It is a particularly useful algorithm for global optimization, such as finding the minimum energy structure for atomic clusters [16].

Since each translational degree of freedom contributes to the total kinetic energy by $\frac{K_B T}{2}$, the temperature of the system may be defined by:

$$T = \frac{1}{3NK_B} \sum_{i=1}^{N} m_i \, \|\vec{v_i}\|^2 \tag{5}$$

where K_B is the Boltzmann constant and N is the total number of atoms in the cluster under consideration.

In this work, we have used a quantitative method for monitoring convergence based on multiple independent simulations starting from four different initial configurations [39]. We quantify the distance between the independent cluster population vectors using the distance $\delta(t)$ defined as:

$$\delta(t) = \frac{1}{2}\max_{j}\left(\sum_{i=1}^{N} \|R_{ij}(t) - \overline{R_i(t)}\| \right), \tag{6}$$

where $R_{ij}(t)$ is the position of the i^{th} particle of the j^{th} simulation at time t, $\overline{R_i(t)} = \frac{1}{4}\sum_{j=1}^{4} R_{ij}(t)$, and N is the number of atoms. This distance is computed against time and the system considered equilibrated when it decreases below a pre-chosen threshold and remains below. A 10^{-2}threshold has been used in this manuscript.

3. Results and discussions

3.1. Parameter values

The first investigation was dedicated to the determination of the parameter values. Let r_2 and r_3 be the equilibrium separation distances in $A\ell_2$ and $A\ell_3$ respectively. Since the $A\ell_3$ cluster had an equilateral triangle geometry with D_{3h} symmetry, we can express p and B as function of q and A as follows:

$$p = q + \frac{r_0 \ln\sqrt{2}}{r_3 - r_2}, \tag{7}$$

$$B = A\left(1 + \frac{r_0 \ln\sqrt{2}}{q(r_3 - r_2)}\right)\exp\left(\frac{r_2 - r_0}{r_2 - r_3}\ln\sqrt{2}\right). \tag{8}$$

Taking into account the experimental values of the cohesive energy and lattice parameters, the approximated values of q and A have been fitted. Under these considerations, the values of the parameters used in this manuscript are given in Table 1.

To verify the many-body Gupta potential for Aluminum parameters

Table 1
Gupta parameters for Aluminum clusters.

Parameters	A	B	p	q
Values	$7.69{\cdot}10^{-2}$ eV	1.1280 eV	15.1194	1.930

listed in Table 1 above, we first determined the optimal configurations of $A\ell_3$, $A\ell_{50}$, $A\ell_{100}$ and $A\ell_{150}$ all presented in Fig. 1 using different initial conditions. The obtained structures are then compared to the results presented by the authors of references [21,22].

Starting with the $A\ell_3$ cluster, we obtained the total energy of − 4.3498 eV. Whatever the initial configuration, we ended up with the same stable configuration or lowest energy structure which was a (D_{3h}) with the only difference being the time taken to reach this final configuration. These results are in good agreement with those obtained by Doye [22]. We also obtained an $A\ell$–$A\ell$ bond of $0.9787r_0$. We tried several initial configurations and we noticed from our analysis that linear initialized coordinates were the ones that required more time to reach the optimized configuration. For illustration, Fig. 2 shows the different optimization steps or paths for $A\ell_3$.

As shown in Fig. 2, there are two stable configurations. The linear one was obtained after $t = 50$ and was maintained until $t = 1850$. During this phase, the kinetic energy of the molecule is approximatively zero and the bond distance is $0.951068r_0$. After this phase, the molecule started a significant modification from the linear to the triangular form. The kinetic energy of the atoms increased to reach 0.5827 eV when $t = 2000$. At $t = 2050$, the kinetic energy was at its maximum (1.2177 eV) and then dropped abruptly to zero. The molecule then reached its most stable configuration at its lowest total energy.

Secondly, we considered $A\ell_{50}$ molecule and proceeded in the same manner as $A\ell_3$ molecule to have an energy of − 139.1150 eV. From different initial configurations, we obtained the same final optimized or stable configuration which is a (C_1). The initial configuration chosen here was a double ring of 25 atoms each and the minimization process for $A\ell_{50}$ is shown in Fig. 3.

The minimum distance between $A\ell_{50}$ atoms is approximately constant and very close to $0.9446r_0$.

From our simulations, we have also observed that the structure remained almost constant until $t = 1250$. Between $t = 1250$ and $t = 3000$, one ring performed a rotation with angle $\frac{\pi}{25}$ around the rings axis. After $t = 3000$, the kinetic energy started to increase and reaches its maximum around $t = 4000$. As shown in the graph of Fig. 3, important modifications of the structure were found after $t = 3000$. The optimized configuration was obtained for $t > 7000$ and is in good agreement with that obtained by the authors of reference [22].

Focusing on $A\ell_{100}$ and $A\ell_{150}$ molecules, we analyzed their optimizations starting from two different initial structures: the simple cubic lattice and the cylindrical configurations for each molecule. As illustrated in Fig. 4 and Fig. 5, we have shown some transformation steps for $A\ell_{100}$ and $A\ell_{150}$ respectively.

For both figures, the black and the blue curves respectively correspond to the simple cubic lattice and cylindrical structures used as

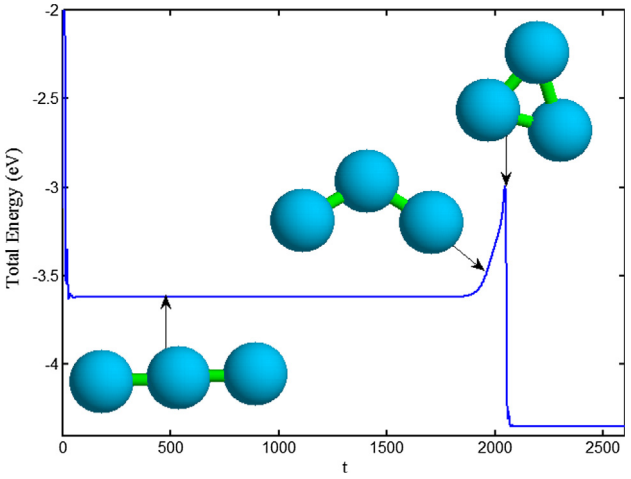

Fig. 2. An illustration of the evolution of the lowest-energy $A\ell_3$ molecule with the Gupta potential starting from a linear initialized coordinates.

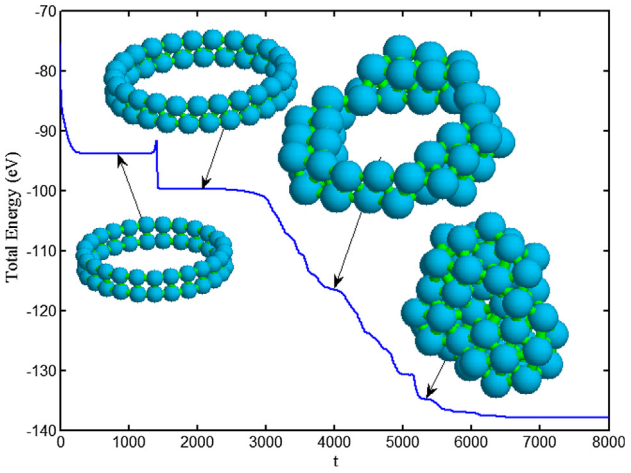

Fig. 3. An illustration of the evolution of the lowest-energy $A\ell_{50}$ molecule with the Gupta potential starting from a cylinder initialized coordinates.

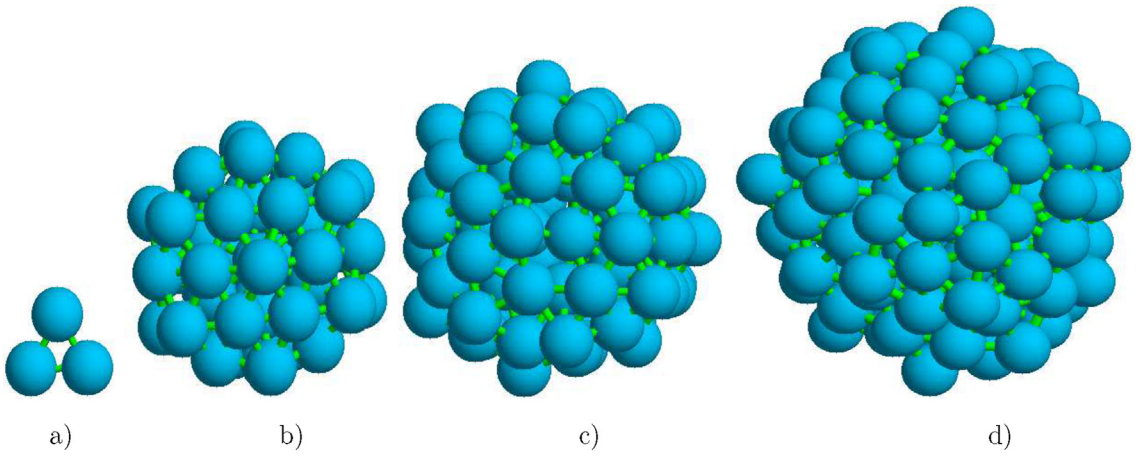

Fig. 1. Final configurations of: a) $A\ell_3$, b) $A\ell_{50}$, c) $A\ell_{100}$ and d) $A\ell_{150}$.

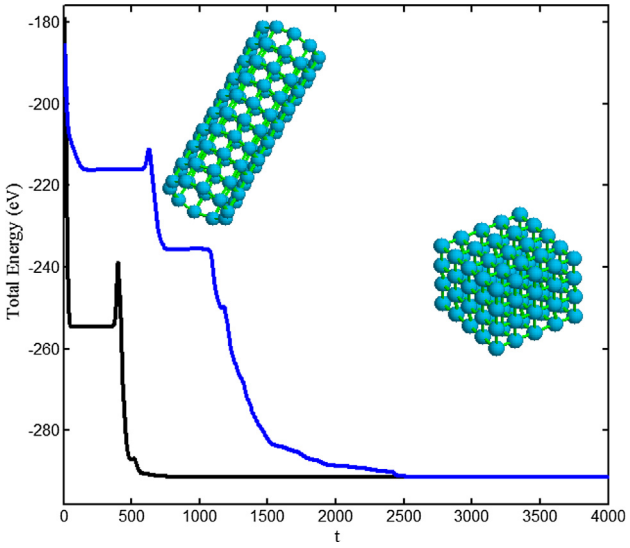

Fig. 4. An illustration of the evolution of the lowest-energy $A\ell_{100}$ molecule starting from a simple cubic lattice (black curve) and from a cylinder initialized coordinates (blue curve). (For interpretation of the references to color in this figure legend, the reader is referred to the web version of this article.)

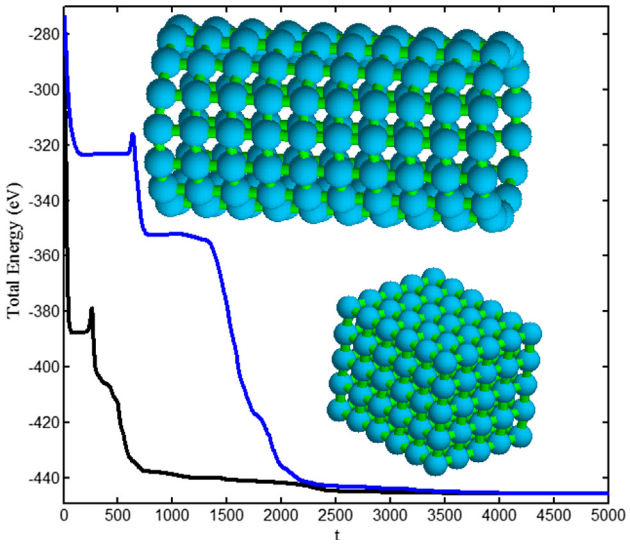

Fig. 5. An illustration of the evolution of the lowest-energy $A\ell_{150}$ molecule starting from a simple cubic lattice (black curve) and from a cylinder initialized coordinates (blue curve). (For interpretation of the references to color in this figure legend, the reader is referred to the web version of this article.)

initial coordinates. From different initials configurations shown in Figs. 4 and 5, we obtained the same final optimized configurations which are respectively (C_1) and (C_s). These structures are shown in Figs. 4 and 5, and Fig. 1d) with energies − 292.1767 eV and − 447.9025 eV respectively which are in good agreement with those of Doye [22]. The minimum distance between $A\ell_{100}$ atoms is approximately constant and very close to $0.9444r_0$ and for $A\ell_{150}$ atoms, it is almost constant and very close to $0.9408r_0$. The peaks observed in the figures corresponded to some important modifications of the structures. We can notice from the two figures that, the simple cubic configurations stabilized first before the cylindrical configurations.

Our results for $A\ell_3$, $A\ell_{50}$, $A\ell_{100}$ and $A\ell_{150}$ molecules, using Gupta potential agrees well in terms of point groups and structures, with those found in the literature [21,22]. The above results permitted us to fixe our parameters as shown in Table 1 above.

3.2. Results

We then proceed to obtain all the global energy minimum structures of the Gupta clusters. The basin-hopping algorithm has proved to be particularly successful in locating putative global minima for a wide variety of cluster systems [16]. Anyway, there is no absolute guarantee that we have located the true global minima, since the probability to miss a global minimum increases with cluster size. However, according to the fact that the same lowest-energy minimum is obtained using different initial conditions, and also according to the good precision between our results and the given cohesive energy of Aluminum, we are confident that our obtained global minima are well estimated. Table 2 depicts the potential energy, Group Point and the length of $A\ell$–$A\ell$ bond of all the clusters for $3 \leqslant N \leqslant 170$. The structural assignment has been made in Table 2 where *C* stands for cyclic, *D* for decahedral, *I* for icosahedral, *T* for tetrahedron and *O* for octahedron.

We can notice from Table 2 that the ground state energy decreases with the number *N* of atoms. In order to go far in our analysis, we plotted on Fig. 6 the ground state energy as a function of *N* (curve in black color).

This curve brought out the following analysis: the shape of the curve is almost linear. Then, the cluster energies of geometric shell clusters are fitted to the following cubic expansion in $N^{1/3}$:

$$E(N) \simeq aN + bN^{2/3} + cN^{1/3} + d. \tag{9}$$

By using the cubic regression method we calculated the parameter values: $a = -3.40444$ eV, $b = 2.17026$ eV, $c = 0.12859$ eV and $d = 1.03007$ eV. To verify our assumption, we have plotted in Fig. 6 (curve in blue) the above relation. A good agreement is obtained here between numerical result and semi-analytical one. The result obtained in Eq. (9) is an important outcome because this can help to predict the ground state energy of any cluster size knowing *N* and without the need for numerical simulation.

To investigate the structural stabilities for $A\ell_N$ clusters, the average binding energy (E_b) for any $A\ell$ cluster is defined as

$$E_b = -\frac{E(N)}{N} \simeq 3.40444 - 2.17026N^{-1/3} - 0.12859N^{-2/3} - \frac{1.03007}{N}, \tag{10}$$

where $E(N)$ is the total energy of the cluster containing *N* aluminum atoms. The average binding energy of the lowest energy isomer of $A\ell_N$ ($3 \leqslant N \leqslant 170$) is plotted, as a function of *N* in Fig. 7.

From Fig. 7, one can see that the average binding energies increase overall but with little fluctuation around a few cluster sizes (which are relevant to the magic-number clusters).

The origin of the magic-number clusters is related to the type of atoms. For noble gas atoms, the magic-number clusters correspond to filled electronic shells, thereby indicating the role of the total number of itinerant electrons on stability. Basing on the magic numbers in clusters that contain more than a few dozen atoms, it has been shown that the most stable species correspond to sizes with complete geometric shells in an icosahedral or cuboctahedral atomic arrangement [33]. Alkali metal clusters (s^1) conform to the jellium model in that, certain nuclearities are relatively stable due to their filled electronic shells [34]. By contrast, clusters of alkaline earth elements (s^2), exhibit magic numbers which correspond to clusters consisting of concentric polyhedral shells of atoms where the relative stability of a given cluster is determined by the competition between packing and surface energy effects [35].

In the case of aluminum, due to the higher atomic valency (+3), the higher density of electronic states and the involvement of $3p^1$, as well as $3s^2$ orbitals in bonding, the origin of these peaks is more complex [36]. It is believed that the crossover from the regime where electronic factors determine cluster stability to where packing and surface energy effects dominate, occurs at lower nuclearities than for the alkali metals [36,37]. Variable temperature experiments by Baguenard et al. have

Table 2
Potential energy, group point and Aℓ–Aℓ bond of the lowest energy configurations.

N	Energy(eV)	Bond(r_0)	PG	N	Energy(eV)	Bond(r_0)	PG	N	Energy(eV)	Bond(r_0)	PG
3	− 4.34983	0.9787	D_{3h}	4	− 6.89561	0.9941	T_d	5	− 9.34712	0.9923	D_{3h}
6	− 12.0278	1.0017	O_h	7	− 14.5962	0.9949	D_{5h}	8	− 17.0885	0.9983	C_{2v}
9	− 19.7611	0.9954	C_{2v}	10	− 22.4982	0.9854	C_{3v}	11	− 25.2357	0.9798	C_{2v}
12	− 28.2547	0.9739	C_{5v}	13	− 31.6329	0.9829	I_h	14	− 33.9797	0.9823	C_{3v}
15	− 36.7320	0.9784	C_{2v}	16	− 39.4368	0.9817	C_s	17	− 42.1397	0.9847	C_2
18	− 45.0494	0.9398	C_s	19	− 48.3574	0.9304	D_{5h}	20	− 51.0270	0.9288	C_{2v}
21	− 53.6976	0.9318	C_1	22	− 56.5141	0.9397	C_s	23	− 59.7394	0.9456	D_{3h}
24	− 62.3914	0.9411	C_{2v}	25	− 65.1848	0.9498	C_s	26	− 68.2925	0.9576	T_d
27	− 71.0629	0.9441	C_{2v}	28	− 73.8040	0.9447	C_s	29	− 76.8017	0.9538	D_{3h}
30	− 79.5915	0.9419	C_{2v}	31	− 82.4369	0.9418	C_s	32	− 85.2960	0.9478	C_{2v}
33	− 88.0976	0.9493	C_{5v}	34	− 90.8948	0.9453	D_{5h}	35	− 94.3272	0.9255	C_{2v}
36	− 97.2693	0.9299	C_s	37	− 100.0447	0.9500	C_s	38	− 103.0710	0.9262	D_{6h}
39	− 106.1741	0.9285	C_{6v}	40	− 109.0568	0.9260	D_{6h}	41	− 111.9302	0.9296	C_{2v}
42	− 115.0334	0.9311	C_1	43	− 118.0820	0.9353	C_s	44	− 120.9767	0.9222	C_{2v}
45	− 124.0708	0.9386	C_1	46	− 127.2073	0.9386	C_s	47	− 130.3143	0.9363	C_{3v}
48	− 133.3006	0.9373	C_s	49	− 136.0027	0.9394	C_s	50	− 139.1150	0.9446	C_1
51	− 141.9827	0.9307	C_1	52	− 145.1069	0.9345	C_s	53	− 148.0852	0.9328	C_{5v}
54	− 153.6278	0.9623	C_s	55	− 156.9316	0.9643	I_h	56	− 157.1739	0.9256	C_{3v}
57	− 160.4398	0.9347	S_4	58	− 163.3002	0.9255	C_s	59	− 166.3712	0.9258	C_{2v}
60	− 169.1812	0.9273	C_{3v}	61	− 172.2358	0.9277	T_d	62	− 175.2437	0.9283	C_s
63	− 178.4397	0.9255	C_1	64	− 181.3260	0.9225	C_{2v}	65	− 184.5851	0.9321	C_1
66	− 187.7525	0.9390	C_1	67	− 190.7509	0.9319	C_1	68	− 193.6235	0.9398	C_1
69	− 196.6888	0.9376	C_3	70	− 199.8774	0.9413	C_2	71	− 202.7042	0.9245	C_s
72	− 205.8481	0.9331	C_s	73	− 208.7526	0.9237	C_s	74	− 212.1544	0.9343	C_s
75	− 215.4319	0.9360	C_s	76	− 218.5124	0.9397	D_{3h}	77	− 221.5578	0.9310	C_{3v}
78	− 224.4132	0.9162	D_{3h}	79	− 227.2243	0.9200	C_s	80	− 230.6202	0.9295	C_s
81	− 233.5749	0.9225	C_s	82	− 236.6836	0.9320	C_2	83	− 239.5451	0.9361	C_1
84	− 242.7113	0.9378	C_s	85	− 245.5700	0.9251	C_{2v}	86	− 248.5707	0.9258	C_s
87	− 252.1090	0.9284	C_1	88	− 255.1910	0.9281	C_s	89	− 258.3163	0.9280	C_s
90	− 261.1174	0.9316	C_s	91	− 264.4623	0.9545	D_{3h}	92	− 267.3222	0.9383	C_2
93	− 270.5029	0.9373	C_1	94	− 273.5429	0.9295	C_{2v}	95	− 276.6024	0.9307	C_s
96	− 279.7527	0.9336	C_2	97	− 282.7939	0.9478	C_1	98	− 286.1358	0.9512	C_1
99	− 289.2391	0.9493	C_1	100	− 292.1767	0.9444	C_1	101	− 295.3935	0.9416	C_1
102	− 298.5960	0.9420	C_1	103	− 301.4776	0.9471	C_1	104	− 304.4115	0.9325	C_1
105	− 307.5460	0.9382	C_s	106	− 310.1656	0.9301	C_1	107	− 313.0646	0.9277	C_s
108	− 316.4403	0.9375	C_s	109	− 320.1979	0.9396	C_1	110	− 323.2767	0.9408	C_1
111	− 326.3590	0.9353	C_1	112	− 329.3589	0.9393	C_1	113	− 332.4441	0.9339	C_1
114	− 335.2425	0.9398	C_s	115	− 338.8164	0.9451	C_1	116	− 341.7280	0.9378	C_s
117	− 344.8550	0.9386	C_1	118	− 347.8365	0.9388	C_1	119	− 350.9419	0.9359	C_1
120	− 354.0818	0.9397	C_2	121	− 356.9454	0.9413	C_1	122	− 359.9576	0.9418	C_2
123	− 363.4546	0.9366	C_1	124	− 366.2721	0.9325	C_1	125	− 369.4206	0.9312	C_1
126	− 372.5688	0.9369	C_1	127	− 376.0505	0.9312	C_1	128	− 379.2189	0.9255	C_1
129	− 381.9535	0.9356	C_3	130	− 385.4508	0.9371	C_1	131	− 388.1855	0.9338	C_1
132	− 391.2332	0.9336	C_2	133	− 394.2573	0.9384	C_s	134	− 397.0438	0.9412	C_2
135	− 400.4313	0.9401	C_s	136	− 403.3256	0.9357	C_s	137	− 406.7123	0.9367	C_s
138	− 409.6199	0.9393	C_{2v}	139	− 412.9599	0.9357	C_s	140	− 416.0248	0.9387	C_s
141	− 419.1856	0.9323	C_s	142	− 422.5587	0.9394	C_{2v}	143	− 425.7004	0.9331	C_s
144	− 428.7183	0.9254	C_{2v}	145	− 431.5097	0.9328	C_1	146	− 434.5826	0.9286	C_1
147	− 446.9617	0.9554	I_h	148	− 441.0488	0.9265	C_s	149	− 444.0072	0.9269	C_1
150	− 447.9025	0.9408	C_s	151	− 451.1330	0.9373	C_{2v}	152	− 454.0891	0.9348	C_s
153	− 457.3169	0.9249	C_{2v}	154	− 459.5114	0.9310	C_s	155	− 462.9513	0.9362	C_s
156	− 465.8317	0.9363	C_{3v}	157	− 469.3694	0.9391	C_1	158	− 472.5375	0.9506	C_2
159	− 475.7368	0.9519	C_s	160	− 478.9933	0.9424	D_{3h}	161	− 482.0470	0.9486	C_1
162	− 485.2691	0.9395	C_s	163	− 488.3247	0.9484	C_s	164	− 491.5816	0.9476	C_2
165	− 494.6451	0.9397	C_s	166	− 497.7476	0.9451	C_s	167	− 500.9590	0.9438	C_1
168	− 503.9306	0.9436	C_2	169	− 507.1065	0.9467	C_1	170	− 510.1182	0.9463	C_s

shown, however, that jellium effects can be seen at much higher nuclearities when the Aℓ clusters are generated at temperatures such that they are either molten or have molten surfaces [38].

The calculated average binding energy of the cluster with the largest-size ($A\ell_{170}$) is about 3.4044 eV, and it is very closed to the cohesive energy of Aℓ crystal (3.3978 eV). This small relative error of 0.19% indicates that there is still a negligible discrepancy between properties of the aluminum clusters investigated and that of the bulk material.

An important feature of this graph is the small peaks at $N = 13$, $N = 55$ and $N = 147$, corresponding to a region of enhanced stability for $N \leqslant 170$. Such regions are more evident when the second difference in the binding energy $D_2(N)$ defined as

$$D_2 = -E_b(N-1) + 2E_b(N) - E_b(N+1), \tag{11}$$

is plotted against N, as presented in Fig. 8.

The second difference is related to the thermodynamic stability of a cluster with respect to disproportionality, assuming a quasi-equilibrium exists during cluster formation [40]. Fig. 8 shows that there are pronounced peaks in $D_2(N)$ at $N = 4$, 6, 13, 19, 53, 55, 56, 146, 147, and 148 and small peaks at 14, 23 and 35.

Experimentally there does appear to be enhanced stability at around 4, 6, 13 and 19 atoms for small clusters with $N \leqslant 20$ [41]. Jellium calculations by Chou and Cohen [42] predict peaks in $D_2(N)$ at $N = 6$, 13 and 19, where the numbers of valence electrons (= $3N$ for neutral clusters) are close to Jellium shell closings [43]. Even here, our results are in good agreement with the experimental ones as well as with those obtained by Chou and Cohen.

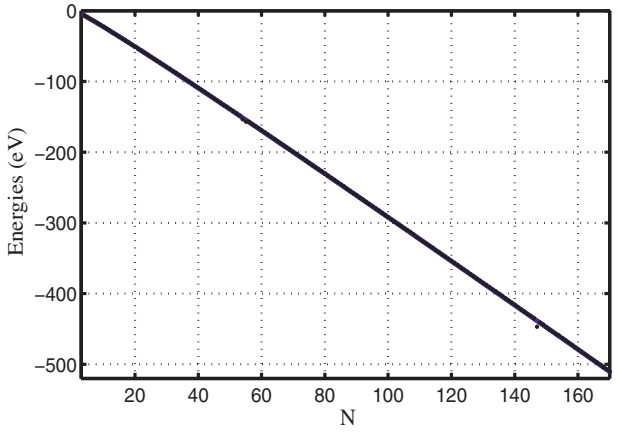

Fig. 6. Ground state energy as a function of the number of atoms curve with a solid line (black) is our numerical result while curve with a dashed line (blue) is our semi-analytical result.

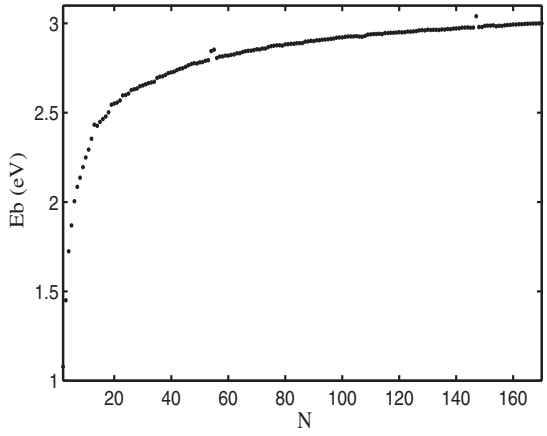

Fig. 7. The average binding energy E_b as a function of cluster size.

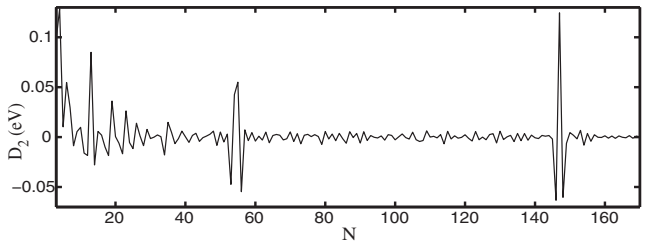

Fig. 8. Second difference in the binding energy D_2 as a function of cluster size.

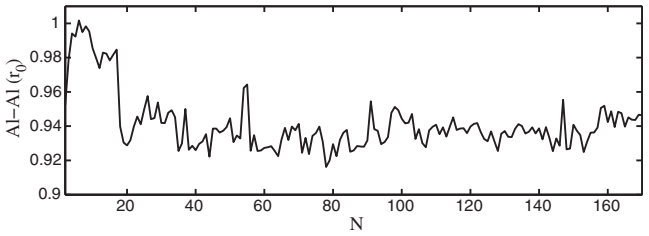

Fig. 9. Aℓ–Aℓ bond as a function of the number of atoms.

On the other hand, the distances between the nearest Aℓ–Aℓ aluminum atoms remained almost constant as shown in Fig. 9.

The average Aℓ–Aℓ bond was found to be $0.9443r_0$ while the lower $0.9162r_0$ and higher $1.0017r_0$ distances were obtained in the case of Aℓ_{78} and Aℓ_6 clusters respectively. Taking into account the lattice constant of the aluminum crystal (404.95pm), the value of r_0 can be determined as $r_0 = 3.0323$Å.

From our simulations, we came out with 15 symmetry groups: D_{3h}, T_d, O_h, D_{5h}, C_{2v}, C_{3v}, C_{5v}, I_h, C_s, C_2, C_1, D_{6h}, C_{6v}, S_4, and C_3. For each of these symmetry groups, one molecule was chosen together with its corresponding global minimum structure and was depicted in Fig. 10. Following the order in which the symmetry groups are given above, structures of Aℓ_3, Aℓ_4, Aℓ_6, Aℓ_7, Aℓ_8, Aℓ_{10}, Aℓ_{12}, Aℓ_{13}, Aℓ_{16}, Aℓ_{17}, Aℓ_{21}, Aℓ_{38}, Aℓ_{39}, Aℓ_{57} and Aℓ_{69} are plotted in Fig. 10a), 10b), 10c), 10d), 10e), 10f), 10g), 10h), 10i), 10j), 10k), 10l), 10m), 10n) and 10o) respectively.

3.3. Comparison

The results obtained here using a Gupta potential agree well with those obtained by Doye [22] and by Noya et al. [44] using the glue potential and the monte-carlo simulations respectively. Even if the minimized energies are approximatively the same, we have noticed that the Gupta potential favored the Icosahedral structures while the Glue potential favored the polytetrahedral structures.

Andrés et al. demonstrated using Kohn sham Density Functional Theory that from Aℓ_{13} to Aℓ_{22}, the icosahedral growth dominates global minima structures and this agrees with our work for Aℓ_{13} to Aℓ_{18} [45]. Also, Khanna et al. had earlier confirmed that from Aℓ_{13} to Aℓ_{18}, icosahedral structures are more stable in all-electron PBE calculations [46].

In general, the structures obtained in this manuscript are similar to those obtained by the authors of reference [23] who also used Gupta potential for their work. Nevertheless, we have noticed two differences between our results and theirs. Firstly, for $N = 9$ as an example, Gilles et al. considered high symmetry structures and found the body-centered cubic to be lowest in energy, in disagreement with our present results. Although the body-centered cubic structure is stable, it is not the optimized structure. To verify this, we used their structure given in Fig. 11a) as initial configuration, after a relatively long simulation time, the structure is transformed as shown in Fig. 11c).

As shown in the curve of Fig. 11b) their simulated body-centered cubic is a stable structure that is 2.0318 eV above the global minimum obtained in this manuscript, and which is, in fact, the second lowest-energy isomer. Secondly, the curve of the binding energy obtained in [23] is qualitatively similar to that obtained in this work. We believe that the quantitative differences that appear between the results are due to the values of the parameters of the potential.

In terms of absolute binding energies, our results are in good agreement with the experimental values. In comparison with some computed ones using Sutton-Chen potential, the Truhlar potential and the Cleri-Rosato potential as reported by Jasper et al. [24,25], the smallest error (0.19%) is found between our results and the experiment.

Next we focus our attention on the performance of the potentials for the description of the Aℓ_2 dimer. The characterization of Aℓ_2 dimer has provided a challenge for both theory and experiment due to the closeness in energy of the singlet and triplet states. Table 3 shows the equilibrium separation values for the Gupta potential, along with the values obtained using the other potentials or methods, as several ab initio and Density Functional Theory calculations, as well as experiment for comparison.

The Aℓ_2 equilibrium separation distance as calculated using the Gupta potential agrees well with the experimental value with a precision of 98.13%. It is followed by the NP-B predicted value 82.01%, while the Sutton-Chen potential presents the lowest precision of 73.79%. This may be due to the Sutton-Chen being fitted to just structural data, which does not take into account the energetics data such as the vacancy formation energy and surface energies.

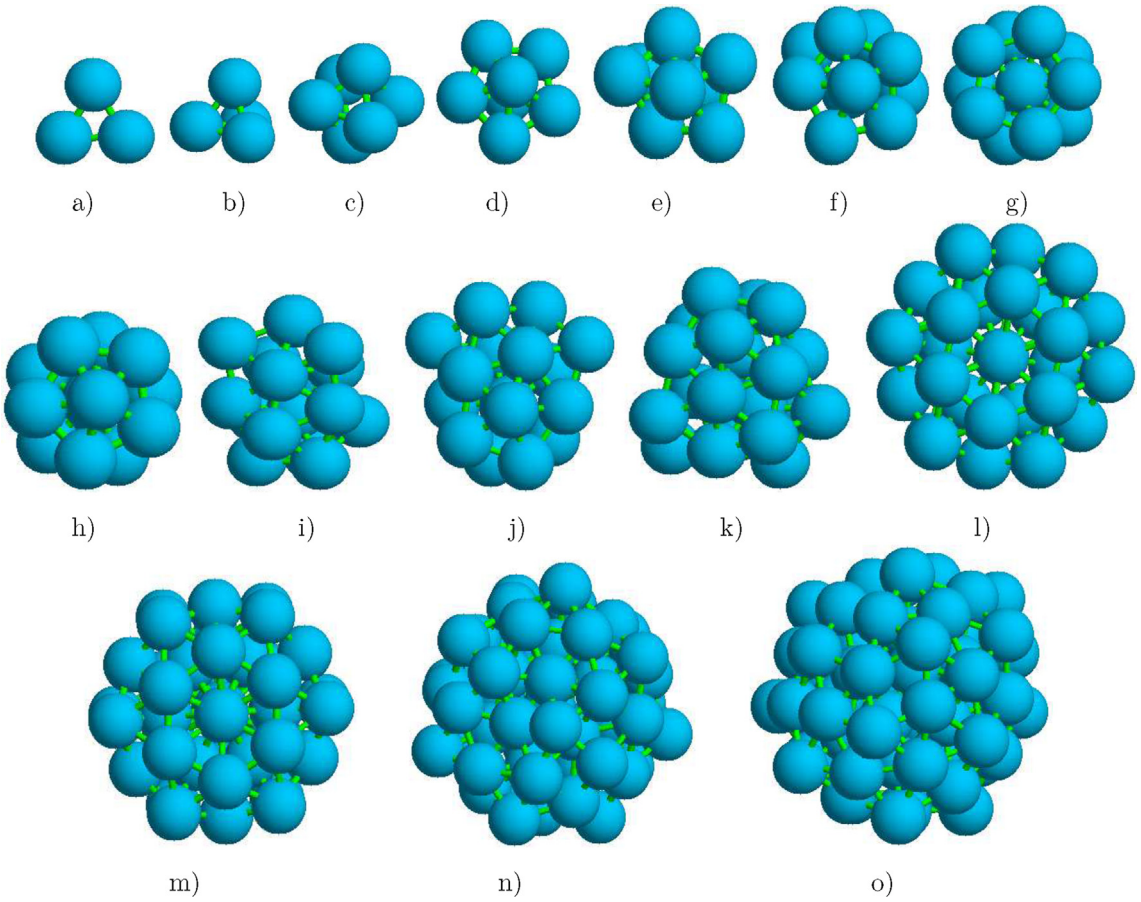

Fig. 10. Ground-state structures for aluminum cluster geometries, as predicted by the Molecular Dynamics with the Gupta potential.

4. Conclusion

In this present work, the optimized geometry, as well as the ground state energy of aluminum clusters with up to 170 atoms, have been analyzed. We have then determined the Gupta parameters for aluminum clusters. Comparison between our results and other results found in the literature have been carried out. We found that for $3 \leqslant N \leqslant 170$, the ground state energy of aluminum cluster obtained using Gupta potential decreases quadratically with the number N of atoms. But the $A\ell$–$A\ell$ bond fluctuates slightly around $0.9443r_0$. In comparison with other results found in the literature, our obtained

Table 3
$A\ell_2$ equilibrium separation values (r_2).

Potentials	r_2 (Å)	Precision
Sutton-Chen [47]	2.092	73.79%
Streitz-Mintmire [48]	2.207	77.85%
Cleri-Rosato [49]	2.325	82.01%
Truhlar potential (NP-B) [25]	2.523	88.99%
Gupta (this work)	2.888	98.13%
Experiment [50]	2.835	–

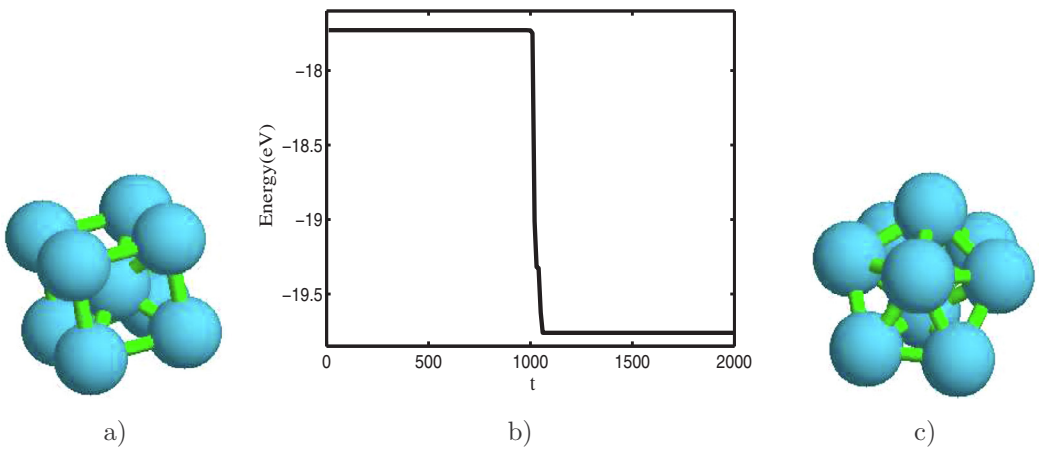

Fig. 11. a) Optimized $A\ell_9$ according to Gilles et al. b) An illustration of the evolution of the lowest-energy $A\ell_9$ molecule with the Gupta potential starting from a body-centered cubic initialized coordinates. c) Optimized $A\ell_9$ obtained here.

values such as binding energy and lattice constant are in very good agreement with the experimental ones. Our next investigation will be to determine the optimized configurations of other atoms and doped materials. We think also that the analysis of the physical properties of some clusters is an interesting subject.

CRediT authorship contribution statement

W.M. Keyampi: Writing - original draft, Data curation. **T.S. Tsasse:** Writing - original draft, Visualization. **B. Nana:** Conceptualization, Methodology, Writing - review & editing. **S. Zekeng:** Supervision, Software.

Declaration of Competing Interest

The authors declare that they have no known competing financial interests or personal relationships that could have appeared to influence the work reported in this paper.

References

[1] G.H. Wang, Cluster Physics, Shanghai Scientific and Technology Press, Shanghai, 2003.
[2] R.L. Johnston, Phil. Trans. R. Soc. Lond. A 356 (1998) 211.
[3] J.T. Liu, H.M. Duan, Acta Phys. Sin. 58 (2009) 4826.
[4] X.J. Kuang, X.Q. Wang, G.B. Liu, J. At. Mol. Phys. 27 (2010) 254.
[5] K. Mailitan, L.L. Chun, M.D. Hai, J. At. Mol. Sci. 4 (2013) 235.
[6] A.W. Castleman, S.N. Khanna, J. Phys. Chem. C 113 (2009) 2664.
[7] Y.C. Bae, V. Kumar, H. Qsnanai, et al., Phys. Rev. B 72 (2005) 125427.
[8] Y.C. Bae, H. Qsnanai, V. Kumar, et al., Phys. Rev. B 70 (2004) 195413.
[9] Y. Shibuta, T. Suzuki, Chem. Phys. Lett. 445 (2007) 265.
[10] A.E. James, H. Marc, S. Yasushi, J. Chem. Phys. 130 (2009) 034704.
[11] I.M.L. Billas, A. Chatelain, W.A. deHeer, J. Magn. Magn. Mater. 168 (1997) 64.
[12] D.E. Bergeron, P.J. Roach, A.W. Castleman, N. Jones, S.N. Khanna, Science 307 (2005) 231.
[13] S.S. Kushvaha, Z. Yan, W. Xiao, M.J. Xu, Q.K. Xue, X.S. Wang, Nanotechnology 18 (2007) 145501.
[14] J. Kanzow, P.S. Horn, M. Kirschmann, V. Zaporojtchenko, K. Dolgner, K.F. Faupel, C. Wehlack, W. Possart, Appl. Surf. Sci. 239 (2005) 227.
[15] B.P. Cao, C.M. Neal, A.K. Starace, Y.N. Ovchinnikov, V.Z. Kresin, M.F. Jarrold, J. Supercond. Nov. Magn. 21 (2008) 163.
[16] D.J. Wales, P.K.D. Jonathan, Phys. Chem. 101 (1997).
[17] S. Goedecker, W. Hellmann, T. Lenosky, Phys. Rev. Lett. 95 (2005) 55501.
[18] R.S. Berry, R.E. Kunz, in: T.P. Martin (Ed.), Kluwer, Dordrecht, 1996, pp. 299.
[19] P.K.D. Jonathan, Comput. Mater. Sci. 35 (2006) 227.
[20] P.K.D. Jonathan, C. Florent, Phys. Rev. Lett. 86 (2001) 3570.
[21] D.L. Lesley, R.L. Johnston, School of Chemistry, University of Birmingham, Edgbaston, Birmingham BB21 2TT, UK.
[22] P.K.D. Jonathan, University Chemical Laboratory, Lensfield Road, Cambridge CB2 1EW, United Kingdom, 2008.
[23] W.T. Giles, L.J. Roy, T.W. Nicholas, Chem. Phys. 112 (2000) 4773.
[24] A.W. Jasper, P. Staszewski, G. Staszewska, N.E. Schultz, D.G. Truhlar, Phys. Chem. B 108 (2004) (2004) 8996.
[25] A.W. Jasper, N.E. Schultz, D.G. Truhlar, Phys. Chem. B 109 (2005) 3915.
[26] K. Michaelian, N. Rendón, I.L. Garzón, Phys. Rev. B 60 (1999) 2000.
[27] J.A. Reyes-Nava, I.L. Garzón, M.R. Beltrán, K. Michaelian, Rev. Mex. Fis. 48 (2002) 450.
[28] R.P. Gupta, Phys. Rev. B 23 (1981) 6265.
[29] F. Ducastelle, J. Phys. Paris 31 (1970) 1055.
[30] J. Friedel, in: J.M. Ziman (Ed.), vol. I, Pergamon, London, 1969.
[31] S. Nouemo, F. Tchoffo, J.M.B. Ndjaka, S. Domngang, J. Taibah Univ Sci. 10 (2016) 430.
[32] S. Yuan, Y. Kong, F. Wen, F. Li, J. Phys.: Condens. Matter 19 (2007) 466203.
[33] T.P. Martin, T. Bergmann, H. Gohlich, T. Lange, Chem. Phys. Lett. 172 (1990) 209.
[34] W.D. Knight, K. Clemenger, W.A. de Heer, W.A. Saunders, M.Y. Chou, M.L. Cohen, Phys. Rev. Lett. 52 (1984) 2141.
[35] T.P. Martin, Phys. Rep. 273 (1996) 199.
[36] J. Lerm, M. Pellarin, B. Baguenard, C. Bordas, E. Cottancin, J.L. Vialle, M. Broyer, T.P. Martin (Ed.), Large Clusters of Atoms and Molecules, Kluwer, Dordrecht, 1996, p. 71.
[37] K.E. Schriver, J.L. Persson, E.C. Honea, R.L. Whetten, Phys. Rev. Lett. 64 (1990) 2539.
[38] B. Baguenard, M. Pellarin, J. Lerm, J.L. Vialle, M. Broyer, J. Chem. Phys. 100 (1994) 754.
[39] B. Knapp, S. Frantal, M. Cibena, W. Schreiner, P. Bauer, J. Computat. Biol. 18 (2011) 8.
[40] W.A. de Heer, Rev. Mod. Phys. 65 (1993) 611.
[41] M.F. Jarrold, in: D.H. Russell (Ed.), Gas Phase Inorganic Chemistry, Plenum, New York, 1989.
[42] M.Y. Chou, M.L. Cohen, Phys. Lett. A 113 (1986) 420.
[43] W.D. Knight, K. Clemenger, W.A. de Heer, W.A. Saunders, M.Y. Chou, M.L. Cohen, Phys. Rev. Lett. 52 (1984) 2141.
[44] E.G. Noya, J.P.K. Doye, Phys. Rev. B73 (2006) 125407.
[45] Andrés Aguadoa, José M. López, J. Chem. Phys. 130 (2009) 064704.
[46] S.N. Khanna, B.K. Rao, P. Jena, Phys. Rev. B 65 (2002) 125105.
[47] A.P. Sutton, J. Chen, Phil. Mag. Let. 61 (1990) 139.
[48] F.H. Streitz, J.W. Mintmire, Phys. Rev. B 50 (1994) 11996.
[49] F. Cleri, V. Rosato, Phys. Rev. B 48 (1993) 22.
[50] S.R. Langhoff, J.C.W. Bauschlicher, Chem. Phys. 92 (1990) 1879.